# Analytical Methods for Phase-Space Integrals

With Applications to Semi-Inclusive Deep-Inelastic Scattering




DISSERTATION ZUR ERLANGUNG DES DOKTORGRADES DER NATURWISSENSCHAFTEN (DR. RER. NAT.) DER FAKULTÄT FÜR PHYSIK DER UNIVERSITÄT REGENSBURG

vorgelegt von

Andreas Rapakoulias aus

Marousi, Attikis, Griechenland

im Jahr 2026

Promotionsgesuch eingereicht am: 11.05.2023

# General Audience Summary

Our most precise description of the subatomic world, the Standard Model of particle physics, makes predictions that can be tested against experiments at facilities such as CERN's Large Hadron Collider and the future Electron–Ion Collider. We compare prediction and measurement to look for deviations from the theory, and through them for new physics. For this comparison to be meaningful, the theoretical prediction must be as precise as the measurement. Improving the precision means computing more terms in a difficult perturbative expansion.

Each such term requires the evaluation of a large number of multidimensional integrals. These come in two kinds. The first is associated with virtual particles that appear and disappear inside a process. It has been studied intensively for decades, and a rich toolbox exists for it. The second is associated with the real radiation of extra particles that fly into the detector. It has received much less attention and is usually evaluated by brute-force numerical methods. The two kinds are linked: only when they are added together do the infinities that affect each separately cancel, leaving the finite answer that nature produces.

This thesis develops analytic tools for the second, less-explored kind. The central idea is to split each real-radiation integral into a "radial" piece, which depends on the particular process, and an "angular" piece, which is universal and reappears unchanged in many different processes. We show how to evaluate these universal angular integrals exactly, as series in the small parameter of dimensional regularisation, by rewriting them as *Mellin–Barnes integrals* and converting them, step by step, into a class of well-understood special functions called *polylogarithms*. We carry this program out in full for the families of angular integrals with three and four denominators, which had never been computed analytically before. We apply the method to semi-inclusive deep-inelastic scattering, a key process for mapping the three-dimensional structure of the proton at the Electron–Ion Collider, at the second non-trivial order of the strong-coupling expansion. The result is a transparent, reusable, and fully validated analytic framework, together with a set of building blocks that the wider community can use directly.

# Abstract

This thesis develops reusable analytic infrastructure for the real-radiation contributions to perturbative calculations in quantum field theory. The central objects are the process-independent angular phase-space integrals that enter the next-to-next-to-leading-order (NNLO) subtraction and slicing frameworks of processes such as Drell–Yan, Higgs production, jet production, and semi-inclusive deep-inelastic scattering. After reviewing the reverse-unitarity formalism that places real and virtual corrections on a common algebraic footing, we use the radial–angular decomposition to isolate these angular building blocks in their rotationally invariant (Somogyi) and frame-dependent (van Neerven) forms. We then construct a systematic Mellin–Barnes-to-polylogarithm method: after analytic continuation in the dimensional regulator and expansion, the balanced Mellin–Barnes integrals are converted into beta functions, then into real parametric integrals, and finally into Goncharov polylogarithms. With this method we compute, for the first time, a complete basis of the three- and four-denominator angular families, both massless and massive, to the orders in the regulator required for NNLO applications, together with partial-fraction and recursion relations for the massive cases and for higher denominator powers. Semi-inclusive deep-inelastic scattering at NNLO in QCD provides the demonstrator application: we combine the angular method with a one-fold radial integration and resolve the soft and collinear singularities, including soft singularities nested inside the angular part that must be extracted to all orders in the regulator. We then extend the same analytic-function technology from real-radiation phase space to the virtual sector, linearizing the generalized harmonic polylogarithms with square-root alphabets that the two-loop electroweak master integrals require. All results are validated against independent calculations, direct numerical Mellin–Barnes integration, permutation symmetries, and an independent differential-equation evaluation. The outcome is thus a durable, validated library of analytic real-radiation building blocks rather than a single process-specific calculation.

# List of Publications

This thesis is based on the following publications, prepared in collaboration with the co-authors listed.

### Published Articles

1. T. Ahmed, S. M. Hasan and A. Rapakoulias, *Angular phase-space integrals with four denominators through Mellin–Barnes*, JHEP 11 (2025) 152, arXiv:2508.15952 [hep-ph]

2. T. Ahmed, S. Goyal, S. M. Hasan, R. N. Lee, S.-O. Moch, V. Pathak, N. Rana, A. Rapakoulias and V. Ravindran, *NNLO phase-space integrals for semi-inclusive deep-inelastic scattering*, Phys.Rev.D 112 (2025) 1, 014020, arXiv:2412.16509 [hep-ph]

3. T. Ahmed, S. M. Hasan and A. Rapakoulias, *Phase-space integrals through Mellin–Barnes representation*, Phys.Rev.D 112 (2025) 5, L051903, arXiv:2410.18886 [hep-ph]

### Conference Proceeding

1. T. Ahmed, S. M. Hasan and A. Rapakoulias, *Phase-space integrals through Mellin-Barnes representation*, RADCOR Conference, arXiv:2604.01505 [hep-ph].

### In Preparation

1. T. Ahmed, Sumit Banik, S. M. Hasan and A. Rapakoulias, *MB2MPL: A Mathematica package for evaluating Mellin-Barnes Integrals in terms of Multiple Polylogarithms*

2. T. Ahmed, S. M. Hasan and A. Rapakoulias, *A symbolic bootstrap for boundary constants in the linearization of generalized harmonic polylogarithms*

The analytic results and their numerical implementation are distributed as ancillary material accompanying these publications (notably the files `3prop0mass.m`, `3prop1mass.m`, `recursion.m`, `massless_ep0.m`, `one_mass_ep0.m`, `de_results.m`, `rad_results.m`, and the evaluation notebooks `Evaluation.nb` and `main.nb`); their organisation is summarised in Section A.2.

# Declaration

I hereby declare that this thesis is my own work and that, to the best of my knowledge, it contains no material previously published or written by another person, except where due reference is made. The research presented here was carried out in collaboration with the co-authors of the publications listed above.

# Acknowledgements

First and foremost, I would like to express my deepest gratitude to my supervisor, Prof. Dr. Taushif Ahmed, for his continuous guidance, encouragement, and unwavering support throughout my PhD studies. His expertise, insightful advice, and patience have been invaluable in shaping my understanding of theoretical particle physics and in helping me develop as an independent researcher. I am sincerely grateful for the trust he placed in me and for the many opportunities he provided during my time in Regensburg.

I would also like to thank Dr. Syed Mehedi Hasan, my colleague, collaborator, and mentor throughout my doctoral studies. I greatly appreciate his constant support, the countless scientific discussions we shared, and his willingness to help whenever challenges arose. His collaboration and friendship made both the research and the day-to-day experience of pursuing a PhD considerably more enjoyable.

My sincere thanks also go to my collaborators in India, Prof. Dr. V. Ravindran, Saurav Goyal, and Vaibhav Pathak. It has been a privilege to work with them on several research projects. I am grateful for the many stimulating discussions, their valuable insights, and their generous hospitality during my visit to India, which was both scientifically enriching and personally memorable.

I would also like to thank all my friends in Regensburg for their companionship and for making my years in Germany enjoyable. Their friendship, encouragement, and the many moments we shared together helped make Regensburg feel like a second home.

Also I gratefully acknowledge the support through the Deutsche Forschungsgemeinschaft (DFG) Research Unit FOR 2926 for making working and doing research in Germany possible.

Finally, and most importantly, I wish to express my heartfelt gratitude to my family. Their unconditional love, endless encouragement, and unwavering belief in me have been my greatest source of strength throughout this journey. Being far away from Greece was often difficult, but their constant support and sacrifices made it possible for me to pursue my goals. This thesis is dedicated to them.

# Dedication

*To my parents and family.*

# Contents

**General Audience Summary** **ii**

**Abstract** **iii**

**List of Publications** **iv**

**Declaration** **v**

**Dedication** **vii**

**1 Introduction** **2**
1.1 Precision as a window on the proton and beyond . . . 2
1.2 The Standard Model ingredients . . . 3
1.3 Deep-inelastic scattering as a probe of the nucleon . . . 4
1.4 From DIS to SIDIS . . . 5
1.5 The Electron–Ion Collider and three-dimensional imaging . . . 6
1.6 Factorisation and higher-order QCD . . . 8
1.7 Electroweak and mixed QCD–electroweak corrections . . . 9
1.8 The ubiquity of infrared divergences . . . 10
1.9 The language of higher-order corrections . . . 11
1.10 The computational bottleneck: real radiation . . . 12
1.10.1 Methods for NNLO real radiation: where this thesis fits . . . 13
1.11 This thesis: idea, contributions, and outline . . . 14

**I Angular Phase-Space Infrastructure for Real Radiation** **16**

**2 Reverse Unitarity, Differential Equations and the Radial–Angular Decomposition** **17**
2.1 From cross sections to angular building blocks . . . 17
2.2 Cross sections and phase space . . . 18
2.3 The optical theorem and cut phase space . . . 18
2.4 Reverse unitarity and cut propagators . . . 19
2.5 IBP identities and the reduction to master integrals . . . 20
2.6 Differential Equations for Feynman Integrals . . . 21
2.7 The radial–angular factorisation . . . 28
2.8 The Somogyi and van Neerven representations . . . 29
2.9 Classification of the angular integrals . . . 30
2.10 Worked example: the single massless denominator . . . 31
2.11 Conventions and notation . . . 32

**3 Mathematical Tools: Mellin–Barnes Integrals and Polylogarithms 33**
3.1 Purpose and the running example . . . 33
3.2 From the Mellin transform to the Mellin–Barnes identity . . . 34
3.3 From the van Neerven form to the angular Mellin–Barnes representation . . . 35
3.4 Residues and analytic continuation in $\epsilon$ . . . 36
3.5 The Barnes lemmas . . . 37
3.6 Balanced integrals, beta conversion, and the delta-collapse . . . 37
3.7 Goncharov polylogarithms . . . 38
3.8 Linear reducibility: when the result is a polylogarithm . . . 39
3.9 The running example, completed . . . 39

**4 Angular Integrals and the Mellin–Barnes-to-Polylogarithm Method 41**
4.1 Scope and conventions . . . 41
4.2 The universal Mellin–Barnes representation . . . 42
4.3 The algorithm . . . 42
4.4 Classification and lower-denominator checks . . . 43
4.5 Linear reducibility and polylogarithmic expressibility . . . 44
4.6 Reduction of the polylogarithms to a fibration basis . . . 44
4.7 Comparison with the differential-equation route . . . 45
4.8 Failure modes and the frontier . . . 45
4.9 MB2MPL Mathematica Package . . . 45

**5 Three- and Four-Denominator Angular Integral Families 47**
5.1 Definitions and scope . . . 47
5.2 Three denominators, massless . . . 48
5.3 Three denominators, single-massive . . . 49
5.4 Partial-fraction reduction: the two-point splitting lemma . . . 49
5.5 Recursion relations . . . 50
5.6 Four denominators, massless . . . 51
5.7 Four denominators, single- and multi-massive . . . 52
5.8 Validation, symmetries, and performance . . . 52
5.9 Summary of the family data . . . 52

**6 Semi-Inclusive Deep-Inelastic Scattering 54**
6.1 Kinematics and scope . . . 54
6.2 The hadronic tensor and structure functions . . . 55
6.3 Collinear factorisation and coefficient functions . . . 55
6.4 Perturbative channels through NNLO . . . 56
6.5 The tagged-parton constraint . . . 57
6.6 From channels to master integrals . . . 58
6.7 State of the art . . . 58
6.8 What this thesis supplies . . . 59

**7 NNLO SIDIS Master Integrals and the Resolution of Singularities 60**
7.1 The constrained phase space and the master integrals . . . 60
7.2 Canonical differential equations . . . 61
7.3 Two relations beyond the IBP reduction . . . 63
7.4 Radial–angular decomposition in the $(k_1, k_2)$ frame . . . 63
7.5 The denominators and a worked mapping . . . 64
7.6 Resolution of the soft and collinear singularities . . . 65

7.7 Summary . . . . . 66

**II Extensions of the Analytic Toolkit 67**

**8 Toward Electroweak and Mixed QCD–Electroweak Corrections 68**
8.1 Motivation and scope . . . . . 68
8.1.1 Vertex corrections and general structure of the form factor . . . . . 69
8.1.2 $\mathcal{O}(\alpha)$ Corrections . . . . . 71
8.1.3 $\mathcal{O}(\alpha\alpha_s)$ Corrections . . . . . 72
8.2 From Lagrangian to Onshell Renormalization . . . . . 72
8.2.1 Renormalization constants at $\mathcal{O}(\alpha)$ for $\gamma qq$ vertex . . . . . 79
8.2.2 Renormalization constants at $\mathcal{O}(\alpha\alpha_s)$ for $\gamma qq$ vertex . . . . . 80
8.3 Linearization of General Harmonic Polylogarithms . . . . . 83
8.4 Status and outlook . . . . . 84

**9 Conclusions and Outlook 85**
9.1 Summary . . . . . 85
9.2 Methodological remarks . . . . . 86
9.3 Outlook . . . . . 86

**A Conventions and Supplementary Material 88**
A.1 Notation and Conventions . . . . . 88
A.2 Map of the Ancillary Files . . . . . 89

**B Evaluation of Angular Phase-Space Integrals 90**
B.1 Spherical Coordinates and the Angular Measure in $d$ Dimensions . . . . . 90
B.2 Integral Representations and Alphabets . . . . . 91
B.3 Partial-Fraction and Recursion Relations . . . . . 92

**C NNLO SIDIS Phase-Space Master Integrals 94**
C.1 Resolution of Singularities: Worked Examples . . . . . 94

**D Electroweak Renormalisation Ingredients 95**
D.1 Feynman Rules . . . . . 95
D.2 Renormalisation Constants and Ingredients . . . . . 97

# List of Figures

1.1 Running of the strong coupling . . . 4
1.2 Inclusive deep-inelastic scattering . . . 5
1.3 Semi-inclusive deep-inelastic scattering . . . 6
1.4 SIDIS azimuthal kinematics . . . 7
1.5 EIC kinematic coverage . . . 7
1.6 Nucleon tomography . . . 8
1.7 Factorisation of SIDIS . . . 9
1.8 Convergence of the perturbative series . . . 10
1.9 Infrared cancellation . . . 11
1.10 NNLO cross-section decomposition . . . 12
1.11 NNLO double-real emission . . . 13

2.1 Chapter roadmap . . . 18
2.2 Reverse unitarity . . . 19
2.3 Integration-by-parts reduction . . . 21
2.4 Geometry of the radial–angular decomposition . . . 29

3.1 The Mellin–Barnes-to-polylogarithm pipeline . . . 34
3.2 The Mellin–Barnes integration contour . . . 35
3.3 Analytic continuation by pole crossing . . . 37

4.1 Classification of angular integrals . . . 43
4.2 Rationalisation of square roots . . . 46

5.1 Propagator structure of the angular integrals . . . 48
5.2 Numerical validation . . . 53

6.1 Partonic channels in SIDIS . . . 57

7.1 Two independent routes to the master integrals . . . 61
7.2 NNLO SIDIS master integrals . . . 62
7.3 Singularity resolution via plus-distribution . . . 65

8.1 Feynman diagrams for set-5 generated by FeynArts. . . . 73
8.2 Feynman diagrams for set-1 generated by FeynArts. . . . 73
8.3 Feynman diagrams for set-8 generated by FeynArts. . . . 74
8.4 Feynman diagrams for set-3 generated by FeynArts. . . . 74
8.5 Bosonic self energy diagrams generated by FeynArts, where “G” represents Goldstone bosons ($\Phi$) and “u” represent Ghosts. . . . 80
8.6 Fermionic self energy diagrams generated by FeynArts. . . . 80
8.7 Fermionic self energy diagrams at $\mathcal{O}(\alpha\alpha_s)$ generated by FeynArts. . . . 81

D.1 QCD Feynman rules . . . . . 96
D.2 Electroweak Feynman rules . . . . . 96

# List of Tables

1.1 Publications and their role in the thesis . . . . . 15

2.1 Classification of angular integrals . . . . . 31
2.2 Notation for the angular formalism . . . . . 32

4.1 MB versus differential equations . . . . . 45

5.1 Numerical validation of the four-denominator integrals . . . . . 53

6.1 SIDIS variables . . . . . 55
6.2 Singularities in NNLO SIDIS . . . . . 56
6.3 Partonic channels by order . . . . . 57

7.1 Pole structure of the SIDIS master integrals . . . . . 66

8.1 The QCD–electroweak double expansion . . . . . 69

A.1 Ancillary files . . . . . 89

# Chapter 1

# Introduction

## Contents

1.1 Precision as a window on the proton and beyond . . . 2
1.2 The Standard Model ingredients . . . 3
1.3 Deep-inelastic scattering as a probe of the nucleon . . . 4
1.4 From DIS to SIDIS . . . 5
1.5 The Electron–Ion Collider and three-dimensional imaging . . . 6
1.6 Factorisation and higher-order QCD . . . 8
1.7 Electroweak and mixed QCD–electroweak corrections . . . 9
1.8 The ubiquity of infrared divergences . . . 10
1.9 The language of higher-order corrections . . . 11
1.10 The computational bottleneck: real radiation . . . 12
1.10.1 Methods for NNLO real radiation: where this thesis fits . . . 13
1.11 This thesis: idea, contributions, and outline . . . 14

## 1.1 Precision as a window on the proton and beyond

The proton admits two distinct descriptions. In the periodic table it is an elementary constituent, fixed by a single unit of electric charge and a spin of one half. In Quantum Chromodynamics it is a strongly coupled bound state of quarks and gluons whose internal dynamics are governed by the strong force of the Standard Model. Reconciling these two descriptions, the simple particle and its composite interior, is a central problem of modern physics. The standard tool for the task is scattering: by scattering a well-understood probe off the proton at ever higher resolution, one resolves ever finer detail of its partonic structure. Building this probe, and sharpening it to the precision now demanded, is a programme to which both experiment and theory contribute. This thesis contributes to the theoretical side of that programme.

Particle physics proceeds by comparing theory with experiment. Our present understanding is encoded in the Standard Model (SM), built on Quantum Chromodynamics (QCD) [1, 2] and the electroweak theory [3, 4, 5], and completed by the discovery of the Higgs boson. The SM describes a large body of data spanning many orders of magnitude in energy. Because it is so successful, the frontier of discovery has shifted from large qualitative effects to *small quantitative deviations*, that is, percent-level or smaller mis-

matches between a measured rate and its prediction, which could signal physics beyond the Standard Model.

The observable used for this comparison is the cross section. An experiment measures a (differential) cross section, and theory predicts it as a perturbative series in the coupling constants. A measured deviation is only as convincing as the prediction it is tested against. To interpret a percent-level discrepancy one needs a prediction whose theoretical uncertainty is well below a percent. Uncomputed higher-order corrections, electroweak effects, or mismodelled hadronic input can each shift a prediction at the percent level. An unaccounted-for shift of this size can mimic or mask a genuine signal of new physics. Precision is therefore a prerequisite for discovery.

Two complementary frontiers drive the present effort. At the Large Hadron Collider (LHC), the emphasis is on hard-scattering processes computed to high orders and compared with data in the search for deviations [6, 7, 8, 9, 10]. At the future Electron–Ion Collider (EIC), the emphasis is on the *structure of matter*, that is, a precise, multidimensional map of how quarks and gluons are distributed inside the nucleon [11, 12]. The two frontiers are linked, because a precise knowledge of nucleon structure is itself an input to LHC predictions. Both demand the same ingredient on the theory side, namely higher-order perturbative calculations controlled to high accuracy.

This thesis develops one such ingredient: a process-independent analytic infrastructure for the *real-radiation* part of higher-order QCD calculations, that is, the part associated with the emission of extra partons into the final state. Rather than treating these integrals as by-products of one process, we isolate them as reusable building blocks that appear in any NNLO subtraction or slicing scheme, from Drell–Yan and Higgs production to semi-inclusive deep-inelastic scattering. The last of these serves as the demanding physical demonstrator, while the angular families are formulated independently of the hard process. The remainder of this chapter builds the phenomenological and theoretical context needed to state the problem precisely, and closes with a summary of the contributions and an outline of the thesis.

## 1.2 The Standard Model ingredients

The Standard Model [13, 14, 15, 16, 1, 2, 17, 18, 19] is a gauge theory with the symmetry group

$$SU(3)_c \times SU(2)_L \times U(1)_Y, \tag{1.1}$$

where the $SU(3)_c$ factor describes the strong interaction and $SU(2)_L \times U(1)_Y$ the electroweak interaction, spontaneously broken to the electromagnetic $U(1)_{\mathrm{em}}$ by the Higgs mechanism. Two features of this structure are essential for what follows.

**QCD and asymptotic freedom:** The strong interaction is described by the QCD Lagrangian

$$\mathcal{L}_{\mathrm{QCD}} = -\tfrac{1}{4} G^a_{\mu\nu} G^{a\,\mu\nu} + \sum_q \bar{q}\,(i\gamma^\mu D_\mu - m_q)\,q, \tag{1.2}$$

with $G^a_{\mu\nu}$ the gluon field strength and $D_\mu$ the covariant derivative. Its defining property is the running of the coupling. At one loop,

$$\mu^2 \frac{\mathrm{d}\alpha_s}{\mathrm{d}\mu^2} = -\beta_0 \frac{\alpha_s^2}{4\pi} + \mathcal{O}(\alpha_s^3), \qquad \beta_0 = \frac{11}{3} C_A - \frac{4}{3} T_R n_f, \tag{1.3}$$

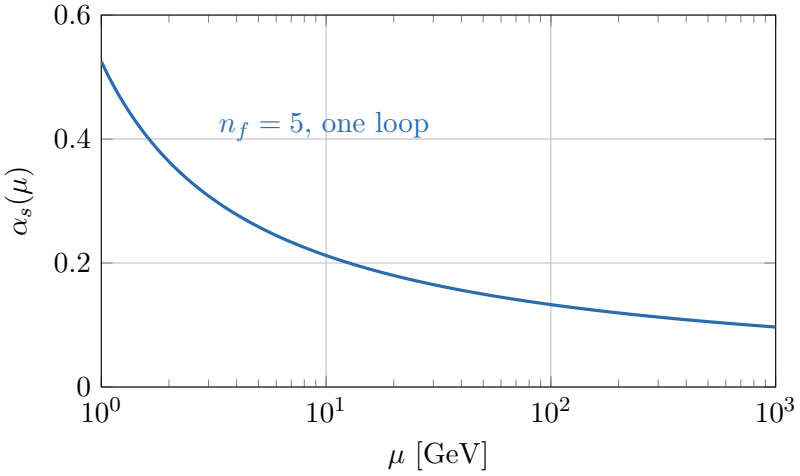



Figure 1.1: The running of the strong coupling $\alpha_s(\mu)$ at one loop ($n_f = 5$, $\Lambda_{\rm QCD} \simeq 0.21\,\text{GeV}$). Asymptotic freedom is the decrease of $\alpha_s$ at large scales; perturbation theory is reliable for $\mu \gtrsim 1\,\text{GeV}$, while confinement dominates at low scales.

with $\beta_0 > 0$ for the physical number of flavours. The coupling therefore *decreases* at large scales (Figure 1.1). This is asymptotic freedom [1, 2], which makes a perturbative expansion in $\alpha_s$ meaningful for hard processes ($\mu \gtrsim 1\,\text{GeV}$), while at low scales the growth of $\alpha_s$ drives confinement and the binding of quarks and gluons into hadrons. The non-perturbative transition between partons and hadrons is what makes the determination of nucleon structure difficult.

**The electroweak sector:** The electroweak interaction unifies electromagnetism and the weak force; after spontaneous symmetry breaking the physical spectrum contains the massless photon and the massive $W^\pm$ and $Z$ bosons, with the weak mixing angle $\theta_W$ relating the gauge couplings. In deep-inelastic scattering the dominant exchange at moderate $Q^2$ is the photon, but at $Q^2$ approaching the weak scale, $Z$ (neutral-current) and $W$ (charged-current) exchange become important. For precision observables the electroweak and mixed QCD×electroweak corrections are not negligible, and their consistent inclusion requires renormalisation of the electroweak sector. I return to this point in Section 1.7 and develop the corresponding ingredients in Chapter 8.

## 1.3 Deep-inelastic scattering as a probe of the nucleon

The cleanest probe of nucleon structure [20, 21, 22, 23, 24, 25, 26, 27, 28] is deep-inelastic scattering (DIS), in which a lepton scatters off a nucleon by exchanging a highly virtual boson,

$$\ell(k) + N(P) \to \ell(k') + X, \qquad q = k - k', \qquad Q^2 = -q^2 > 0, \tag{1.4}$$

as illustrated in Figure 1.2. The standard invariants are

$$x_B = \frac{Q^2}{2P\cdot q}, \qquad y = \frac{P\cdot q}{P\cdot k}, \qquad W^2 = (P+q)^2, \tag{1.5}$$

with $x_B$ the Bjorken variable, $y$ the inelasticity, and $W$ the invariant mass of the hadronic final state. The large virtuality $Q^2$ provides the hard scale that resolves the partonic

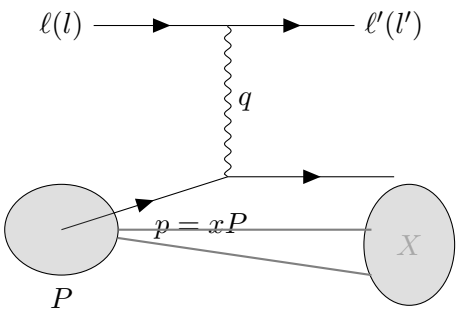



Figure 1.2: Inclusive deep-inelastic scattering, $\ell + P \to \ell' + X$. A lepton of momentum $l$ scatters off the proton $P$ by exchanging a virtual boson $\gamma^*/Z$ of momentum $q = l - l'$ and virtuality $Q^2 = -q^2$; the boson strikes a parton carrying a fraction $x$ of the proton momentum, and the hadronic remnant $X$ is summed over. Inclusive DIS probes the one-dimensional parton distributions $f(x, Q^2)$.

constituents, and the resolution of DIS improves with $Q^2$.

The hadronic side of the process is encoded in the hadronic tensor, which for electromagnetic exchange decomposes into structure functions,

$$W^{\mu\nu} = \Big(-g^{\mu\nu} + \frac{q^\mu q^\nu}{q^2}\Big) F_1(x_B, Q^2) + \Big(P^\mu - \frac{P\cdot q}{q^2} q^\mu\Big)\Big(P^\nu - \frac{P\cdot q}{q^2} q^\nu\Big) \frac{F_2(x_B, Q^2)}{P\cdot q} + \cdots , \quad (1.6)$$

the ellipsis denoting parity-violating and spin-dependent terms relevant for weak exchange and polarised beams. In the parton model, the structure functions acquire a simple interpretation: at leading order

$$F_2(x_B, Q^2) = x_B \sum_q e_q^2 \left[q(x_B, Q^2) + \bar{q}(x_B, Q^2)\right], \qquad F_2 = 2x_B F_1, \quad (1.7)$$

the latter being the Callan–Gross relation, a consequence of the spin-$\frac{1}{2}$ nature of quarks. Here $q(x, Q^2)$ is the parton distribution function (PDF): the number density of quarks of flavour $q$ carrying a longitudinal momentum fraction $x$ of the nucleon. The PDFs are intrinsically non-perturbative, but their *scale dependence* is calculable in perturbation theory through the DGLAP evolution equations,

$$\frac{\mathrm{d} f_i(x,\mu)}{\mathrm{d}\ln\mu^2} = \sum_j P_{ij}(x, \alpha_s) \otimes f_j(x, \mu), \quad (1.8)$$

with $P_{ij}$ the splitting functions and $\otimes$ a convolution in $x$. The logarithmic violation of Bjorken scaling encoded in this equation is one of the most precisely tested predictions of QCD. The work in this thesis serves the precise extraction of such distributions and of their fragmentation-function counterparts.

## 1.4 From DIS to SIDIS

Inclusive DIS detects only the scattered lepton and therefore integrates over the entire hadronic final state. Semi-inclusive DIS (SIDIS) [29, 30, 31, 32, 33, 34] goes one step

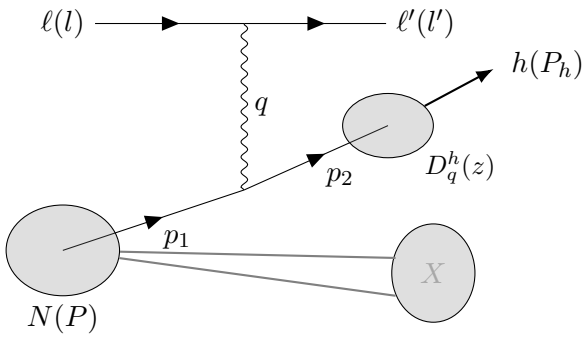



Figure 1.3: Semi-inclusive deep-inelastic scattering, $\ell + N \to \ell' + h + X$. In addition to the scattered lepton, one hadron $h$ of momentum $P_h$ is identified. The struck parton $p_2$ fragments into $h$, a process described by the fragmentation function $D_q^h(z)$. The detected hadron grants access to transverse-momentum and spin correlations, and hence to the three-dimensional structure of the nucleon.

further: it detects, in addition, at least one identified hadron,

$$\ell(p_\ell) + N(P) \to \ell(p'_\ell) + h(P_h) + X, \tag{1.9}$$

as in Figure 1.3. The identified hadron carries the additional variable

$$z_h = \frac{P \cdot P_h}{P \cdot q}, \tag{1.10}$$

the fraction of the virtual-photon energy transferred to the hadron, and a transverse momentum $P_{hT}$ relative to the photon direction. At the partonic level, with $p_1, p_2$ the momenta of the incoming and fragmenting partons, one works with

$$x' = \frac{Q^2}{2p_1 \cdot q}, \qquad z' = \frac{p_1 \cdot p_2}{p_1 \cdot q}, \qquad 0 < x', z' < 1. \tag{1.11}$$

The transition from the fragmenting parton to the observed hadron is non-perturbative and is described by a fragmentation function (FF) $D_{h/i}(z, \mu)$, the density for parton $i$ to produce hadron $h$ with momentum fraction $z$.

This single additional measurement changes the physics qualitatively. Detecting a hadron of definite species and momentum provides *flavour sensitivity* (different hadrons tag different parton flavours), access to *fragmentation* dynamics, and, through $P_{hT}$ and the azimuthal angle $\phi_h$ between the lepton and hadron planes (Figure 1.4), direct sensitivity to the *transverse motion and spin correlations* of partons inside the nucleon. For this reason, SIDIS is a cornerstone process for mapping the three-dimensional structure of the nucleon [35].

## 1.5 The Electron–Ion Collider and three-dimensional imaging

The facility that makes SIDIS timely is the Electron–Ion Collider [12, 36, 37, 38], the next-generation facility to be built at Brookhaven National Laboratory. The EIC is designed to deliver a variable electron–proton centre-of-mass energy in the range $\sqrt{s} \simeq 20$–$100\,\mathrm{GeV}$, upgradable towards $140\,\mathrm{GeV}$, at an instantaneous luminosity of $10^{33}$–$10^{34}\,\mathrm{cm}^{-2}\mathrm{s}^{-1}$, with

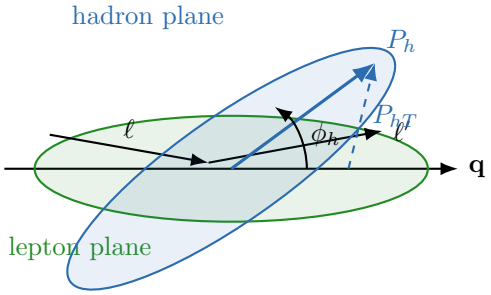



Figure 1.4: Azimuthal kinematics of SIDIS in the photon–nucleon frame. The virtual-photon momentum $\mathbf{q}$ defines the axis; the incoming and scattered leptons define the lepton plane, and the observed hadron $P_h$ defines the hadron plane. The azimuthal angle $\phi_h$ between the two planes, together with the hadron transverse momentum $P_{hT}$, encodes the spin–orbit and transverse-momentum correlations accessed at the EIC.

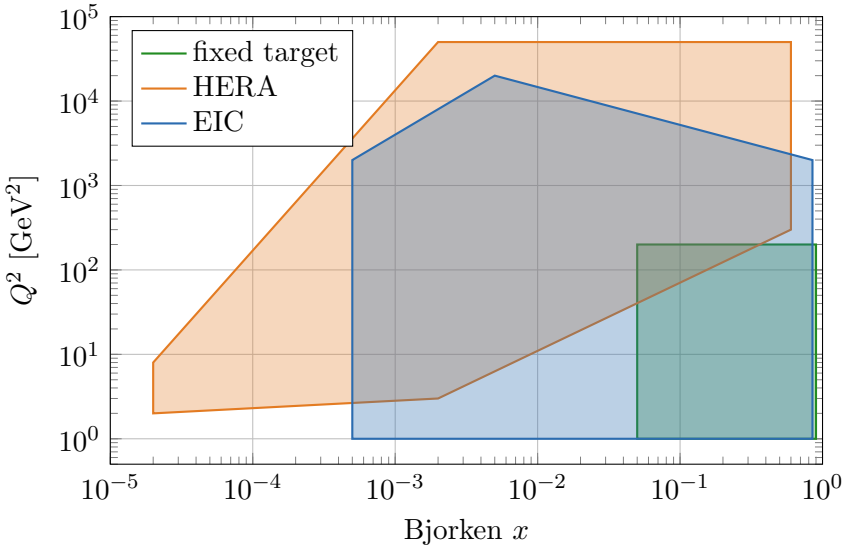


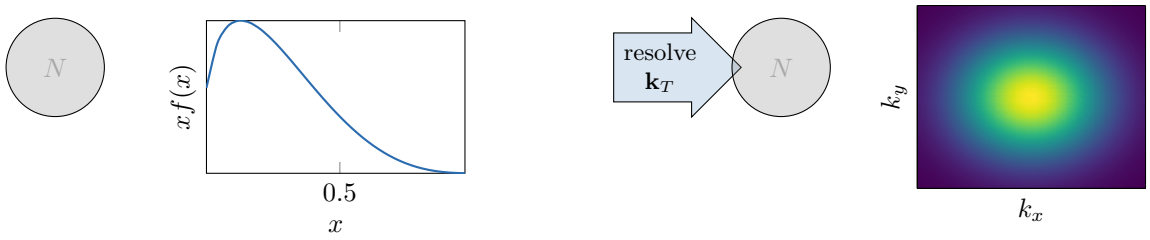

Figure 1.5: Schematic kinematic coverage in the $(x, Q^2)$ plane for the Electron–Ion Collider compared with fixed-target experiments and HERA. The EIC bridges the high-$x$ valence region and the low-$x$ sea/gluon region with high luminosity, enabling multidimensional imaging of the nucleon. Boundaries are indicative; cf. the EIC Yellow Report [39].

polarised electron and ion beams [12, 39]. Figure 1.5 shows, schematically, the kinematic reach in the $(x, Q^2)$ plane: the EIC bridges the high-$x$ valence region explored by fixed-target experiments and the low-$x$ sea- and gluon-dominated region opened by HERA, with the luminosity and polarisation needed for differential, multidimensional measurements.

The central goal is *nucleon tomography*, that is, the high-resolution, multidimensional imaging of the quark and gluon content of nucleons and nuclei (Figure 1.6). Where inclusive DIS yields the one-dimensional longitudinal distributions $f(x)$, SIDIS, by resolving the parton transverse momentum, grants access to transverse-momentum-dependent distributions (TMDs),

$$f_{i/N}(x, \boldsymbol{k}_T; \mu, \zeta), \qquad D_{h/i}(z, \boldsymbol{p}_T; \mu, \zeta), \tag{1.12}$$

which encode the correlation between a parton's longitudinal momentum, its transverse momentum, and the nucleon spin. These objects underlie a phenomenology of azimuthal and spin asymmetries, namely the Sivers, Boer–Mulders, transversity and Collins effects,




inclusive DIS:
1D longitudinal $f(x)$

SIDIS: 3D imaging $f(x, \mathbf{k}_T)$

Figure 1.6: From one-dimensional to three-dimensional nucleon structure. Inclusive DIS yields the longitudinal momentum distribution $f(x)$; SIDIS, sensitive to the parton transverse momentum $\mathbf{k}_T$, enables a tomographic image $f(x, \mathbf{k}_T)$ of the nucleon in momentum space, a central goal of the EIC.

which the EIC will measure with high precision [40, 11]. (Generalised parton distributions, accessed in exclusive processes, provide the complementary spatial imaging; they are not the subject of this thesis.)

These two descriptions form a single picture of the nucleon viewed at different transverse scales. TMD factorisation applies in the regime of small hadron transverse momentum, with the hierarchy $P_{hT} \ll Q$; collinear factorisation, used in the bulk of this thesis, applies after integration over transverse momentum or at $P_{hT} \sim Q$. They are not competing theories but complementary frameworks, joined by matching relations. The high-precision collinear coefficient functions to which this thesis contributes are therefore not confined to the high-$P_{hT}$ regime. They are an ingredient of the matching that bridges both regimes, and hence of the full EIC tomography programme.

## 1.6 Factorisation and higher-order QCD

Perturbative QCD phenomenology [11, 41, 42, 43, 44, 45, 46, 47] rests on the *separation of scales*. When the hard scale $Q$ is far above the confinement scale, $Q \gg \Lambda_{\mathrm{QCD}}$, the short-distance dynamics of the partonic hard scattering decouple from the long-distance dynamics of hadron binding and formation. The factorisation theorem makes this decoupling precise: it writes the cross section as a convolution of a perturbatively calculable hard kernel with non-perturbative distributions, the two being separated at an arbitrary factorisation scale $\mu_F$ (Figure 1.7). Physics above $\mu_F$ is absorbed into the hard kernel and computed order by order in $\alpha_s$; physics below $\mu_F$ is absorbed into the distributions and measured. The independence of any physical observable from the choice of $\mu_F$ is what the DGLAP evolution equations enforce.

A key property of this construction is *universality*. The parton distributions and fragmentation functions are properties of the nucleon and of the hadronisation process, not of the particular hard process in which they are measured. Once extracted, for instance from a global fit to DIS and $e^+e^-$ data, they may be used to predict any other process, with only the hard kernel changing. This predictive transfer is the basis of collider phenomenology, and it requires the precise, process-by-process computation of the hard coefficient functions. It is to those coefficient functions that this thesis contributes.

For SIDIS in collinear factorisation, the (semi-inclusive) structure functions take the

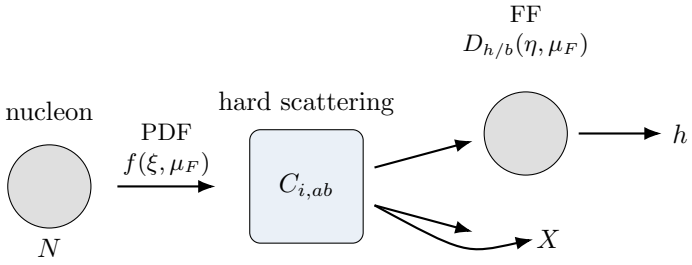



Figure 1.7: The factorisation of SIDIS into long- and short-distance physics. At the hard scale $Q \gg \Lambda_{\mathrm{QCD}}$ the nucleon is resolved into partons described by a (universal) parton distribution $f(\xi, \mu_F)$; these undergo the perturbatively calculable hard scattering $C_{i,ab}$; and the outgoing parton fragments into the observed hadron through a (universal) fragmentation function $D_{h/b}(\eta, \mu_F)$. The factorisation scale $\mu_F$ marks the boundary between the two regimes.

schematic form

$$\widetilde{F}_i(x, z, Q^2) = \sum_{a,b} f_{a/N}(\xi, \mu_F) \otimes C_{i,ab}\Big(\tfrac{x}{\xi}, \tfrac{z}{\eta}, Q^2, \mu_F, \mu_R\Big) \otimes D_{h/b}(\eta, \mu_F), \tag{1.13}$$

a double convolution of a PDF, a fragmentation function, and a partonic coefficient function $C_{i,ab}$. The coefficient functions are the perturbatively calculable hard kernels,

$$C_{i,ab} = C^{(0)}_{i,ab} + \frac{\alpha_s}{2\pi} C^{(1)}_{i,ab} + \left(\frac{\alpha_s}{2\pi}\right)^2 C^{(2)}_{i,ab} + \cdots, \tag{1.14}$$

and it is these that connect measured cross sections to the distributions one wishes to extract.

The state of the art reflects the difficulty of the calculation. The analogous coefficient functions are known to next-to-next-to-leading order (NNLO) for $e^+e^-$ annihilation and to next-to-leading order (NLO) for hadron–hadron collisions. For SIDIS the NLO coefficient functions have long been available, and the NNLO coefficient functions have only recently been computed [35], in parallel by independent groups, with threshold-enhanced resummed results also available. The phase-space integrals evaluated in this thesis are ingredients of this NNLO SIDIS calculation.

Why is NNLO necessary? Successive orders reduce the dependence on the unphysical factorisation and renormalisation scales, and the residual scale variation is the standard proxy for the theoretical uncertainty. Figure 1.8 sketches the expected pattern, in which the central prediction stabilises and the uncertainty band narrows from LO to NLO to NNLO. To match the percent-level precision targeted at the EIC, and to extract fragmentation functions and related quantities without theory-dominated errors, control through NNLO is required.

Moreover, at each order the infrared singularities of the real and virtual contributions cancel only when both are included. I now make this structural necessity precise.

## 1.7 Electroweak and mixed QCD–electroweak corrections

At the precision of the EIC, the perturbative expansion in $\alpha_s$ is not the whole story. Electromagnetic and weak effects enter through QED radiation off the leptonic and hadronic lines, through genuine weak loops, and through the interference of photon and $Z$ exchange;

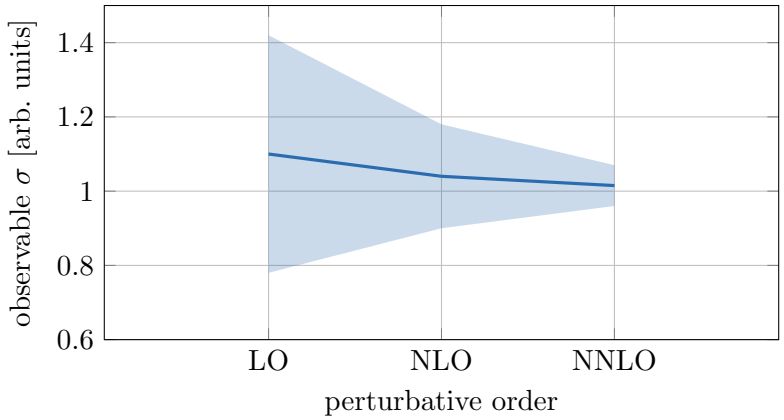



Figure 1.8: Schematic convergence of a perturbative prediction: the central value (solid) stabilises and the scale-variation uncertainty band (shaded) narrows from LO to NLO to NNLO. Matching the percent-level precision targeted at the EIC requires control through (at least) NNLO.

at higher $Q^2$ the neutral- and charged-current channels must be treated together. A useful bookkeeping organises the structure functions in a double expansion,

$$F_i = F_i^{(0,0)} + \frac{\alpha}{\pi} F_i^{(1,0)} + \frac{\alpha_s}{\pi} F_i^{(0,1)} + \frac{\alpha}{\pi}\frac{\alpha_s}{\pi} F_i^{(1,1)} + \cdots , \tag{1.15}$$

in which the mixed $\mathcal{O}(\alpha\alpha_s)$ term is the first place where the strong and electroweak corrections genuinely interfere. The consistent inclusion of these effects requires the renormalisation of the electroweak sector: the definition of the couplings, masses, and mixing angle, the treatment of $\gamma_5$ in dimensional regularisation, and the cancellation of ultraviolet poles by counterterms [48].

The $\gamma qq$ vertex provides the relevant building block. Its general decomposition involves vector and axial form factors,

$$\Gamma^\mu = -ig_V \Big[ F_1\, \gamma^\mu + \frac{i}{2m} F_2\, \sigma^{\mu\nu} q_\nu \Big] + g_A \Big[ G_1\, \gamma^\mu \gamma_5 + \frac{1}{2m} G_2\, q^\mu \gamma_5 \Big], \tag{1.16}$$

which simplifies for massless external quarks. In this thesis the electroweak strand is developed only at the level of *renormalisation ingredients*, namely the form factors and the on-shell counterterms of the $\gamma qq$ vertex at $\mathcal{O}(\alpha)$ and $\mathcal{O}(\alpha\alpha_s)$, summarised in Chapter 8. I do *not* claim a complete mixed QCD–electroweak SIDIS prediction; assembling one is identified as future work in Chapter 9.

## 1.8 The ubiquity of infrared divergences

Before stating the computational problem I describe the obstacle that pervades it [49, 50, 51, 52, 53, 54]. When massless partons are involved, individual perturbative contributions to a cross section are afflicted by *infrared* (IR) singularities, of two physical origins. A *soft* singularity arises when an emitted gluon carries vanishing energy; a *collinear* singularity arises when a massless parton is emitted exactly parallel to another. In both limits an extra emission becomes *unresolvable*: the final state with the soft or collinear parton is physically indistinguishable, by any finite-resolution detector, from the state without it. In dimensional regularisation, $d = 4 - 2\epsilon$, these singularities appear as poles in $\epsilon$, up to

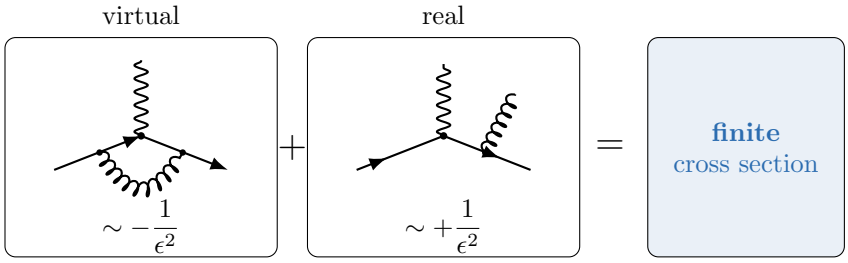



Figure 1.9: The cancellation of infrared singularities. The virtual correction and the real-emission contribution are each separately divergent in $d = 4 - 2\epsilon$, with poles of opposite sign; by the Kinoshita–Lee–Nauenberg theorem the poles cancel in a sufficiently inclusive sum, leaving a finite cross section. This cancellation makes the double-real part inseparable from the virtual parts.

$1/\epsilon^2$ per loop or emission at one order, one factor for the soft and one for the collinear limit.

That such poles appear in separate pieces is not a pathology but a reflection of a degeneracy of physical states, and the resolution is the content of the Kinoshita–Lee–Nauenberg (KLN) theorem [50, 51], together with the older Bloch–Nordsieck argument [55]: for a *sufficiently inclusive* observable, in which one sums over the degenerate soft and collinear final states, the singularities cancel. Specifically, the virtual correction (an extra parton in a loop, then reabsorbed) and the real correction (the same parton emitted into the final state) carry IR poles of opposite sign, and their sum is finite (Figure 1.9). Initial-state collinear singularities, which do not cancel this way, are instead absorbed into the parton distributions by mass factorisation, the same renormalisation that gives rise to DGLAP evolution.

This cancellation has a structural consequence for the present work: *the real-emission contribution cannot be computed or even defined in isolation from the virtual one.* Its $1/\epsilon$ poles are physical and must be retained, in analytic form, to all the orders in $\epsilon$ at which they cancel against the virtual poles. An analytic, pole-by-pole control of the real-radiation phase-space integrals is therefore required, and providing it is the purpose of this thesis.

## 1.9 The language of higher-order corrections

One more ingredient must be introduced, because it determines the mathematical character of the results. The loop and phase-space integrals of perturbative QCD do not, in general, evaluate to elementary functions. As the number of loops, legs, and scales grows, the answers populate an ascending hierarchy of *special functions*: ordinary logarithms at the lowest level, then the classical polylogarithms $\mathrm{Li}_n$, then their multi-variable generalisations, the Goncharov, or multiple, polylogarithms (MPLs), and, beyond the reach of these, elliptic polylogarithms and functions associated with higher-genus geometries. Identifying the function class of a given integral, and computing it within that class, is a central activity of modern higher-order calculations. The angular phase-space integrals studied in this thesis turn out to live in the polylogarithmic class. A recurring question, taken up in the outlook, is exactly where the boundary to elliptic generalisations lies. Chapter 3 develops the required mathematics from the ground up.

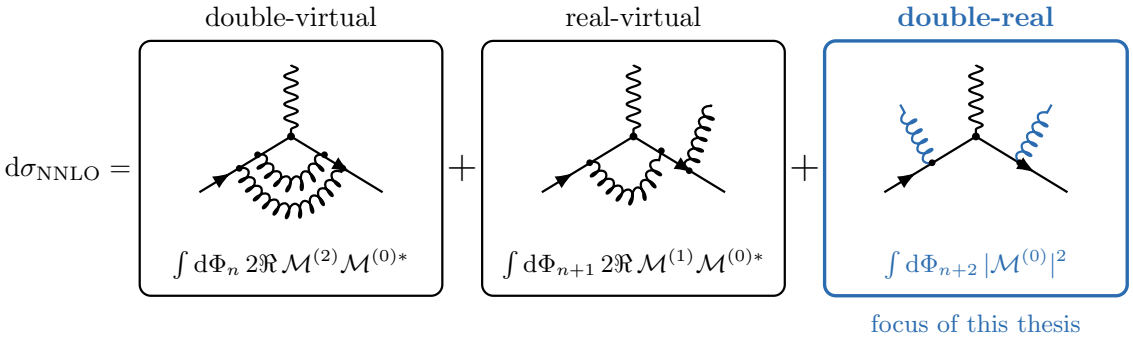



Figure 1.10: The three contributions to an NNLO cross section: the double-virtual term with two virtual gluon corrections to the photon–quark vertex, the real–virtual term with one virtual gluon correction and one real gluon emission, and the double-real term with two real gluon emissions and no virtual correction. Each contribution is separately infrared divergent in $d = 4 - 2\epsilon$, but the poles cancel in the sum.

## 1.10 The computational bottleneck: real radiation

I can now state the technical problem. At NNLO a cross section is the sum of three separately divergent pieces (Figure 1.10),

$$\mathrm{d}\sigma_{\mathrm{NNLO}} = \mathrm{d}\sigma_{\mathrm{VV}} + \mathrm{d}\sigma_{\mathrm{RV}} + \mathrm{d}\sigma_{\mathrm{RR}}, \tag{1.17}$$

the double-virtual (VV, two loops, no extra emission), the real–virtual (RV, one loop and one emission), and the double-real (RR, two emissions). As discussed in Section 1.8, each is separately afflicted by soft and collinear poles in $\epsilon$, which cancel only in the sum. A complete prediction therefore requires all three pieces, computed consistently to the same order in $\epsilon$.

The three pieces are, however, very unequally developed. The virtual contributions (VV, RV) are loop integrals, for which a mature analytic technology exists: integration-by-parts (IBP) reduction [56, 57, 58], the method of differential equations [59, 60, 61], and a detailed understanding of the polylogarithmic functions in which the answers are expressed. The double-real contribution,

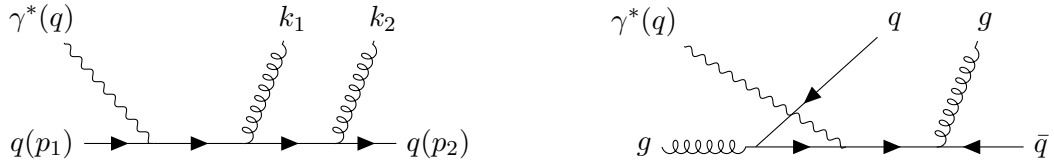
$$\mathrm{d}\sigma_{\mathrm{RR}} \sim \int \mathrm{d}\Phi_{n+2} \, |\mathcal{M}^{(0)}_{n+2}|^2, \tag{1.18}$$

is instead a multifold integral over the phase space of the unresolved partons (Figure 1.11), and its analytic evaluation has received far less attention. It is usually done numerically. This is the bottleneck the thesis addresses.

The method that makes the real part tractable is reverse unitarity [62]. The on-shell phase-space delta function is the discontinuity of a propagator,

$$\delta_+(p^2) \;\longleftrightarrow\; \frac{1}{2\pi i}\Big(\frac{1}{p^2 - i0} - \frac{1}{p^2 + i0}\Big), \tag{1.19}$$

so that a phase-space integral becomes a cut loop integral, and the full loop technology, in particular IBP reduction to master integrals, becomes available for the real part as well. For SIDIS the additional measurement of the fragmenting parton imposes an extra




(a) quark-initiated, $\gamma^* q \to q\, g\, g$ (b) gluon-initiated, $\gamma^* g \to q\, \bar{q}\, g$

Figure 1.11: Representative double-real-emission contributions to the NNLO partonic cross section: (a) the quark-initiated channel and (b) one of the gluon-initiated channels. In each case two extra partons are radiated relative to the Born process, and the analytic evaluation of the phase-space integral over their momenta is the central problem addressed in this thesis.

constraint on the three-particle phase space,

$$[\mathrm{d}PS_3]_{z'} = \mathrm{d}PS_3\, \delta\Big(z' - \frac{p_1 \cdot p_2}{p_1 \cdot q}\Big), \tag{1.20}$$

which in full reads

$$[\mathrm{d}PS_3]_{z'} = \frac{\mathrm{d}^d k_1\, \mathrm{d}^d k_2\, \mathrm{d}^d p_2}{(2\pi)^{3d-3}}\, \delta_+(k_1^2)\delta_+(k_2^2)\delta_+(p_2^2)\, (2\pi)^d \delta^{(d)}(p_2+k_1+k_2-p_1-q)\, \delta\Big(z' - \frac{p_1 \cdot p_2}{p_1 \cdot q}\Big). \tag{1.21}$$

This tagging delta function is what distinguishes SIDIS from inclusive DIS and what makes the phase-space integrals hard. After reverse unitarity and IBP reduction, the NNLO SIDIS double-real contribution reduces to twenty master integrals organised into thirteen families [35], which are the central objects evaluated in this thesis.

### 1.10.1 Methods for NNLO real radiation: where this thesis fits

The difficulty of the real-radiation integrals has driven two decades of methodological development [63, 64, 65, 66, 67, 68, 69, 70, 71], and it is useful to situate the present approach within it. The dominant strategy is *subtraction*: one constructs local counterterms that reproduce the soft and collinear singularities of the real-emission matrix elements pointwise, renders the subtracted real contribution finite and integrable in four dimensions, and adds back the analytically integrated counterterms. The mature NNLO realisations of this idea, namely antenna subtraction [72], the sector-improved residue (STRIPPER) scheme [73], the Somogyi–Trócsányi–Del Duca / CoLoRFulNNLO construction [74, 75], and local analytic sector subtraction [76], differ in how they parametrise and integrate the unresolved regions, but all ultimately require analytic control of integrals over the single- and double-unresolved phase space. A second strategy is *slicing*: a resolution variable such as transverse momentum [77] or $N$-jettiness [78, 79] separates the singular region, where the cross section is known from a factorisation theorem, from a finite remainder, and the projection-to-Born method [80] is a related device. Underlying every analytic variant, finally, is sector decomposition [81], which remains the standard *numerical* fallback when closed forms are unavailable.

What unites these methods, and what makes the present work relevant to all of them, is that their integrated counterterms and factorised ingredients are built from the same elementary object: the angular integral over the direction of an unresolved parton, weighted by eikonal denominators. This object has a long history. The two-denominator massless and massive cases were given in closed form by van Neerven [82], and the systematic $d$-

dimensional treatment of the single- and two-denominator families is due to Somogyi [83]. The thesis takes up this lineage at the point where it had stalled, the three- and four-denominator families with general masses, and supplies them analytically through the Mellin–Barnes-to-polylogarithm method. Because the angular integrals are process- and scheme-independent, the results are not tied to SIDIS or to any one subtraction formalism. They are reusable infrastructure for whichever of the methods above a given calculation employs. Reverse unitarity [62], which converts the tagged SIDIS phase space into cut loop integrals amenable to IBP reduction, connects this analytic angular technology to a realistic NNLO observable.

## 1.11 This thesis: idea, contributions, and outline

**The idea:** Rather than solving the real-radiation master integrals by differential equations, we exploit a structural simplification. In a suitable frame the phase-space integral factorises into a *radial* part, which is process-dependent, and an *angular* part, which is universal. The angular integrals,

$$\Omega_{j_1,\ldots,j_n} = \int \mathrm{d}\Omega_{d-1}(\hat{q}) \prod_{r=1}^{n} \frac{1}{(p_r \cdot \hat{q})^{j_r}}, \tag{1.22}$$

recur unchanged across many processes, and their singularity structure is already transparent at the master-integral level. We evaluate them analytically through their Mellin–Barnes representation, built from the elementary splitting identity

$$\frac{1}{(A+B)^{\lambda}} = \frac{1}{\Gamma(\lambda)} \int_{-i\infty}^{+i\infty} \frac{\mathrm{d}z}{2\pi i}\, \Gamma(-z)\Gamma(\lambda+z)\, \frac{A^z}{B^{\lambda+z}}, \tag{1.23}$$

and convert them, through a chain of exact steps developed in Chapters 3 and 4, into Goncharov polylogarithms. The universal angular results are then recombined with the radial part through a single one-fold integration, with a dedicated procedure to disentangle the soft and collinear singularities.

**Contributions:** The original results of this thesis, obtained in collaboration as recorded in the List of Publications, are:

1. a systematic Mellin–Barnes-to-polylogarithm method for angular phase-space integrals (Chapters 3 and 4);
2. the first analytic evaluation of the three-denominator angular families, massless to $\mathcal{O}(\epsilon^2)$ and single-massive to $\mathcal{O}(\epsilon)$, with partial-fraction and recursion relations (Chapter 5);
3. the first analytic evaluation of the four-denominator angular families, with their seventeen- and eleven-letter alphabets and the partial-fraction construction for the multi-massive cases (Chapter 5);
4. the radial–angular evaluation of the NNLO SIDIS master integrals, cross-checked against an independent differential-equation computation, together with a systematic resolution of the soft and collinear singularities of the radial integration (Chapter 7);

Table 1.1: The publications underlying the thesis and the chapters that develop them.

| Publication | Content | Chapters |
|---|---|---|
| arXiv:2410.18886 | Three-denominator angular integrals (MB) | 4, 5 |
| arXiv:2508.15952 | Four-denominator angular integrals (MB) | 4, 5 |
| arXiv:2412.16509 | NNLO SIDIS phase-space master integrals | 6, 7 |

5. a complete validation of all results, and the electroweak-renormalisation ingredients toward a future mixed QCD–electroweak treatment ( Chapter 8).

The publications underlying these results, and the chapters that develop them, are listed in Table 1.1.

**Outline:** The thesis is organised so that the physical setup precedes the mathematics, which in turn precedes the results and their validation. Chapter 2 develops reverse unitarity and the radial–angular decomposition and defines the angular integrals. Chapter 3 is a self-contained account of Mellin–Barnes integrals and Goncharov polylogarithms, built around a single running example. Chapter 4 formulates the general method and contrasts it with the differential-equation route. Chapter 5 presents the core new results: the three- and four-denominator families, their alphabets, and the partial-fraction and recursion relations. Chapter 6 introduces SIDIS and its role at the EIC, and Chapter 7 applies the method to the NNLO SIDIS master integrals and the resolution of their singularities. Chapter 8 develops the electroweak-renormalisation ingredients. Chapter 9 summarises the achievements and discusses the open frontiers: the five-denominator integrals and the question of elliptic generalisations, the automation of the method, and the assembly of complete physical observables.

# Part I

# Angular Phase-Space Infrastructure for Real Radiation

# Chapter 2

# Reverse Unitarity, Differential Equations and the Radial–Angular Decomposition

## Contents

2.1 From cross sections to angular building blocks . . . 17
2.2 Cross sections and phase space . . . 18
2.3 The optical theorem and cut phase space . . . 18
2.4 Reverse unitarity and cut propagators . . . 19
2.5 IBP identities and the reduction to master integrals . . . 20
2.6 Differential Equations for Feynman Integrals . . . 21
2.7 The radial–angular factorisation . . . 28
2.8 The Somogyi and van Neerven representations . . . 29
2.9 Classification of the angular integrals . . . 30
2.10 Worked example: the single massless denominator . . . 31
2.11 Conventions and notation . . . 32

## 2.1 From cross sections to angular building blocks

Chapter 1 ended at a precise technical demand: the double-real contribution to an NNLO cross section is a multifold phase-space integral whose analytic evaluation is the bottleneck of the calculation. The strategy of this thesis is to transform such an intractable, process-specific integral into a sum of products of two far simpler objects, a process-dependent but one-dimensional *radial* integral, and a process-independent, reusable *angular* building block. Everything in this chapter serves that factorisation.

The chain of reductions that achieves it is shown in Figure 2.1: reverse unitarity [62] rewrites the phase-space integral as a cut loop integral; integration-by-parts (IBP) reduction expresses it through a finite set of master integrals; and a decomposition into radial and angular parts isolates the angular integrals $\Omega_{j_1,\dots,j_n}$ [83, 84]. This is a *bottom-up* strategy, complementary to the more common *top-down* route in which each master integral is solved as a whole by differential equations [61]. Rather than solving the masters directly, we isolate the universal angular structures common to many of them and to many




Figure 2.1: The chain of reductions developed in this chapter. Reverse unitarity turns the real-radiation phase-space integrals into cut loop integrals; IBP reduction expresses these through a finite set of master integrals; and the radial–angular decomposition isolates the process-independent angular integrals $\Omega_{j_1,\ldots,j_n}$ that are the subject of the rest of the thesis.

processes, and compute those once and for all. Throughout this and the following three chapters I work in $d = 4 - 2\epsilon$ dimensions.

## 2.2 Cross sections and phase space

A hadronic cross section [85, 86] is built from squared amplitudes integrated over the final-state phase space. For a partonic process $a\,b \to n$ with momenta $p_1, \ldots, p_n$,

$$\mathrm{d}\sigma_n = \frac{1}{2\lambda^{1/2}(s, m_a^2, m_b^2)} \frac{1}{S_n} \sum_{\text{spins, colours}} |\mathcal{M}_{ab\to n}|^2 \,\mathrm{d}\Phi_n, \tag{2.1}$$

with $\lambda$ the Källén function and $S_n$ the symmetry factor for identical final-state particles. For massless incoming partons, the case of interest, the flux simplifies to $2\lambda^{1/2} \to 2s$. The $n$-particle Lorentz-invariant phase space in $d$ dimensions is

$$\mathrm{d}\Phi_n(P; p_1, \ldots, p_n) = (2\pi)^d\, \delta^{(d)}\Big(P - \sum_{i=1}^{n} p_i\Big) \prod_{i=1}^{n} \frac{\mathrm{d}^d p_i}{(2\pi)^{d-1}}\, \delta_+(p_i^2 - m_i^2), \tag{2.2}$$

where $\delta_+(p_i^2 - m_i^2) = \delta(p_i^2 - m_i^2)\,\theta(p_i^0)$ enforces both the on-shell condition and positive energy. Integrating the energy component against the delta function gives the familiar three-momentum measure,

$$\mathrm{d}^d p\, \delta_+(p^2 - m^2) = \frac{\mathrm{d}^{d-1}\mathbf{p}}{2E_{\mathbf{p}}}, \qquad E_{\mathbf{p}} = \sqrt{\mathbf{p}^2 + m^2}. \tag{2.3}$$

The difficulty at higher orders is not this measure as such but the proliferation of scalar products $p_i \cdot p_j$ in the squared matrix element, which turn $\mathrm{d}\Phi_n$ into a non-trivial multidimensional integral. Loop-integral technology becomes indispensable at this point.

## 2.3 The optical theorem and cut phase space

The link between phase-space integrals and loop integrals is unitarity [87, 88]. Writing $S = 1 + iT$, the unitarity condition $S^\dagger S = 1$ gives

$$-i\,(T - T^\dagger) = T^\dagger T, \tag{2.4}$$

and, taking the matrix element between identical states $|i\rangle$ and inserting a complete set of intermediate states,

$$2\,\mathrm{Im}\,\langle i|T|i\rangle = \sum_X \int \mathrm{d}\Phi_X\, \langle i|T^\dagger|X\rangle\langle X|T|i\rangle. \tag{2.5}$$

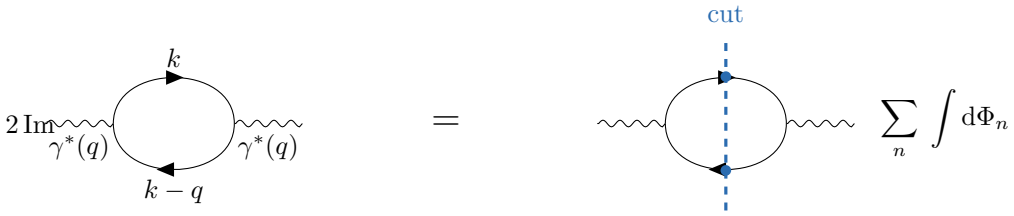



Figure 2.2: The optical theorem underlying reverse unitarity: the imaginary part of a forward-scattering amplitude (left) equals the sum over on-shell intermediate states, obtained by cutting the diagram (right), which is a phase-space integral. Reverse unitarity inverts this relation, treating each on-shell delta function as a cut propagator so that the phase-space integral can be manipulated with loop-integral technology.

The right-hand side is a sum over on-shell intermediate states, a phase-space integral, while the left-hand side is the imaginary part of a forward amplitude, a loop integral. The total cross section is the optical-theorem special case $\sigma_{\text{tot}} = \text{flux}^{-1}\, 2\,\text{Im}\,\mathcal{M}^{\text{forward}}_{i\to i}$. Applied not only to forward matrix elements but to general ones, the same unitarity condition $S^\dagger S = 1$ yields the Cutkosky cutting rules [89], which equate the discontinuity of a diagram across a given channel to the diagram with the channel's lines put on shell. Figure 2.2 depicts the identity: cutting a forward diagram through its intermediate lines puts them on shell and produces the phase-space integral.

The bridge in the other direction rests on the distributional identity

$$\frac{1}{x \pm i0} = \mathcal{P}\,\frac{1}{x} \mp i\pi\,\delta(x), \tag{2.6}$$

which rearranges to express the delta function as a discontinuity,

$$\delta(x) = \frac{1}{2\pi i}\Big(\frac{1}{x - i0} - \frac{1}{x + i0}\Big). \tag{2.7}$$

This is the seed of reverse unitarity [89, 62].

## 2.4 Reverse unitarity and cut propagators

Reverse unitarity [90, 62, 91] promotes (2.7) into a calculational device. Define the *cut propagator*

$$\Big[\frac{1}{D^a}\Big]_c \equiv \frac{1}{2\pi i}\Big[\frac{1}{(D - i0)^a} - \frac{1}{(D + i0)^a}\Big], \tag{2.8}$$

so that, by (2.7), for $a = 1$ one has $[1/D]_c = \delta(D)$, the positive-energy restriction $\delta_+$ being supplied by the physical momentum routing. For higher powers,

$$\Big[\frac{1}{D^a}\Big]_c = \frac{(-1)^{a-1}}{(a-1)!}\,\delta^{(a-1)}(D), \tag{2.9}$$

a derivative of the delta function. Each on-shell constraint in (2.2) is therefore a cut propagator, and a phase-space integral becomes a loop integral with some lines cut. For the simplest case of one massless emission against a massive system,

$$\int \mathrm{d}^d k\,\delta_+(k^2)\,\delta_+\big((P-k)^2 - Q^2\big) \;\longrightarrow\; \int \mathrm{d}^d k\,\Big[\frac{1}{k^2}\Big]_c\Big[\frac{1}{(P-k)^2 - Q^2}\Big]_c. \tag{2.10}$$

The crucial point, a subtlety that must be respected throughout, is how cut propagators behave under the algebraic manipulations that follow. They are *differentiated like ordinary propagators*,

$$\frac{\partial}{\partial k^\mu}\Big[\frac{1}{D^a}\Big]_c = -a\,\frac{\partial D}{\partial k^\mu}\Big[\frac{1}{D^{a+1}}\Big]_c, \tag{2.11}$$

and a propagator power may be raised or lowered by multiplying or cancelling factors of $D$,

$$D\,\Big[\frac{1}{D^a}\Big]_c = \Big[\frac{1}{D^{a-1}}\Big]_c. \tag{2.12}$$

However, cancelling the *last* factor would set $a = 0$, and a cut line with non-positive power is not an uncut line: it is the removal of the cut. Therefore

$$\boxed{\Big[\frac{1}{D^0}\Big]_c = 0.} \tag{2.13}$$

Operationally, this prunes the IBP system: whenever a generated relation contains an integral in which one of the *required* phase-space cuts has been cancelled to non-positive power, that integral is set to zero *within the relation*. This single rule keeps the cut family closed under IBP and distinguishes the reverse-unitarity calculus from an ordinary loop calculation.

## 2.5 IBP identities and the reduction to master integrals

With phase-space integrals recast as cut loop integrals, the full reduction machinery applies [57, 56, 58, 92, 93, 94, 95, 96]. An integral family is the set

$$I(\vec{a}) = \int \prod_{r=1}^{L} \mathrm{d}^d\ell_r \prod_{i\notin C} \frac{1}{D_i^{a_i}} \prod_{c\in C} \Big[\frac{1}{D_c^{a_c}}\Big]_c, \tag{2.14}$$

labelled by the integer powers $\vec{a} = (a_1, \ldots, a_N)$, with $C$ the set of cut lines. Integration-by-parts identities follow from the vanishing of a total derivative in dimensional regularisation,

$$0 = \int \prod_{r=1}^{L} \mathrm{d}^d\ell_r \,\frac{\partial}{\partial \ell_i^\mu}\Big[v^\mu \prod_{j\notin C} D_j^{-a_j} \prod_{c\in C} \big(D_c^{-a_c}\big)_c\Big], \tag{2.15}$$

for any loop or external vector $v^\mu$. Expanding the derivative produces linear relations among integrals with shifted powers,

$$0 = \sum_{\vec{b}} c_{\vec{b}}(d, s_{ij})\, I(\vec{b}), \tag{2.16}$$

with coefficients rational in $d$ and the kinematic invariants $s_{ij}$. Solving the (large, sparse) linear system by the Laporta algorithm [58] expresses every integral of the family through a finite basis of master integrals,

$$I(\vec{a}) = \sum_{m=1}^{N_{\mathrm{MI}}} r_m(\vec{a}; d, s_{ij})\, M_m, \tag{2.17}$$

as illustrated schematically in Figure 2.3. To see how a single such relation arises, take the one-loop massive bubble with one cut line, $I(a_1, a_2) = \int \mathrm{d}^d k\,[1/(k^2)]_c\,(1/((k-P)^2-Q^2)^{a_2})$,

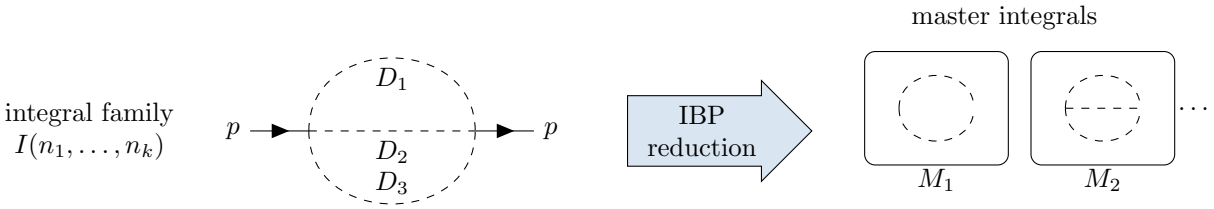



Figure 2.3: Integration-by-parts (IBP) reduction. Every integral of a given family—a fixed topology with propagators $D_i$ raised to arbitrary integer powers $n_i$—is expressed, through the linear relations following from the vanishing of total derivatives in dimensional regularisation, as a combination of a finite basis of master integrals $M_k$. For cut (phase-space) integrals the same relations hold, with the constraint that a cut propagator cannot be cancelled against a numerator.

and apply the operator $\partial_{k^\mu} k^\mu$ inside the integral. Using $\partial_{k^\mu} k^\mu = d$ and $k^\mu \partial_{k^\mu} (k^2)^0 = 0$, $k^\mu \partial_{k^\mu} ((k-P)^2 - Q^2) = 2k^2 - 2k\cdot P = (k^2) + \big((k-P)^2 - Q^2\big) + (Q^2 - P^2)$, the vanishing of the total derivative gives, after expressing the dot products through the denominators,

$$0 = \big(d - 2a_2\big) I(1, a_2) - a_2 \,(Q^2 - P^2)\, I(1, a_2 + 1) + a_2\, I(0, a_2 + 1), \tag{2.18}$$

and the last term vanishes by the cut-propagator rule $[1/(k^2)^0]_c = 0$. The relation thus lowers $a_2$ and, iterated, reduces the whole tower to the single master $I(1,1)$. In practice such reductions are automated with dedicated software [56, 57, 97, 98]; for the NNLO SIDIS application of Chapter 7 they yield twenty master integrals [35]. Two features specific to the cut case deserve emphasis: the cut-propagator rule of Section 2.4 removes from the basis any would-be master with a cancelled cut, and the measurement constraints that define a semi-inclusive observable enter as additional cut propagators, as we shall see for the SIDIS tagging delta function.

## 2.6 Differential Equations for Feynman Integrals

The evaluation of multi-loop Feynman integrals represents one of the principal challenges in perturbative quantum field theory. While the perturbative expansion of scattering amplitudes is conceptually straightforward, the complexity of the corresponding loop integrals increases rapidly with the number of loops, external legs and independent kinematic scales. Modern precision calculations in Quantum Chromodynamics (QCD) and the electroweak sector require the evaluation of thousands or even millions of scalar integrals after the reduction of tensor structures. Fortunately, these integrals are not independent. Owing to the existence of linear relations generated by integration-by-parts (IBP) identities, all integrals belonging to a given topology can be expressed in terms of a finite set of master integrals. Consequently, the determination of these master integrals constitutes the central problem in contemporary multi-loop calculations.

Several techniques have been developed for the evaluation of master integrals, including direct integration in Feynman parameters, Mellin–Barnes representations, sector decomposition, dimensional recurrence relations and difference equations. Among these methods, the differential equation approach [59, 60, 99, 61, 100, 101, 102] has proven to be one of the most powerful and systematic techniques for obtaining analytic results. Since its introduction by Kotikov [59] and its subsequent development by Remiddi and collaborators [60, 99], the method has become a standard tool in higher-order perturbative

calculations. Its success stems from the observation that Feynman integrals are smooth functions of the external kinematic invariants and internal masses. Rather than attempting to evaluate an integral directly, one instead studies its variation with respect to these parameters. The resulting differential equations encode the complete analytic information of the master integrals and often admit solutions in terms of generalized polylogarithms or, for more complicated integral families, elliptic and even more general classes of special functions.

The differential equation method is particularly attractive because it naturally complements the reduction of Feynman integrals through IBP identities. Once the reduction has been performed, the remaining task is to determine a finite-dimensional vector of master integrals. Differentiation with respect to an external invariant produces integrals belonging to the same family, which may again be reduced to the master basis using the same IBP relations. The original problem of evaluating complicated multidimensional integrals is therefore transformed into the solution of a coupled system of first-order differential equations. From the mathematical point of view, this represents a considerable simplification, since many powerful analytical techniques developed for ordinary differential equations become directly applicable. Moreover, the singularity structure of the differential equations reflects the physical singularities of the scattering process, making the analytic properties of the master integrals particularly transparent.

To illustrate the general framework, consider an $L$-loop family of scalar Feynman integrals defined by

$$I(\nu_1, \ldots, \nu_N) = \int \prod_{l=1}^{L} \frac{d^d k_l}{i\pi^{d/2}} \frac{1}{D_1^{\nu_1} D_2^{\nu_2} \cdots D_N^{\nu_N}}, \tag{2.19}$$

where the propagator denominators are given by

$$D_i = q_i^2 - m_i^2 + i0, \tag{2.20}$$

with $q_i$ denoting linear combinations of loop and external momenta. Throughout this chapter dimensional regularization is employed, so that the space-time dimension is taken to be

$$d = 4 - 2\epsilon. \tag{2.21}$$

The infinitesimal imaginary part appearing in the propagators specifies the causal prescription and determines the analytic continuation of the integrals across their branch cuts. The exponents $\nu_i$ are arbitrary integers, allowing both higher powers of propagators and irreducible numerators to be incorporated into the same integral family.

The large number of scalar integrals generated in practical calculations is substantially reduced by exploiting integration-by-parts identities. These identities follow from the observation that, within dimensional regularization, total derivatives with respect to the loop momenta vanish,

$$\int \prod_{l=1}^{L} d^d k_l \, \frac{\partial}{\partial k_i^\mu} \left( v^\mu \frac{1}{D_1^{\nu_1} \cdots D_N^{\nu_N}} \right) = 0, \tag{2.22}$$

where $v^\mu$ may be chosen as either a loop momentum or an external momentum. Since the surface terms vanish in dimensional regularization, Eq. (2.22) generates a large system of linear relations among integrals belonging to the same topology. Solving these relations using algorithms such as the Laporta algorithm makes it possible to express every integral

of the family as a linear combination of a finite number of master integrals,

$$I_i = \sum_{a=1}^{N_{\mathrm{MI}}} c_{ia}(\epsilon, \{s\}, \{m^2\})\, M_a, \tag{2.23}$$

where the coefficients $c_{ia}$ are rational functions of the dimensional regulator, the independent kinematic invariants and the internal masses. The entire problem of computing the scattering amplitude therefore reduces to determining the master integrals $M_a$.

The key observation underlying the differential equation method is that the master integrals depend continuously on the external kinematic variables. Let the independent variables be collectively denoted by

$$\mathbf{x} = (x_1, x_2, \ldots, x_n), \tag{2.24}$$

where each variable may represent a Mandelstam invariant, a momentum transfer or an internal mass. The master integrals can then be regarded as smooth functions

$$M_a = M_a(\mathbf{x}, \epsilon), \tag{2.25}$$

whose derivatives with respect to any of the kinematic variables may be evaluated by differentiating under the integral sign. For example,

$$\frac{\partial M_a}{\partial x_i} = \frac{\partial}{\partial x_i} \int \prod_{l=1}^{L} \frac{d^d k_l}{i\pi^{d/2}}\, \mathcal{I}_a, \tag{2.26}$$

where $\mathcal{I}_a$ denotes the corresponding loop integrand. Since differentiation acts only on the propagators and not on the integration measure, it commutes with the loop integration, leading to

$$\frac{\partial M_a}{\partial x_i} = \int \prod_{l=1}^{L} \frac{d^d k_l}{i\pi^{d/2}}\, \frac{\partial \mathcal{I}_a}{\partial x_i}. \tag{2.27}$$

The differentiated integrand generally contains propagators raised to higher powers together with additional scalar products originating from the differentiation. However, these new integrals still belong to the same integral family and may therefore be reduced using exactly the same IBP identities employed in the original reduction. Consequently, every derivative of a master integral can be expressed as a linear combination of the master integrals themselves,

$$\frac{\partial M_a}{\partial x_i} = \sum_{b=1}^{N_{\mathrm{MI}}} A^{(i)}_{ab}(\mathbf{x}, \epsilon)\, M_b, \tag{2.28}$$

where the coefficients $A^{(i)}_{ab}$ are rational functions of the kinematic variables and the dimensional regulator. Equation (2.28) constitutes the fundamental result upon which the differential equation method is based. Rather than attempting to evaluate each master integral independently, one instead determines the complete vector of master integrals by solving a finite system of coupled differential equations.

It is convenient to assemble the master integrals into the vector

$$\mathbf{M}(\mathbf{x},\epsilon) = \begin{pmatrix} M_1 \\ M_2 \\ \vdots \\ M_{N_{\mathrm{MI}}} \end{pmatrix}, \tag{2.29}$$

in terms of which the complete system assumes the compact matrix form

$$\frac{\partial}{\partial x_i}\mathbf{M} = A_i(\mathbf{x},\epsilon)\,\mathbf{M}, \tag{2.30}$$

where $A_i$ denotes an $N_{\mathrm{MI}} \times N_{\mathrm{MI}}$ matrix. This representation emphasizes that the master integrals form a vector-valued function on the space of kinematic variables, while the coefficient matrices describe how this vector evolves as the external parameters are varied. The analytic structure of the Feynman integrals is therefore encoded entirely in the properties of the matrices $A_i$, whose poles determine the singular hypersurfaces of the differential equations. The solution of Eq. (2.30), supplemented by appropriate boundary conditions, completely determines all master integrals belonging to the chosen integral family. As will be discussed in the following sections, the efficiency of the method depends crucially on the choice of the master basis. An appropriate basis transformation can dramatically simplify the structure of the differential equations, ultimately leading to the canonical form introduced by Henn [61], in which the dependence on the dimensional regulator factorizes and the iterative structure of the solution becomes manifest. The matrix form of Eq. (2.30) provides a convenient description of the complete system of differential equations satisfied by the master integrals. In the presence of several independent kinematic variables, the derivatives with respect to each variable define a corresponding matrix of rational functions. Denoting the independent variables by $x_1, \ldots, x_n$, the complete system may therefore be written as

$$\frac{\partial}{\partial x_i}\mathbf{M}(\mathbf{x},\epsilon) = A_i(\mathbf{x},\epsilon)\mathbf{M}(\mathbf{x},\epsilon), \qquad i = 1,\ldots,n, \tag{2.31}$$

where each matrix $A_i$ depends on the kinematic variables and on the dimensional regulator. The coefficient matrices are entirely determined by the IBP reduction and therefore inherit the analytic structure of the underlying Feynman integrals. Their matrix elements are rational functions of the external invariants and masses, while their poles coincide with the singular hypersurfaces of the corresponding Feynman graph. These singularities originate from physical thresholds, pseudo-thresholds and exceptional momentum configurations, and therefore reflect the Landau singularities of the underlying scattering process. Consequently, the differential equations not only provide a computational method for determining the master integrals but also encode important information about their analytic properties.

Since the master integrals are smooth functions of the independent variables away from their singular points, mixed partial derivatives must commute. This requirement imposes a non-trivial consistency condition on the coefficient matrices. Differentiating Eq. (2.31) first with respect to $x_i$ and subsequently with respect to $x_j$ yields

$$\frac{\partial^2 \mathbf{M}}{\partial x_i \partial x_j} = \frac{\partial A_i}{\partial x_j}\mathbf{M} + A_i \frac{\partial \mathbf{M}}{\partial x_j}, \tag{2.32}$$

while exchanging the order of differentiation gives

$$\frac{\partial^2 \mathbf{M}}{\partial x_j \partial x_i} = \frac{\partial A_j}{\partial x_i}\mathbf{M} + A_j \frac{\partial \mathbf{M}}{\partial x_i}. \tag{2.33}$$

Substituting Eq. (2.31) into the derivatives of the master integrals and requiring the equality of mixed derivatives leads to

$$\left(\frac{\partial A_i}{\partial x_j} - \frac{\partial A_j}{\partial x_i} + [A_i, A_j]\right)\mathbf{M} = 0, \tag{2.34}$$

where

$$[A_i, A_j] = A_i A_j - A_j A_i \tag{2.35}$$

denotes the matrix commutator. Since the master integrals are linearly independent, the coefficient multiplying the vector $\mathbf{M}$ must vanish identically, resulting in the integrability condition

$$\boxed{\frac{\partial A_i}{\partial x_j} - \frac{\partial A_j}{\partial x_i} + [A_i, A_j] = 0.} \tag{2.36}$$

Equation (2.36) is one of the fundamental consistency conditions satisfied by the differential equations. Mathematically, it expresses the vanishing of the curvature associated with the matrix-valued connection defined by the differential equations. Physically, it guarantees that the solution obtained by integrating the system does not depend on the particular path chosen in the space of kinematic variables, provided no singularity is crossed during the deformation of the integration contour. This property plays an important role in practical calculations, since it allows one to determine the master integrals by integrating along any convenient path connecting a boundary point to the desired kinematic configuration.

The singular structure of the coefficient matrices determines the analytic behaviour of the solutions. Since every matrix element is a rational function of the kinematic variables, one may write

$$A_i(\mathbf{x}, \epsilon) = \frac{P_i(\mathbf{x}, \epsilon)}{Q_i(\mathbf{x})}, \tag{2.37}$$

where $P_i$ and $Q_i$ denote polynomial matrices. The zeros of the denominator define the singular hypersurfaces of the differential equations. In the vicinity of such hypersurfaces the coefficient matrices develop poles whose residues govern the local behaviour of the solutions. For regular singular points the coefficient matrix admits the Laurent expansion

$$A(x) = \frac{R}{x - x_0} + A_0 + \mathcal{O}(x - x_0), \tag{2.38}$$

where $R$ is the residue matrix associated with the singular point $x = x_0$. The local behaviour of the master integrals then follows from the classical theory of linear differential equations. Introducing the ansatz

$$\mathbf{M}(x) = (x - x_0)^R \sum_{n=0}^{\infty} \mathbf{c}_n (x - x_0)^n, \tag{2.39}$$

one obtains a Frobenius expansion whose coefficients are determined recursively after substituting Eq. (2.39) into the differential equations. The eigenvalues of the residue ma-

trix determine the leading powers appearing in the local solution, while non-trivial Jordan blocks generate logarithmic contributions. This behaviour is familiar from many one-loop and multi-loop examples, where logarithms arise naturally at threshold singularities and branch points.

The differential equations determine the master integrals only up to integration constants, and therefore suitable boundary conditions must be supplied in order to obtain a unique solution. In practical applications the boundary point is usually chosen in a Euclidean region where all invariants are negative and the master integrals are real and free from physical branch cuts. Such kinematic configurations are particularly advantageous because they avoid threshold singularities and often permit either direct integration or asymptotic expansions. Alternative choices include soft limits, collinear limits or pseudo-thresholds at which the regularity of the master integrals provides sufficient information to determine the integration constants. The selection of an appropriate boundary point is therefore guided both by mathematical simplicity and by the analytic structure of the integral family under consideration.

Once the boundary conditions are known, the formal solution of the system may be written as a path-ordered exponential. Introducing an initial point $\mathbf{x}_0$ at which the vector of master integrals is known, the solution at any other point is formally given by

$$\mathbf{M}(\mathbf{x},\epsilon) = \mathcal{P}\exp\left(\int_\gamma A(\mathbf{x},\epsilon)\right)\mathbf{M}(\mathbf{x}_0,\epsilon), \tag{2.40}$$

where

$$A(\mathbf{x},\epsilon) = \sum_{i=1}^{n} A_i(\mathbf{x},\epsilon)\,dx_i \tag{2.41}$$

is the matrix-valued differential one-form and $\gamma$ denotes an arbitrary path connecting the initial and final kinematic points. The symbol $\mathcal{P}$ indicates path ordering, which is required because the coefficient matrices evaluated at different points generally do not commute. Although Eq. (2.40) provides a formally exact solution, it is not immediately useful for practical calculations owing to the complicated structure of the path-ordered exponential. The principal objective of modern developments in the differential equation method is therefore to perform a transformation of the master basis that simplifies the coefficient matrices as much as possible. In the most favourable situations this transformation converts the system into the canonical form introduced by Henn, where the dependence on the dimensional regulator factorizes completely and the path-ordered exponential reduces to an expansion in iterated integrals. This canonical representation will be developed in the following section and forms the foundation of most contemporary analytic calculations of multi-loop Feynman integrals. The matrix representation of the differential equations given in Eq. (2.30) is completely general and is valid for any choice of master integrals. However, this representation is by no means unique. Since the master integrals form a basis of the vector space generated by the integral family, any invertible linear transformation defines an equally valid set of master integrals. If the original basis is denoted by $\mathbf{M}$ and a new basis by $\mathbf{F}$, the two are related through

$$\mathbf{M} = T(\mathbf{x},\epsilon)\mathbf{F}, \tag{2.42}$$

where $T$ is an invertible matrix whose entries are generally rational functions of the kinematic variables and the dimensional regulator. The existence of such transformations reflects the freedom in choosing the master integrals and plays a central role in the modern

formulation of the differential equation method.

Differentiating Eq. (2.42) with respect to an arbitrary kinematic variable and making use of Eq. (2.30) leads to

$$\frac{\partial T}{\partial x_i}\mathbf{F} + T\frac{\partial \mathbf{F}}{\partial x_i} = A_i T\mathbf{F}, \tag{2.43}$$

from which one immediately obtains

$$\frac{\partial \mathbf{F}}{\partial x_i} = B_i\mathbf{F}, \tag{2.44}$$

where the transformed coefficient matrix is given by

$$B_i = T^{-1}A_iT - T^{-1}\frac{\partial T}{\partial x_i}. \tag{2.45}$$

Equation (2.45) shows that the differential equations transform exactly like a gauge connection under a local change of basis. Consequently, many apparently different systems of differential equations are mathematically equivalent, differing only by the choice of master basis. The practical objective is therefore to identify a basis in which the matrices $B_i$ assume the simplest possible form.

In general, the matrices obtained directly from an IBP reduction possess a rather complicated dependence on both the dimensional regulator and the kinematic variables. Their entries typically contain high-order poles, non-factorized dependence on $\epsilon$, and complicated rational functions involving several scales. Solving such systems directly is usually difficult even when the number of master integrals is relatively small. It is therefore advantageous to exploit the freedom provided by Eq. (2.42) in order to simplify the analytic structure of the differential equations before attempting to solve them.

An important simplification consists in transforming the system into a Fuchsian form, in which all singularities are regular singular points. In the vicinity of a singular point $x = x_k$, the coefficient matrix then behaves as

$$A(x) = \frac{R_k}{x - x_k} + \mathcal{O}(1), \tag{2.46}$$

where $R_k$ denotes the residue matrix associated with the singularity. The absence of higher-order poles considerably simplifies the local analysis of the solutions and ensures that the singular behaviour is entirely governed by logarithms and algebraic powers. In many applications this Fuchsian form can be achieved through an appropriate sequence of basis transformations together with suitable changes of the kinematic variables.

Although the Fuchsian form already represents a significant simplification, an even more remarkable structure emerges for a suitable choice of master integrals. Henn observed that for a large class of Feynman integrals it is possible to construct a basis in which the dependence on the dimensional regulator completely factorizes from the kinematic dependence. In this basis the differential equations take the form

$$d\mathbf{F} = \epsilon\, dA\, \mathbf{F}, \tag{2.47}$$

where the matrix-valued differential one-form $dA$ is independent of $\epsilon$. Equation (2.47) is commonly referred to as the canonical or $\epsilon$-form of the differential equations. Its importance lies in the fact that the perturbative expansion in the dimensional regulator becomes completely transparent. Since the coefficient matrix no longer depends on $\epsilon$, the solution may be constructed recursively order by order in the Laurent expansion around $\epsilon = 0$.

Each successive order is obtained by performing one additional integration of the previous order, revealing the iterative structure characteristic of multiple polylogarithms.

The differential one-form appearing in Eq. (2.47) can often be written as

$$dA = \sum_{i=1}^{N} A_i \, d\log W_i(\mathbf{x}), \tag{2.48}$$

where the matrices $A_i$ are constant and the functions $W_i(\mathbf{x})$ are algebraic functions of the kinematic variables. The collection of functions

$$\mathcal{A} = \{W_1, W_2, \ldots, W_N\} \tag{2.49}$$

is known as the alphabet of the differential equation. Each letter corresponds to a possible logarithmic singularity of the solution and therefore determines the analytic structure of the master integrals. Once the alphabet has been identified, the solution naturally organizes itself into Chen iterated integrals whose integration kernels are precisely the logarithmic differentials appearing in Eq. (2.48).

The existence of a canonical basis is one of the central developments in the modern theory of Feynman integrals. It transforms the problem of solving coupled differential equations into the study of iterated integrals over a finite alphabet, thereby establishing a direct connection between perturbative quantum field theory and several branches of modern mathematics, including algebraic geometry, mixed Hodge structures and the theory of multiple polylogarithms. In the following section the solution of the canonical system will be discussed in detail, together with its representation in terms of Chen iterated integrals and generalized polylogarithms.

## 2.7 The radial–angular factorisation

The master integrals could now be solved by differential equations. The alternative pursued here exploits a factorisation of the phase-space measure [103, 104, 105, 106, 107, 108], performed in a definite frame: the rest frame of the total momentum of the unresolved system (for a single emission, equivalently the frame in which the fixed vectors $p_i$ are specified). In this frame a massless unresolved momentum is parametrised by its energy and direction,

$$q^\mu = \rho\,(1, \hat{\mathbf{q}}), \qquad q^2 = 0, \qquad \rho = q^0 > 0, \tag{2.50}$$

with $\hat{\mathbf{q}}$ a unit vector in $d-1$ spatial dimensions. The on-shell measure then factorises into a radial and an angular piece. Indeed, writing $\mathrm{d}^d q = \mathrm{d}q^0\,\mathrm{d}^{d-1}\mathbf{q}$ and using $\delta_+(q^2) = \delta(q_0^2 - \mathbf{q}^2)\theta(q^0) = \delta(q^0 - |\mathbf{q}|)/(2|\mathbf{q}|)$ to do the energy integral, then passing the spatial integral to hyperspherical coordinates $\mathrm{d}^{d-1}\mathbf{q} = |\mathbf{q}|^{d-2}\mathrm{d}|\mathbf{q}|\,\mathrm{d}\Omega_{d-1}(\hat{\mathbf{q}})$ and setting $\rho = |\mathbf{q}|$, one obtains

$$\mathrm{d}^d q\,\delta_+(q^2) = \frac{|\mathbf{q}|^{d-2}}{2|\mathbf{q}|}\,\mathrm{d}|\mathbf{q}|\,\mathrm{d}\Omega_{d-1} = \tfrac{1}{2}\,\rho^{d-3}\,\mathrm{d}\rho\,\mathrm{d}\Omega_{d-1}(\hat{\mathbf{q}}). \tag{2.51}$$

For fixed external vectors written in the same frame as $p_i^\mu = E_i(1, \beta_i\hat{\mathbf{p}}_i)$ with $\beta_i = \sqrt{1 - p_i^2/E_i^2}$, the denominators become

$$p_i \cdot q = E_i\,\rho\,\big(1 - \beta_i\,\hat{\mathbf{p}}_i \cdot \hat{\mathbf{q}}\big), \tag{2.52}$$

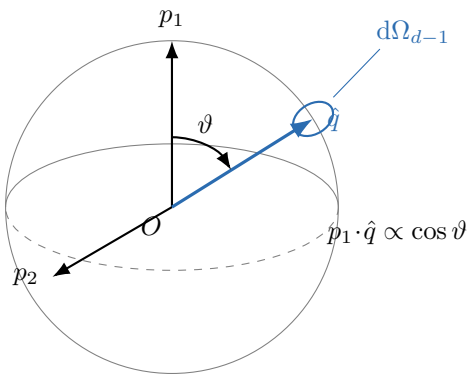



Figure 2.4: Geometry of the radial–angular decomposition. After the radial magnitude is integrated out, the remaining integral is over the direction $\hat{q}$ of the massless reference vector on the unit sphere, with measure $\mathrm{d}\Omega_{d-1}$. The denominators are dot products $p_r\cdot\hat{q}$ with the fixed external vectors $p_r$; for $p_1$ along the polar axis, $p_1\cdot\hat{q}\propto\cos\vartheta$, so the angular integrand is a non-trivial function of the polar and azimuthal angles.

which depend on $\rho$ only through an overall power. Consequently a generic integral factorises into a radial integral and an *angular* integral,

$$\int \mathrm{d}^d q\,\delta_+(q^2)\,\frac{R(\rho)}{\prod_i (p_i\cdot q)^{j_i}} = \tfrac{1}{2}\Big(\prod_i E_i^{-j_i}\Big)\int_0^\infty \mathrm{d}\rho\,\rho^{d-3-j}R(\rho)\,\Omega_{j_1,\ldots,j_n}, \qquad j=\sum_i j_i, \tag{2.53}$$

where $R(\rho)$ collects the process-dependent radial dependence (propagators not of the form $p_i\cdot q$, and the measurement function). The angular integral

$$\Omega_{j_1,\ldots,j_n} = \int \mathrm{d}\Omega_{d-1}(\hat{\mathbf{q}})\,\frac{1}{\prod_i (1-\beta_i\hat{\mathbf{p}}_i\cdot\hat{\mathbf{q}})^{j_i}} \tag{2.54}$$

is *universal*: it depends only on the directions and velocities of the fixed vectors, not on the process. The universality is genuine but qualified: it emerges only after the radial powers and energy factors are extracted, and the radial integral itself remains process-dependent.

Consider what this universality buys, because it is the central payoff of the approach. The angular integral $\Omega_{j_1,\ldots,j_n}$ depends only on the directions and velocities of the fixed vectors $p_i$, not on the process that produced it. The very same $\Omega$ therefore appears in the double-real corrections to Drell–Yan production, to Higgs production, to other SIDIS structure functions, and to any process with the same number and mass pattern of hard partons radiating the unresolved momentum. Computing these angular building blocks once, analytically and to all orders in $\epsilon$, thus pays of over an entire class of calculations; the process-specific work is reduced to the (one-dimensional) radial integral. This is the economy that motivates treating the angular integrals as objects of study in their own right, which the next three chapters do.

## 2.8 The Somogyi and van Neerven representations

The angular integral admits two complementary representations. The *Somogyi* form is manifestly rotationally invariant,

$$\Omega_{j_1,\ldots,j_n} = \int \mathrm{d}\Omega_{d-1}(q)\,\frac{1}{(p_1\cdot q)^{j_1}\cdots(p_n\cdot q)^{j_n}}, \tag{2.55}$$

and depends on the fixed vectors only through the scalar products

$$v_{kl} = \begin{cases} \dfrac{p_k \cdot p_l}{2}, & k \neq l, \\ \dfrac{p_k^2}{4}, & k = l. \end{cases} \tag{2.56}$$

To compute it one chooses a frame. Aligning $p_1$ with the polar axis and successively fixing the orientations of $p_2, \dots, p_n$ gives the standard configuration

$$\begin{aligned} p_1^\mu &= (1, \mathbf{0}_{d-2}, \beta_1), \\ p_2^\mu &= (1, \mathbf{0}_{d-3}, \beta_2 \sin\chi_2^{(1)}, \beta_2 \cos\chi_2^{(1)}), \\ &\vdots \\ p_n^\mu &= \Big(1, \mathbf{0}_{d-1-n}, \beta_n \prod_{k=1}^{n-1} \sin\chi_n^{(k)}, \beta_n \cos\chi_n^{(n-1)} \prod_{k=1}^{n-2} \sin\chi_n^{(k)}, \dots, \beta_n \cos\chi_n^{(1)}\Big), \end{aligned} \tag{2.57}$$

and the integration vector

$$q^\mu = \Big(1, \dots, \cos\vartheta_n \prod_{k=1}^{n-1} \sin\vartheta_k, \dots, \cos\vartheta_2 \sin\vartheta_1, \cos\vartheta_1\Big). \tag{2.58}$$

From hyperspherical coordinates the measure factorises, in $d = 4 - 2\epsilon$, as

$$\mathrm{d}\Omega_{d-1}(q) = \Big[\prod_{k=1}^{n} \mathrm{d}(\cos\vartheta_k)\,(\sin\vartheta_k)^{-k+1-2\epsilon}\Big]\mathrm{d}\Omega_{d-1-n}(q), \tag{2.59}$$

the trivial $d-1-n$ angles integrating to a constant. Inserting this gives the *van Neerven* representation [82, 83],

$$\begin{aligned} \Omega_{j_1,\dots,j_n} = \int \mathrm{d}\Omega_{d-1-n}(q) \int_{-1}^{1} \Big[\prod_{k=1}^{n} \mathrm{d}(\cos\vartheta_k)\,(\sin\vartheta_k)^{-k+1-2\epsilon}\Big] \\ \times \prod_{k=1}^{n} \Big\{1 - \beta_k \sum_{l=1}^{k} \Big[\big(\delta_{lk} + (1-\delta_{lk})\cos\chi_k^{(l)}\big)\cos\vartheta_l \prod_{m=1}^{l-1} \big(\sin\chi_k^{(m)} \sin\vartheta_m\big)\Big]\Big\}^{-j_k}. \end{aligned} \tag{2.60}$$

The distinction between the two forms is conceptual as well as practical: (2.55) is coordinate-free and makes the rotational invariance manifest, whereas (2.60) is a particular coordinate realisation, fixed by an ordering of the vectors and a choice of frame. They represent the same integral, but only the Somogyi variables $v_{kl}$ make the symmetry transparent, and the Mellin–Barnes representation of Chapter 3 is most naturally written in those variables.

## 2.9 Classification of the angular integrals

The angular integrals are organised by the number of denominators $n$ and the number of massive legs (a leg being massless when $p_i^2 = 0$, i.e. $v_{ii} = 0$). Table 2.1 records the resulting function classes. The low-$n$ entries are classical and serve as checks; for $n \geq 3$ the only known closed form is in terms of the multivariable $H$-function, which is prohibitively difficult to expand in $\epsilon$. This is the gap that the method of this thesis fills.

Table 2.1: Angular integrals by denominator number and mass pattern, with the classical function class and the role each case plays in this thesis.

| $n$ | mass pattern | function class | role |
|---|---|---|---|
| 1 | massless | $\Gamma$ ratio | worked example (Section 2.10) |
| 1 | massive | ${}_2F_1$ | known check [109] |
| 2 | two massless | ${}_2F_1$ | running example for Chapter 3 |
| 2 | massive | Appell $F_1$ / Lauricella | SIDIS checks |
| $\geq 3$ | general | multivariable $H$-function | MB-to-GPL method needed |

This chapter claims no new analytic results: it defines the objects and explains why the later Mellin–Barnes construction is required. An independent differential-equation treatment of the same angular integrals has been developed in parallel [110, 111, 112], and is compared with the present method in Chapter 4.

## 2.10 Worked example: the single massless denominator

To make the formalism concrete we evaluate the simplest case in full. Take one massless fixed vector along the polar axis, $p^\mu = (1, \mathbf{0}_{d-2}, 1)$, so that with $q^\mu = (1, \ldots, \cos\theta)$ the single denominator is $p \cdot q = 1 - \cos\theta$. The integral is

$$\Omega_j = \int \mathrm{d}\Omega_{d-1}(q)\, \frac{1}{(p\cdot q)^j}. \tag{2.61}$$

Only the polar angle $\theta$ appears in the integrand. Splitting the $(d-1)$-sphere measure as $\mathrm{d}\Omega_{d-1} = \mathrm{d}\Omega_{d-2}\sin^{d-3}\theta\,\mathrm{d}\theta$ and writing $x = \cos\theta$, the polar factor becomes $\sin^{d-3}\theta\,\mathrm{d}\theta = (1-x^2)^{(d-4)/2}\mathrm{d}x = (1-x^2)^{-\epsilon}\mathrm{d}x$ in $d = 4-2\epsilon$, while the remaining $(d-2)$-sphere integrates to a constant,

$$\mathrm{d}\Omega_{d-1} = \mathrm{d}\Omega_{d-2}\,(1-x^2)^{-\epsilon}\,\mathrm{d}x, \qquad \Omega_{d-2} = \frac{2\pi^{1-\epsilon}}{\Gamma(1-\epsilon)}. \tag{2.62}$$

Hence

$$\Omega_j = \Omega_{d-2}\int_{-1}^{1}\mathrm{d}x\,(1-x^2)^{-\epsilon}(1-x)^{-j} = \Omega_{d-2}\int_{-1}^{1}\mathrm{d}x\,(1-x)^{-j-\epsilon}(1+x)^{-\epsilon}. \tag{2.63}$$

The substitution $t = (1-x)/2$ (so $1-x = 2t$, $1+x = 2(1-t)$, $\mathrm{d}x = -2\,\mathrm{d}t$, and the limits become $t: 1 \to 0$) gives

$$\Omega_j = \Omega_{d-2}\,2^{1-j-2\epsilon}\int_0^1 \mathrm{d}t\, t^{-j-\epsilon}(1-t)^{-\epsilon} = \Omega_{d-2}\,2^{1-j-2\epsilon}\,B(1-j-\epsilon,\,1-\epsilon), \tag{2.64}$$

where $B(a,b) = \int_0^1 t^{a-1}(1-t)^{b-1}\mathrm{d}t$ is the Euler beta function. Using $\Omega_{d-2} = 2\pi^{1-\epsilon}/\Gamma(1-\epsilon)$ and $B(a,b) = \Gamma(a)\Gamma(b)/\Gamma(a+b)$,

$$\boxed{\Omega_j = 2^{2-j-2\epsilon}\,\pi^{1-\epsilon}\,\frac{\Gamma(1-j-\epsilon)}{\Gamma(2-j-2\epsilon)}} \tag{2.65}$$

For positive integer $j$ the angular integral is endpoint divergent and the boxed result is understood by analytic continuation in $\epsilon$, a recurring theme that is treated systematically

Table 2.2: Symbols used in the angular-integral formalism.

| symbol | meaning |
|---|---|
| $d = 4 - 2\epsilon$ | dimension and regulator (this chapter) |
| $q^\mu$ | massless reference / integration vector, $q^2 = 0$ |
| $p_i^\mu$ | fixed external vectors, $i = 1, \dots, n$ |
| $\beta_i$ | velocity of $p_i$, $\beta_i = \sqrt{1 - p_i^2/E_i^2}$ |
| $\chi_i^{(k)}$ | relative angles fixing the configuration of $p_i$ |
| $\vartheta_k$ | polar integration angles |
| $j_i,\ j = \sum_i j_i$ | denominator powers and their sum |
| $v_{kl}$ | $p_k \cdot p_l/2$ $(k \neq l)$, $p_k^2/4$ $(k = l)$ |
| $z_{kl}$, $z_k$ | Mellin–Barnes variables (Chapter 3); $z_{kk}$ counted twice in $z_k$ |
| $\Omega_{j_1,\dots,j_n}$ | angular integral, eq. (2.55) |

in Chapter 3.

The two-denominator massless case already needs the Mellin–Barnes representation that the next chapter develops in full; here I only record where it leads. Its one-fold representation,

$$\Omega_{j_1,j_2} = \frac{2^{2-j-2\epsilon}\pi^{1-\epsilon}}{\Gamma(j_1)\Gamma(j_2)\Gamma(2-j-2\epsilon)} \int \frac{\mathrm{d}z}{2\pi i}\, \Gamma(-z)\Gamma(j_1+z)\Gamma(j_2+z)\Gamma(1-j-\epsilon-z)\,(v_{12})^z, \tag{2.66}$$

is evaluated by closing the contour and summing residues, which produces a Gauss series $\sum_{m\geq 0} \frac{(j_1)_m (j_2)_m}{(j+\epsilon)_m} \frac{v_{12}^m}{m!}$ and hence a hypergeometric function ${}_2F_1(j_1, j_2; j+\epsilon; v_{12})$, with branch conventions fixed in Chapter 3. This is the running example carried through the next chapter.

## 2.11 Conventions and notation

*Remark* 2.1 (Regulator convention). I use $d = 4 - 2\epsilon$ *throughout* the thesis. The SIDIS master integrals of Chapter 7 were originally computed in the differential-equation convention $d = 4 + \epsilon_{\mathrm{p}}$ of Ref. [35]; for uniformity I convert all of their results to $d = 4 - 2\epsilon$ using $\epsilon_{\mathrm{p}} = -2\epsilon$.

# Chapter 3

# Mathematical Tools: Mellin–Barnes Integrals and Polylogarithms

## Contents


3.1 Purpose and the running example . . . 33
3.2 From the Mellin transform to the Mellin–Barnes identity . . . 34
3.3 From the van Neerven form to the angular Mellin–Barnes representation . . . 35
3.4 Residues and analytic continuation in $\epsilon$ . . . 36
3.5 The Barnes lemmas . . . 37
3.6 Balanced integrals, beta conversion, and the delta-collapse . . . 37
3.7 Goncharov polylogarithms . . . 38
3.8 Linear reducibility: when the result is a polylogarithm . . . 39
3.9 The running example, completed . . . 39


This chapter collects, around a single running example, the two mathematical ingredients used in the rest of the thesis: Mellin–Barnes (MB) integrals and Goncharov (multiple) polylogarithms (GPLs). The treatment is pedagogical rather than encyclopaedic. I motivate, derive, and immediately test every tool on the running example, so that by the end of the chapter the reader has followed one angular integral from its MB representation to a closed polylogarithmic answer and its symbol. I then formulate the general method in Chapter 4 and apply it in Chapter 5.

## 3.1 Purpose and the running example

The example I carry throughout is the two-denominator massless angular integral

$$\Omega_{1,1}(v_{12},\epsilon) = \int \mathrm{d}\Omega_{d-1}(q)\, \frac{1}{(p_1\cdot q)(p_2\cdot q)}, \qquad p_1^2 = p_2^2 = 0, \quad v_{12} = \frac{p_1\cdot p_2}{2}. \tag{3.1}$$

It is the simplest case that already requires the full pipeline of Figure 3.1, and its closed form is known in terms of a Gauss hypergeometric function [109], which provides an independent check at the end of the chapter. The pipeline has six exact steps. Only the final truncation of the Laurent series in $\epsilon$ is an approximation.

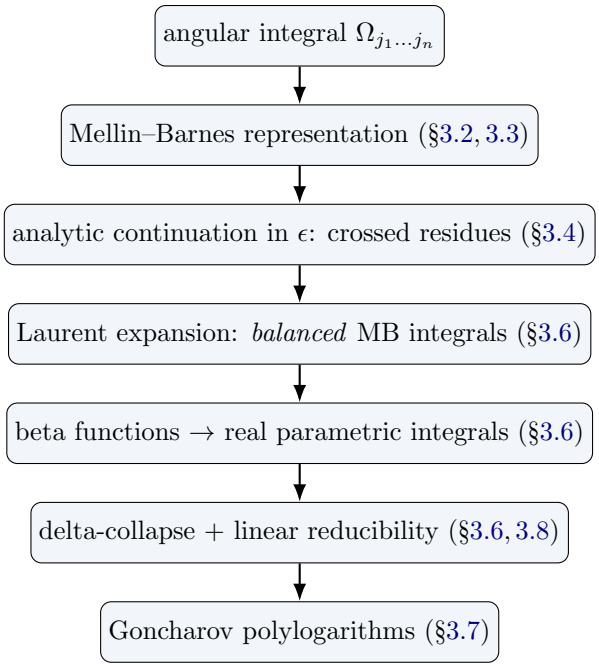



Figure 3.1: The evaluation pipeline followed throughout the thesis, with the section that develops each step. Each step is exact; the only approximation is the truncation of the Laurent series in $\epsilon$.

The Mellin–Barnes route taken here is not the only analytic technique available. The main alternative is the method of differential equations in a canonical basis [59, 60, 61], which solves each master integral as a whole and is the standard tool of modern multiloop calculations. The two are complementary, as discussed in Chapter 4. The Mellin–Barnes method is well suited to the angular integrals studied in this thesis because it acts directly on their universal denominator structure and produces reusable building blocks, whereas the differential-equation method is most powerful once a canonical basis and boundary data for a specific topology are in hand.

## 3.2 From the Mellin transform to the Mellin–Barnes identity

The Mellin transform [113, 114, 115, 116] of a function $f$ and its inverse are

$$\mathcal{M}[f](s) = \int_0^\infty x^{s-1} f(x)\,\mathrm{d}x, \qquad f(x) = \frac{1}{2\pi i}\int_{c-i\infty}^{c+i\infty} x^{-s}\,\mathcal{M}[f](s)\,\mathrm{d}s, \tag{3.2}$$

the contour lying in the fundamental strip where the transform converges. Applied to $f(x) = (1+x)^{-\lambda}$ the transform is a beta function,

$$\mathcal{M}[f](s) = \int_0^\infty x^{s-1}(1+x)^{-\lambda}\,\mathrm{d}x = B(s, \lambda - s) = \frac{\Gamma(s)\Gamma(\lambda - s)}{\Gamma(\lambda)}, \qquad 0 < \Re s < \Re\lambda. \tag{3.3}$$

Inverting and substituting $s = -z$ gives

$$\frac{1}{(1+x)^\lambda} = \frac{1}{\Gamma(\lambda)}\frac{1}{2\pi i}\int_{c-i\infty}^{c+i\infty} \mathrm{d}z\,\Gamma(-z)\Gamma(\lambda+z)\,x^z, \tag{3.4}$$

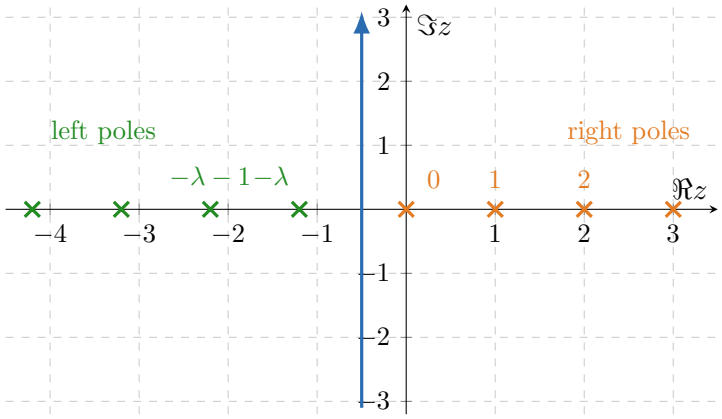



Figure 3.2: The complex $z$-plane for a Mellin–Barnes integral with integrand $\Gamma(\lambda+z)\Gamma(-z)\,(\cdots)$. The vertical contour $\mathcal{C}$ at $\Re z = c$ separates the *left* poles of $\Gamma(\lambda+z)$ at $z=-\lambda,-\lambda-1,\ldots$ from the *right* poles of $\Gamma(-z)$ at $z=0,1,2,\ldots$.

and replacing $x \to A/B$ yields the *Mellin–Barnes splitting identity*

$$\frac{1}{(A+B)^{\lambda}} = \frac{1}{\Gamma(\lambda)}\frac{1}{2\pi i}\int_{c-i\infty}^{c+i\infty} \mathrm{d}z\,\Gamma(-z)\Gamma(\lambda+z)\,A^{z}B^{-\lambda-z} \tag{3.5}$$

valid for $\Re\lambda > 0$. The single non-trivial datum is the contour: it is the vertical line $\Re z = c$ with

$$-\Re\lambda < c < 0, \tag{3.6}$$

chosen so that the *right* poles of $\Gamma(-z)$ (at $z=0,1,2,\ldots$) lie to its right and the *left* poles of $\Gamma(\lambda+z)$ (at $z=-\lambda,-\lambda-1,\ldots$) lie to its left. Figure 3.2 shows the configuration. Respecting it is the whole content of the residue calculus to follow.

## 3.3 From the van Neerven form to the angular Mellin–Barnes representation

The splitting identity converts the angular integral into gamma functions. Starting from the van Neerven representation of Chapter 2,

$$\Omega_{j_1,\ldots,j_n} = \int \mathrm{d}\Omega_{d-1-n}\int_{-1}^{1}\prod_{k=1}^{n}\mathrm{d}(\cos\vartheta_k)\,(\sin\vartheta_k)^{-k+1-2\epsilon}\prod_{r=1}^{n}D_r^{-j_r}, \tag{3.7}$$

one applies (3.5) to each denominator $D_r = 1-\beta_r\,\hat{\mathbf{p}}_r\cdot\hat{\mathbf{q}}$, trading it for an MB integral over a variable $z_{kl}$ (one per propagator pair) at the price of gamma functions; the now-elementary angular integrations over the $\vartheta_k$ produce further gamma functions. The result, written in the invariant variables $v_{kl}$, is the Somogyi MB representation [83]

$$\begin{aligned}\Omega_{j_1,\ldots,j_n}(\{v_{kl}\},\epsilon) = {}& \frac{2^{2-j-2\epsilon}\pi^{1-\epsilon}}{\prod_{k=1}^{n}\Gamma(j_k)\,\Gamma(2-j-2\epsilon)}\int_{-i\infty}^{+i\infty}\Big[\prod_{k=1}^{n}\prod_{l=k}^{n}\frac{\mathrm{d}z_{kl}}{2\pi i}\,\Gamma(-z_{kl})\,(v_{kl})^{z_{kl}}\Big]\\ &\times\Big[\prod_{k=1}^{n}\Gamma(j_k+z_k)\Big]\Gamma(1-j-\epsilon-z),\end{aligned} \tag{3.8}$$

with $z = \sum_{k\le l} z_{kl}$ and $z_k = \sum_{l=1}^{k} z_{lk} + \sum_{l=k}^{n} z_{kl}$ (so that $z_{kk}$ is counted twice), and $j = \sum_k j_k$. Integrations associated with a vanishing $v_{kl}$ (as for a massless leg, $v_{kk} = 0$) are omitted.

For the running example, $n = 2$, $j = 2$, and $v_{11} = v_{22} = 0$, so only $z_{12} \equiv z$ survives; then $z_1 = z_2 = z$ and (3.8) collapses to a one-fold integral,

$$\Omega_{1,1}(v_{12},\epsilon) = \frac{2^{-2\epsilon}\pi^{1-\epsilon}}{\Gamma(-2\epsilon)} \int_{-i\infty}^{+i\infty} \frac{\mathrm{d}z}{2\pi i}\, \Gamma(-z)\,\Gamma(1+z)^2\,\Gamma(-1-\epsilon-z)\,(v_{12})^z \tag{3.9}$$

where the last gamma is $\Gamma(1-j-\epsilon-z) = \Gamma(-1-\epsilon-z)$ and the prefactor gamma is $\Gamma(2-j-2\epsilon) = \Gamma(-2\epsilon)$. This is the object we now evaluate.

## 3.4 Residues and analytic continuation in $\epsilon$

For foundational, standard, and representative treatments directly relevant to the material discussed in this section, see [117, 118].

The elementary building block of every MB evaluation is the residue of $\Gamma(-z)$ at its right poles,

$$\mathrm{Res}_{z=n}\,\Gamma(-z) = \frac{(-1)^n}{n!}, \qquad n = 0, 1, 2, \ldots \tag{3.10}$$

Closing the contour of the fundamental identity (3.5) to the right and summing these residues reproduces the binomial series,

$$\frac{1}{2\pi i}\int \mathrm{d}z\,\Gamma(-z)\Gamma(\lambda+z)\,x^z = \Gamma(\lambda)\sum_{n=0}^{\infty}\frac{(-1)^n(\lambda)_n}{n!}\,x^n = \Gamma(\lambda)(1+x)^{-\lambda}, \tag{3.11}$$

which is a sanity check on contour orientation.

A naive expansion in $\epsilon$ is illegitimate, as is already visible in (3.9). Its integrand has three pole families,

$$z = n \ \text{(from } \Gamma(-z)\text{)}, \qquad z = -1-\epsilon+n \ \text{(from } \Gamma(-1-\epsilon-z)\text{)}, \qquad z = -1-n \ \text{(from } \Gamma(1+z)^2\text{)}, \tag{3.12}$$

and as $\epsilon \to 0$ the pole at $z = -1-\epsilon$ approaches, and would cross, a contour placed to separate the left and right families at finite $\epsilon$. Expanding the integrand in $\epsilon$ before this crossing is resolved would drop the contribution of the crossing pole. The cure is analytic continuation [119, 120, 121], performed by either of two equivalent algorithms:

- *fixed contour, moving poles*: hold $\mathcal{C}$ fixed, track the poles as $\epsilon$ varies, and add the residue of each pole that crosses;
- *moving contour, fixed poles*: deform $\mathcal{C}$ to keep all poles on their original sides, adding the residue of each pole the deformation sweeps past.

Figure 3.3 illustrates the first. For (3.9) the single crossing is at $z_\star = -1-\epsilon$, where $\mathrm{Res}_{z=z_\star}\,\Gamma(-1-\epsilon-z) = -1$, contributing a term proportional to

$$-\,\Gamma(1+\epsilon)\,\Gamma(-\epsilon)^2\,(v_{12})^{-1-\epsilon}, \tag{3.13}$$

the overall sign being fixed by the orientation of the deformation. The original integral is thus written as this residue term plus a remainder integral whose contour is now pole-free as $\epsilon \to 0$, and only then is the Laurent expansion legitimate. This residue term carries the leading $1/\epsilon$ pole of $\Omega_{1,1}$, and the remainder supplies the finite part.

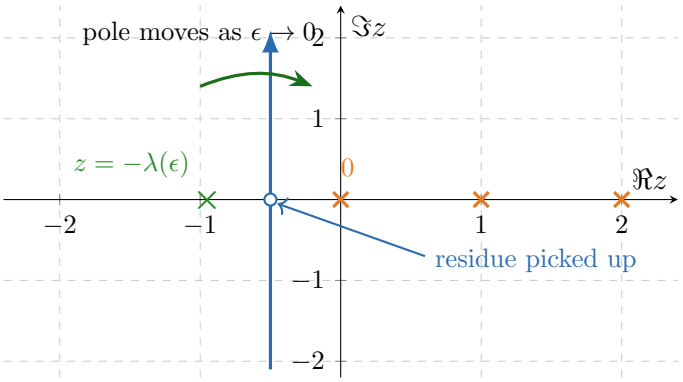



Figure 3.3: Analytic continuation in the regulator. As $\epsilon \to 0$ a pole at $z = -\lambda(\epsilon)$, here from a $\Gamma(\cdot - z)$ factor, migrates rightward and crosses the fixed contour $\mathcal{C}$; to keep the contour pole-free it is deformed, and the residue of the crossed pole (circled) is added to the integral. Collecting such residues is what makes the subsequent Laurent expansion in $\epsilon$ legitimate.

## 3.5 The Barnes lemmas

The remainder integrals are evaluated in closed form with the Barnes lemmas [113]. The *first Barnes lemma* is

$$\frac{1}{2\pi i}\int_{-i\infty}^{+i\infty} \mathrm{d}z\, \Gamma(a+z)\Gamma(b+z)\Gamma(c-z)\Gamma(d-z) = \frac{\Gamma(a+c)\Gamma(a+d)\Gamma(b+c)\Gamma(b+d)}{\Gamma(a+b+c+d)}. \tag{3.14}$$

*Proof sketch.* Close the contour to the right, enclosing the poles of $\Gamma(c-z)\Gamma(d-z)$ at $z = c+n$ and $z = d+n$ ($n \geq 0$). Summing the residues at $z = c+n$ produces a Gauss series $\propto {}_2F_1(a+c, b+c; 1+c-d; 1)$, and those at $z = d+n$ the analogous series with $c \leftrightarrow d$. Each is a hypergeometric function at unit argument; resumming both with Gauss's theorem

$${}_2F_1(\alpha, \beta; \gamma; 1) = \frac{\Gamma(\gamma)\Gamma(\gamma-\alpha-\beta)}{\Gamma(\gamma-\alpha)\Gamma(\gamma-\beta)} \tag{3.15}$$

and combining the two contributions yields the right-hand side of (3.14). □

The *second Barnes lemma*,

$$\begin{aligned}\frac{1}{2\pi i}\int \mathrm{d}z\, &\frac{\Gamma(a+z)\Gamma(b+z)\Gamma(c+z)\Gamma(d-z)\Gamma(e-z)}{\Gamma(a+b+c+d+e+z)} \\ &= \frac{\prod_{r\in\{a,b,c\}}\Gamma(r+d)\Gamma(r+e)}{\Gamma(a+b+d+e)\Gamma(a+c+d+e)\Gamma(b+c+d+e)},\end{aligned} \tag{3.16}$$

holds under the analogous separation and convergence conditions. These lemmas, together with their corollaries obtained by shifting parameters, suffice to evaluate every one-fold integral that arises in this thesis.

## 3.6 Balanced integrals, beta conversion, and the delta-collapse

Multifold MB integrals are reduced to real integrals when they possess a special structure.

**Definition 3.1** (Balanced MB integral)**.** A one-fold MB integral $\int \frac{\mathrm{d}z_j}{2\pi i} \prod_k \Gamma(a_k+z_j)^{\alpha_k} \prod_l \Gamma(b_l-z_j)^{\beta_l}$ with $\alpha_k, \beta_l \in \mathbb{Z}$ is *balanced* in $z_j$ if $\sum_k \alpha_k = \sum_l \beta_l$; a multifold integral is balanced if it is balanced in each variable.

The integrand of (3.9) has $\sum \alpha = 2$ (from $\Gamma(1+z)^2$) and $\sum \beta = 2$ (from $\Gamma(-z)$ and $\Gamma(-1-\epsilon-z)$), so it is balanced, and so is each coefficient integral generated by the $\epsilon$-expansion. I record the inheritance of this property as a proposition, since the whole method relies on it.

**Proposition 3.2** (Stability of balance)**.** *The angular MB representation* (3.8) *is balanced in each variable, and balance is preserved by the analytic continuation and the Laurent expansion of Section 3.4.*

A balanced integrand is built entirely from beta functions, and each beta function has a real integral representation,

$$B(a,b) = \frac{\Gamma(a)\Gamma(b)}{\Gamma(a+b)} = \int_0^1 \mathrm{d}t\, t^{a-1}(1-t)^{b-1} = \int_0^\infty \mathrm{d}t\, t^{a-1}(1+t)^{-a-b}, \qquad \Re a, \Re b > 0. \tag{3.17}$$

Substituting these and exchanging the (convergent) real and MB integrations brings a balanced multifold MB integral to the form

$$\int_0^\kappa \Big(\prod_i \mathrm{d}x_i\Big) R_0(\mathbf{x},\mathbf{u}) \int \prod_l \frac{\mathrm{d}\tilde{z}_l}{2\pi i} \big[R_l(\mathbf{x},\mathbf{u})\big]^{\tilde{z}_l}, \qquad \kappa \in \{1,\infty\}, \tag{3.18}$$

with the $R_l$ ratios of monomials in $x_i$, $(1\pm x_i)$ and the external parameters. The remaining MB integrations are removed by the delta-collapse.

**Lemma 3.3** (Delta-collapse)**.** *For real $A > 0$ and a contour with vanishing real part,* $\int_{-i\infty}^{+i\infty} \frac{\mathrm{d}z}{2\pi i} A^z = \delta(1-A)$.

*Proof.* Write $A^z = e^{z\ln A}$ and parametrise the contour as $z = it$, $t \in (-\infty,\infty)$. Then $\int \frac{\mathrm{d}z}{2\pi i} A^z = \frac{1}{2\pi}\int_{-\infty}^{\infty} \mathrm{d}t\, e^{it\ln A} = \delta(\ln A)$, and $\delta(\ln A) = A\,\delta(A-1) = \delta(A-1)$ since the Jacobian at the root $A=1$ is unity. □

*Remark* 3.4 (Status of the delta-collapse). Lemma 3.3 is a distributional identity, valid inside a convergent real integral with $A > 0$, a fixed branch of $\ln A$, and a legitimate exchange of the MB and real integrations; no endpoint terms are dropped. we use it only where these conditions hold.

Each delta function sets one of the $R_l$ to unity, removing one real integration and leaving a finite set of integrals of rational integrands,

$$\int_0^\kappa \Big(\prod_i \mathrm{d}x_i\Big) R_0(\mathbf{x},\mathbf{u}) \prod_l \delta\big[1-R_l(\mathbf{x},\mathbf{u})\big]. \tag{3.19}$$

Whether these integrate to polylogarithms is the question settled in Section 3.8.

## 3.7 Goncharov polylogarithms

The functions produced by the remaining real integrations are Goncharov (multiple) polylogarithms [122, 123, 124, 125, 126, 127], defined as the iterated integrals [128, 129]

$$G(a_1,\dots,a_n;z) = \int_0^z \frac{\mathrm{d}t}{t-a_1}\, G(a_2,\dots,a_n;t), \qquad G(;z) = 1, \tag{3.20}$$

with weight $n$ equal to the number of indices (letters) $a_i$. When all indices vanish,

$$G(\underbrace{0,\dots,0}_{n};z)=\frac{1}{n!}\ln^n z, \tag{3.21}$$

and the classical functions are recovered as

$$G(\mathbf{a}_n;z)=\frac{1}{n!}\ln^n\Big(1-\frac{z}{a}\Big),\qquad G(\underbrace{0,\dots,0}_{n-1},1;z)=-\operatorname{Li}_n(z). \tag{3.22}$$

Two algebraic structures make GPLs usable. First, as iterated integrals with a common endpoint they satisfy the *shuffle product*

$$G(\vec{a};z)\,G(\vec{b};z)=\sum_{\vec{c}\in\vec{a}\,\sqcup\!\sqcup\,\vec{b}}G(\vec{c};z), \tag{3.23}$$

the sum running over all interleavings $\vec{c}$ of $\vec{a}$ and $\vec{b}$ preserving their internal orders. (3.23) follows by writing the product as an integral over a square $0<t_i,s_j<z$ and decomposing the square into the ordered simplices, each of which is one shuffle term. The shuffle relation allows products of results to be re-expressed in a chosen basis and weights to be reduced. GPLs with a trailing-zero (endpoint-divergent) index are defined by *shuffle regularisation*: one solves, e.g., $G(a;z)G(0;z)=G(a,0;z)+G(0,a;z)$ for the ill-defined $G(a,0;z)$ in terms of convergent objects. Finally, the *fibration basis* rewrites every GPL so that the active integration variable appears as the rightmost argument, which makes the next real integration in (3.18) immediate. The manipulations are automated in PolyLogTools [130].

## 3.8 Linear reducibility: when the result is a polylogarithm

The rational integrals left by the delta-collapse evaluate to GPLs precisely when they are *linearly reducible* [131, 132]. The criterion is constructive: the integrations can be ordered so that, at each step, every denominator polynomial is linear in the next integration variable. An integration of the form

$$\int_0^1 \mathrm{d}x\,\frac{F(x)}{x-a}\;\rightsquigarrow\;G(a,\dots;1) \tag{3.24}$$

then yields a GPL whose new letter is the root $a$, and iterating produces the full result with a finite alphabet. When instead irreducible quadratics or several non-rationalisable square roots survive, one is forced beyond ordinary GPLs, to algebraic GPLs or to elliptic generalisations [132, 133, 134, 135, 136]. For the three- and four-denominator families of Chapter 5 the criterion is met after a suitable ordering and the rationalisation of a single root. The boundary where it fails is the subject of the outlook in Chapter 9.

## 3.9 The running example, completed

For the one-fold integral (3.9) the evaluation is carried out directly by residues (the beta-conversion and delta-collapse of Section 3.6 are the tools for the genuinely multi-fold integrals, $n\geq 3$, of Chapter 5). Assuming $|v_{12}|$ small enough that the right arc vanishes, we close the contour to the right and pick up the poles of $\Gamma(-z)$ at $z=n$, with residue $(-1)^n/n!$. Using $\Gamma(1+n)^2=(n!)^2$ and the reflection $\Gamma(-1-\epsilon-n)=$

$(-1)^n\Gamma(-1-\epsilon)/(2+\epsilon)_n$, the residue sum is

$$\sum_{n\geq 0}\frac{(-1)^n}{n!}(n!)^2\,\Gamma(-1-\epsilon-n)\,v_{12}^n=\Gamma(-1-\epsilon)\sum_{n\geq 0}\frac{(1)_n(1)_n}{(2+\epsilon)_n\,n!}\,v_{12}^n=\Gamma(-1-\epsilon)\,{}_2F_1(1,1;2+\epsilon;v_{12}), \tag{3.25}$$

so that

$$\Omega_{1,1}(v_{12},\epsilon)=\frac{2^{-2\epsilon}\pi^{1-\epsilon}\,\Gamma(-1-\epsilon)}{\Gamma(-2\epsilon)}\,{}_2F_1(1,1;2+\epsilon;v_{12}). \tag{3.26}$$

This is the explicit closed form, reached within the pipeline. It agrees with the result quoted in the literature [109], which after a standard hypergeometric transformation to the variable $x$ defined by $1-x=v_{12}/(v_{12}-2)$ reads $\Omega_{1,1}=\mathcal{N}(\epsilon,v_{12})\,{}_2F_1(1,1;1-\epsilon;1-x)$ with $\mathcal{N}$ the prefactor of (3.26) carried through the transformation; expanding the hypergeometric function gives

$${}_2F_1(1,1;1-\epsilon;1-x)=\frac{1}{x}\Big[1-\epsilon\ln x+\epsilon^2\Big(\mathrm{Li}_2(1-x)+\tfrac{1}{2}\ln^2 x\Big)+\mathcal{O}(\epsilon^3)\Big]. \tag{3.27}$$

This is the logarithm-and-dilogarithm endpoint: weight grows by one at each order in $\epsilon$, exactly the pattern of the general families. agreement of this output with the direct $\epsilon$-expansion of the known ${}_2F_1$ closes the running example and validates the pipeline in miniature.

To summarise what the chapter has established: the Mellin–Barnes representation separates sums into products; analytic continuation extracts the poles in $\epsilon$ legitimately; the balanced structure turns the integrand into beta functions and hence real integrals; the delta-collapse renders those integrals rational; linear reducibility makes them polylogarithmic.

# Chapter 4

# Angular Integrals and the Mellin–Barnes-to-Polylogarithm Method

## Contents


4.1 Scope and conventions . . . 41
4.2 The universal Mellin–Barnes representation . . . 42
4.3 The algorithm . . . 42
4.4 Classification and lower-denominator checks . . . 43
4.5 Linear reducibility and polylogarithmic expressibility . . . 44
4.6 Reduction of the polylogarithms to a fibration basis . . . 44
4.7 Comparison with the differential-equation route . . . 45
4.8 Failure modes and the frontier . . . 45
4.9 MB2MPL Mathematica Package . . . 45


Chapter 3 presented the Mellin–Barnes-to-polylogarithm pipeline on a single running example. In this chapter I abstract it into a reusable *method*. I state a boxed algorithm, classify the integrals it applies to, give the explicit lower-denominator results that check it, describe the in-house procedure that reduces the output to a canonical form and state where it succeeds and where it fails. I then compute the concrete three- and four-denominator families in Chapter 5.

## 4.1 Scope and conventions

The object of study is the angular integral

$$\Omega_{j_1,\dots,j_n}(\{p_i\},d)=\int \mathrm{d}\Omega_{d-1}(q)\,\prod_{i=1}^{n}\frac{1}{(p_i\cdot q)^{j_i}},\qquad d=4-2\epsilon, \tag{4.1}$$

with $q$ the massless reference vector, the $p_i$ fixed, and $j=\sum_i j_i$. As before the invariant data are the scalar products $v_{kl}=p_k\cdot p_l/2$ $(k\neq l)$ and $v_{kk}=p_k^2/4$. One qualification applies throughout the chapter: *the algorithm below is general as an algorithmic representation, but its reduction to ordinary Goncharov polylogarithms is conditional on the linearly reducible, genus-zero structure of the real integrals it produces* (Section 4.5).

## 4.2 The universal Mellin–Barnes representation

For foundational, standard, and representative treatments directly relevant to the material discussed in this section, see [137, 138, 116].

Every angular integral has the Somogyi Mellin–Barnes representation derived in Chapter 3,

$$\Omega_{j_1,\dots,j_n} = \frac{2^{2-j-2\epsilon}\pi^{1-\epsilon}}{\prod_{k=1}^{n}\Gamma(j_k)\,\Gamma(2-j-2\epsilon)} \int_{-i\infty}^{+i\infty} \prod_{1\le k\le l\le n} \frac{\mathrm{d}z_{kl}}{2\pi i}\,\Gamma(-z_{kl})\,v_{kl}^{z_{kl}} \times \prod_{k=1}^{n}\Gamma(j_k+z_k)\,\Gamma(1-j-\epsilon-z), \tag{4.2}$$

with $z=\sum_{k\le l} z_{kl}$ and $z_k=\sum_{l<k} z_{lk}+2z_{kk}+\sum_{l>k} z_{kl}$. The contours are vertical lines with the poles of $\Gamma(-z_{kl})$ to the right and those of $\Gamma(j_k+z_k)$ to the left; integrations with $v_{kk}=0$ are dropped. This single formula, valid for any $n$ and any mass pattern, is the input to the method.

## 4.3 The algorithm

**Algorithm 4.1 (MB-to-GPL evaluation of an angular integral).**

1. Fix the mass pattern and drop the MB variables of the vanishing $v_{kk}$.
2. Write the Somogyi MB representation (4.2).
3. Analytically continue to a neighbourhood of $\epsilon=0$, either by *contour deformation* (moving the path to keep poles on their original sides as $\epsilon$ changes) or by *fixed-contour pole tracking* (holding the path and summing the residues of poles that cross it as $\epsilon\to 0$).
4. Add the crossed-pole residues until every remaining contour is admissible at $\epsilon=0$.
5. Laurent-expand each resulting MB integral in $\epsilon$.
6. For each coefficient, verify the balanced condition (Definition 3.1): in every variable $z_r$, the total power of $\Gamma(\cdots+z_r)$ equals that of $\Gamma(\cdots-z_r)$. This is the prerequisite for the beta-function conversion of the next step.
7. Pair the gamma functions into beta functions and insert their real representations.
8. Exchange the MB and real integrations, reaching $\int_0^\kappa \prod_i \mathrm{d}x_i\, R_0 \int \prod_r \frac{\mathrm{d}z_r}{2\pi i} R_r^{z_r}$.
9. Collapse the MB integrations with $\int \frac{\mathrm{d}z}{2\pi i} A^z = \delta(1-A)$.
10. Integrate the remaining rational/logarithmic real integrals.
11. Reduce all GPLs to a common fibration basis (Section 4.6).
12. Validate numerically and against symmetries and known limits.

Steps 3–6 carry the only structural assumption: that balance survives the continuation and expansion. We establish this for every family treated in this thesis and conjecture it in general (Proposition 3.2); I state it explicitly rather than assume it silently. Steps 9–10

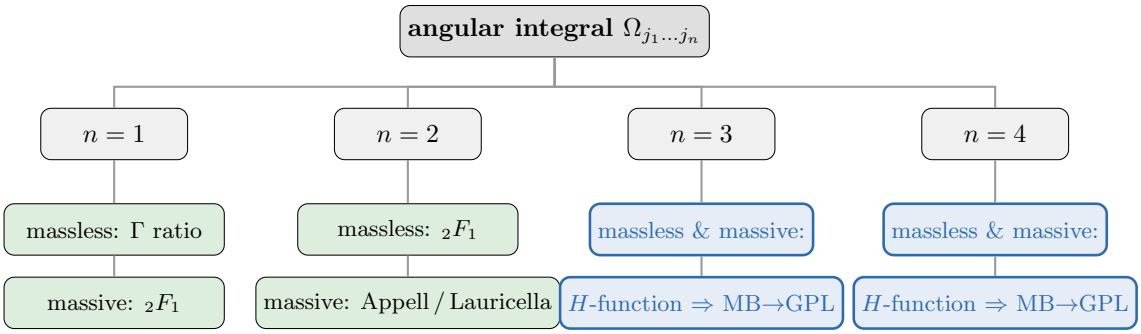



Figure 4.1: Classification of the angular integrals by the number of denominators $n$ and the mass pattern. For $n = 1, 2$ the integrals are classical special functions (Gamma ratios, ${}_2F_1$, Appell $F_1$/Lauricella). For $n \geq 3$, highlighted in blue, the only known closed form is the multivariable $H$-function, which cannot be expanded in $\epsilon$ in practice; these are the cases computed in this thesis through their Mellin–Barnes representation and expressed in Goncharov polylogarithms.

succeed precisely when the real integrals are linearly reducible, the criterion of Section 4.5. Figure 3.1 summarises the flow of the algorithm.

## 4.4 Classification and lower-denominator checks

The method is needed only from $n = 3$ onwards; for $n \leq 2$ the integrals are classical special functions whose $\epsilon$-expansions provide exact checks. Figure 4.1 organises the cases. Reading down each column, the integrals of one and two denominators reduce to Gamma ratios, ${}_2F_1$, and Appell/Lauricella functions, while the three- and four-denominator cases (highlighted) have no usable closed form and are handled by the method. I record the explicit closed forms [109], in the normalisation $I^{(0)}(\epsilon) = 2\pi/(1-2\epsilon)$ for the total angular volume.

*One denominator, massless:*

$$I_j^{(0)}(\epsilon) = I^{(0)}(\epsilon)\,\frac{(2-j-2\epsilon)_j}{2^j(1-j-\epsilon)_j} = 2^{2-j-2\epsilon}\pi^{1-\epsilon}\,\frac{\Gamma(1-j-\epsilon)}{\Gamma(2-j-2\epsilon)}, \tag{4.3}$$

the form derived from first principles in Section 2.10.

*One denominator, massive:*

$$I_j^{(1)}(v_{11};\epsilon) = I^{(0)}(\epsilon)\,{}_2F_1\Big(\tfrac{j}{2},\tfrac{j+1}{2};\tfrac{3}{2}-\epsilon;1-v_{11}\Big). \tag{4.4}$$

*Two denominators, both massless:*

$$I_{j,l}^{(0)}(v_{12};\epsilon) = I^{(0)}(\epsilon)\,\frac{(2-j-l-2\epsilon)_{j+l}}{2^{j+l}(1-j-\epsilon)_j(1-l-\epsilon)_l}\,{}_2F_1\Big(j,l;1-\epsilon;1-\tfrac{v_{12}}{2}\Big), \tag{4.5}$$

the case carried through Chapter 3.

*Two denominators, one massive:* the result is an Appell function of the first kind,

$$I_{j,l}^{(1)}(v_{12},v_{11};\epsilon) = I_l^{(0)}(\epsilon)\,v_{12}^j\,F_1\big(j,1-l-\epsilon,1-l-\epsilon;2-l-2\epsilon;\tau_+,\tau_-\big), \quad \tau_\pm = 1-\frac{1\pm\sqrt{1-v_{11}}}{v_{12}}, \tag{4.6}$$

with $F_1(a,b_1,b_2;c;x,y)=\sum_{m,n\geq 0}\frac{(a)_{m+n}(b_1)_m(b_2)_n}{(c)_{m+n}}\frac{x^m y^n}{m!\,n!}$. normalisation $v_{12}=p_1\cdot p_2/2$ used here. The double-massive two-denominator case is a third-order Lauricella function $F_B^{(3)}$. For $n\geq 3$ no such elementary closed form exists. The all-order result is a multivariable $H$-function that cannot be expanded in $\epsilon$ in practice, and the Mellin–Barnes method gives its Laurent coefficients.

## 4.5 Linear reducibility and polylogarithmic expressibility

Whether step 10 of Algorithm 4.1 terminates in GPLs is decided by linear reducibility [132, 133, 139, 131]. A parametric integral

$$\mathcal{I}=\int_0^1 \mathrm{d}x_1\cdots\mathrm{d}x_m\,\frac{P(\mathbf{x})}{\prod_a Q_a(\mathbf{x})^{r_a}}\prod_b \ln R_b(\mathbf{x}) \tag{4.7}$$

is GPL-expressible in an integration order $x_{\sigma(1)},\ldots,x_{\sigma(m)}$ if, at every step, all the irreducible polynomials that produce poles in the next variable are *linear* in it, $Q_a=A_a(\hat{\mathbf{x}})\,x_{\sigma(k)}+B_a(\hat{\mathbf{x}})$. Each such polynomial then contributes a GPL letter through its root $x_{\sigma(k)}=-B_a/A_a$, and the integration $\int_0^1 \mathrm{d}x\,F(x)/(x-a)\rightsquigarrow G(a,\ldots;1)$ proceeds letter by letter. The criterion requires that on integrating out one variable at a time the denominator always factorises into terms linear in the next variable, so that the poles encountered define admissible letters. When instead an irreducible quadratic survives in the active variable, its roots are algebraic functions of the remaining parameters that cannot serve as GPL letters, and the final integration is blocked, so ordinary GPLs are no longer guaranteed. I examine this obstruction in Section 4.8.

## 4.6 Reduction of the polylogarithms to a fibration basis

The real integrations of step 10 deliver GPLs whose letters depend non-linearly on the remaining variables and which are not in a canonical form [122, 125, 140]. The in-house procedure of Ref. [141] brings them to a unique fibration basis by lowering the weight through differentiation. For a weight-$n$ candidate $G(\vec{a}_n(z);1)$ we write

$$G(\vec{a}_n(z);1)=G(\vec{a}_n(z_0);1)+\int_{z_0}^{z}\mathrm{d}s\,\frac{\partial}{\partial s}G(\vec{a}_n(s);1),\qquad \frac{\partial}{\partial s}G(\vec{a}_n(s);1)=\sum_r R_r(s)\,G(\vec{b}_r(s);\xi_r), \tag{4.8}$$

the derivative being a weight-$(n-1)$ object times a rational kernel $R_r$.

**Algorithm 4.2 (weight reduction):** (1) choose the active variable $z$; (2) differentiate the GPLs whose letters depend non-linearly on $z$; (3) partial-fraction the rational kernels $R_r(z)$; (4) reduce the weight-$(n-1)$ GPLs recursively; (5) move $z$ to the rightmost argument (fibration basis); (6) integrate back in $z$; (7) fix the boundary constant at a regular point $z=z_0$; (8) check numerically before and after.

As a minimal illustration, consider rewriting $F(z)=G\big(\frac{1}{1-z},0;1\big)$, a weight-two GPL whose *first letter depends on* $z$ so that $z$ is not yet a fibration variable, into the basis in which $z$ is the rightmost argument. Following Algorithm 4.2 we differentiate with respect to $z$ (lowering the weight to one and producing a rational kernel), reduce the weight-one piece, and integrate back in $z$, fixing the constant at a convenient point. The reduction

Table 4.1: The Mellin–Barnes and differential-equation routes to the angular master integrals, stage by stage.

| stage | Mellin–Barnes route | differential-equation route |
|---|---|---|
| input | universal angular blocks | full topology after IBP |
| reduction | analytic continuation, residues | canonical-basis search |
| core data | balanced MB integrals | boundary constants |
| output | GPLs (if linearly reducible) | GPLs from canonical system |
| strength | reusable, exposes collinear poles | systematic for whole MI systems |
| weak point | balance/reducibility not guaranteed | basis and boundary search can dominate |

yields

$$F(z) = G(0,1;z) + \frac{\pi^2}{6} = \frac{\pi^2}{6} - \mathrm{Li}_2(z), \tag{4.9}$$

now in the fibration basis with $z$ the rightmost argument. As a check, differentiating the right-hand side reproduces the weight-one kernel $\mathrm{d}F/\mathrm{d}z = G(1;z)/z$, and the value at $z = 0$ fixes the constant $\pi^2/6$. Applied systematically, the procedure reduces an entire result to one basis, in which relations among functions become explicit and the symbol is read off directly. I carry out the manipulations with PolyLogTools [130].

## 4.7 Comparison with the differential-equation route

The same master integrals can be obtained by reverse unitarity, IBP reduction, and canonical differential equations [110, 111, 112, 142, 143, 144]. Table 4.1 contrasts the two routes stage by stage. They are complementary rather than competing: the SIDIS calculation of Chapter 7 is convincing precisely because we carry out both routes and they agree.

## 4.8 Failure modes and the frontier

I now state where the method can break down. Seven obstructions can arise: (i) an explosion in the number of crossed-pole residues during analytic continuation; (ii) the balanced-conversion property not being established for arbitrary $n$ (Proposition 3.2); (iii) the absence of any integration order making all kernels linear; (iv) several square roots that are individually but not simultaneously rationalisable (Figure 4.2); (v) an underlying geometry of positive genus, where elliptic or more general iterated integrals appear [145, 146, 147]; (vi) expression swell, a correct but unwieldy GPL representation before basis reduction; and (vii) numerical branch instability near thresholds. For the families treated in this thesis none of these is fatal: after the stated reductions the three- and four-denominator integrals remain in the GPL class. This does *not* imply that all five-denominator angular integrals do, and the five-denominator frontier, in particular the question of where elliptic structures first appear, is taken up in the outlook of Chapter 9.

## 4.9 MB2MPL Mathematica Package

For a large class of Mellin–Barnes (MB) integrals, it is possible to obtain fully analytic expressions in terms of multiple polylogarithms (MPLs). Such representations are particularly valuable because they reveal the analytic structure of the result and can be

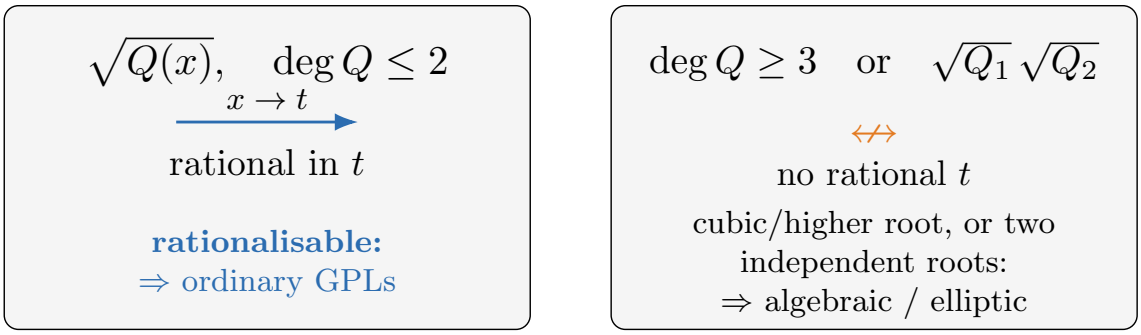



Figure 4.2: The obstruction that bounds the method. A single algebraic square root $\sqrt{Q(x)}$ of the integration variable is rationalisable by a change of variables $x \to t$ only when $Q$ is at most quadratic, $\deg Q \le 2$; the substitution then leaves rational integrands and hence ordinary Goncharov polylogarithms. If $Q$ is cubic or of higher degree the curve $y^2 = Q(x)$ has positive genus (it is elliptic for $\deg Q = 3, 4$) and cannot be rationalised, and likewise two or more algebraically independent square roots cannot in general be rationalised simultaneously. In either case the result leaves the polylogarithmic class for algebraic or elliptic generalisations.

evaluated efficiently with existing numerical libraries. However, deriving these expressions manually is often a highly technical and time-consuming task, involving contour deformations, residue summations, analytic continuations, and the identification of the resulting special functions.

To facilitate this process, a Mathematica package currently under development by our research group, MB2MPL, has been designed to automate the conversion of Mellin–Barnes representations into expressions involving multiple polylogarithms whenever such a representation exists within its range of applicability. Starting from an MB integral, the package systematically performs the necessary analytic manipulations and produces compact expressions in terms of MPLs that are immediately suitable for both symbolic manipulation and fast numerical evaluation.

Although no algorithm can treat every possible Mellin–Barnes representation, MB2MPL covers a broad class of integrals that frequently arise in perturbative quantum field theory. Its primary goal is to bridge the gap between Mellin–Barnes representations and the polylogarithmic functions commonly used in modern precision calculations, thereby providing an efficient and user-friendly tool for obtaining analytic results. At the time of writing, the package is in its final stages of development and is expected to become publicly available in the near future.

## Bridge to the next chapter

Chapter 5 now applies this machinery to the three- and four-denominator families, where the conditions of this chapter become explicit: definite Mellin–Barnes representations, seventeen- and eleven-letter alphabets, partial-fraction formulae for the massive cases, recursion relations, and validation tables.

# Chapter 5

# Three- and Four-Denominator Angular Integral Families

## Contents


5.1 Definitions and scope . . . . . 47
5.2 Three denominators, massless . . . . . 48
5.3 Three denominators, single-massive . . . . . 49
5.4 Partial-fraction reduction: the two-point splitting lemma . . . . . 49
5.5 Recursion relations . . . . . 50
5.6 Four denominators, massless . . . . . 51
5.7 Four denominators, single- and multi-massive . . . . . 52
5.8 Validation, symmetries, and performance . . . . . 52
5.9 Summary of the family data . . . . . 52

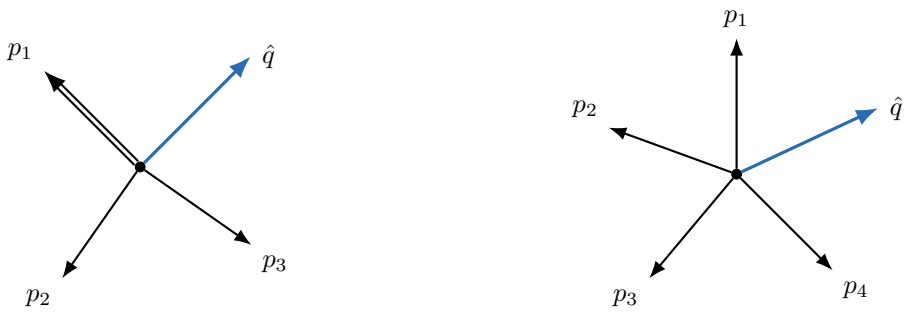

This chapter presents the central new results of the thesis: the analytic evaluation of the three- and four-denominator angular integral families. For each family I give the Mellin–Barnes representation, enough of the derivation to make the result reproducible, the polylogarithmic function space, representative closed forms, and the partial-fraction and recursion relations that organise the massive cases. The chapter closes with the numerical and structural validation.

## 5.1 Definitions and scope

The object computed is the angular family

$$\Omega_{j_1,\dots,j_n}(\{p_i\},d) = \int \mathrm{d}\Omega_{d-1}(q)\,\frac{1}{(p_1\cdot q)^{j_1}\cdots(p_n\cdot q)^{j_n}}, \qquad d=4-2\epsilon, \tag{5.1}$$

in the invariant variables $v_{kl} = p_k\cdot p_l/2$ $(k\neq l)$, $v_{kk}=p_k^2/4$. Throughout I include the normalisation $C_\epsilon = 2^{-1+2\epsilon}\pi^\epsilon\,\Gamma(1-2\epsilon)/\Gamma(1-\epsilon)$ and compute $I^{(m)}_{j_1,\dots,j_n} = C_\epsilon\,\Omega^{(m)}_{j_1,\dots,j_n}$, the superscript $(m)$ counting the massive legs. Figure 5.1 fixes the geometry. The cases $n=3,4$ are treated here: the massless and single-massive integrals are computed directly through their Mellin–Barnes representation, and the multi-massive cases are reduced to the single-massive one by partial fractioning (Section 5.4) [84, 141].




(a) three denominators ($p_1$ massive) (b) four denominators (all massless)

Figure 5.1: Geometric structure of the angular integrals. The integration runs over the direction $\hat{q}$ (blue) of the massless reference vector; the denominators are the dot products $(p_i \cdot q)$ with the fixed external vectors $p_i$, a massive leg drawn as a doubled line. (a) the three-denominator family with one massive leg; (b) the four-denominator massless family.

**Computational strategy:** Every family in this chapter is treated by the same workflow, which I state once so that the case-by-case presentation reads as variations on a single theme. (i) Start from the Somogyi Mellin–Barnes representation of Chapter 3. (ii) Analytically continue in $\epsilon$ and convert the balanced coefficient integrals to real parametric integrals. (iii) Integrate to Goncharov polylogarithms and identify the symbol alphabet, that is, the function space. (iv) Reduce to a fibration basis and, for the massive cases, organise the results through the partial-fraction and recursion *structure relations* of Sections 5.4 and 5.5. (v) Validate numerically and by permutation symmetry. The denominator number controls the number of Mellin–Barnes folds and hence the difficulty, while the mass pattern controls whether square-root letters appear.

## 5.2 Three denominators, massless

For foundational, standard, and representative treatments directly relevant to the material discussed in this section, see [137, 138].

The massless three-denominator integral is the three-fold Mellin–Barnes integral

$$\Omega_{j_1,j_2,j_3} = \frac{2^{2-j-2\epsilon}\pi^{1-\epsilon}}{\Gamma(j_1)\Gamma(j_2)\Gamma(j_3)\Gamma(2-j-2\epsilon)} \int_{-i\infty}^{+i\infty} \frac{\mathrm{d}z_{12}\,\mathrm{d}z_{13}\,\mathrm{d}z_{23}}{(2\pi i)^3} \prod_{a<b} \Gamma(-z_{ab})\, v_{ab}^{z_{ab}} \times \Gamma(j_1+z_{12}+z_{13})\,\Gamma(j_2+z_{12}+z_{23})\,\Gamma(j_3+z_{13}+z_{23})\,\Gamma(1-j-\epsilon-z), \quad (5.2)$$

with $z = z_{12}+z_{13}+z_{23}$, $j = j_1+j_2+j_3$, and contours parallel to the imaginary axis. For $j_i = 1$ the analytic continuation of Chapter 4 produces four distinct Mellin–Barnes integrals at $\mathcal{O}(\epsilon)$ and eight at $\mathcal{O}(\epsilon^2)$ (four of them genuinely new), each balanced and integrated to Goncharov polylogarithms [84]. The result is a Laurent series

$$I^{(0)}_{1,1,1} = \frac{1}{\epsilon} I^{(0),-1}_{1,1,1} + I^{(0),0}_{1,1,1} + \epsilon\, I^{(0),1}_{1,1,1} + \epsilon^2\, I^{(0),2}_{1,1,1} + \mathcal{O}(\epsilon^3), \quad (5.3)$$

whose leading terms are

$$I^{(0),-1}_{1,1,1} = -\frac{\pi}{4}\Big(\frac{1}{v_{12}v_{13}} + \frac{1}{v_{12}v_{23}} + \frac{1}{v_{13}v_{23}}\Big), \quad (5.4)$$

$$I^{(0),0}_{1,1,1} = \frac{\pi}{4}\Bigg[\Big(\tfrac{1}{v_{12}v_{13}} + \tfrac{1}{v_{12}v_{23}} - \tfrac{1}{v_{13}v_{23}}\Big)\ln v_{12} + \Big(\tfrac{1}{v_{12}v_{13}} - \tfrac{1}{v_{12}v_{23}} + \tfrac{1}{v_{13}v_{23}}\Big)\ln v_{13} + \Big(-\tfrac{1}{v_{12}v_{13}} + \tfrac{1}{v_{12}v_{23}} + \tfrac{1}{v_{13}v_{23}}\Big)\ln v_{23}\Bigg]. \tag{5.5}$$

At higher orders the coefficients become weight-two and weight-three Goncharov polylogarithms. The full coefficient-level GPL representation is supplied in the ancillary files `3prop0mass.m` and `cofs0mass.m`.

## 5.3 Three denominators, single-massive

With $p_1^2 \neq 0$ the representation gains a fourth variable,

$$\begin{aligned}\Omega_{1,1,1}(v_{11},\{v_{ij}\}) = \frac{2^{-1-2\epsilon}\pi^{1-\epsilon}}{\Gamma(-1-2\epsilon)}\int_{-i\infty}^{+i\infty}\frac{\mathrm{d}z_{11}\mathrm{d}z_{12}\mathrm{d}z_{13}\mathrm{d}z_{23}}{(2\pi i)^4}\,\Gamma(-z_{11})\Gamma(-z_{12})\Gamma(-z_{13})\Gamma(-z_{23}) \\ \times\,\Gamma(1+2z_{11}+z_{12}+z_{13})\,\Gamma(1+z_{12}+z_{23})\,\Gamma(1+z_{13}+z_{23}) \\ \times\,\Gamma(-2-\epsilon-z_{11}-z_{12}-z_{13}-z_{23})\,v_{11}^{z_{11}}v_{12}^{z_{12}}v_{13}^{z_{13}}v_{23}^{z_{23}}.\end{aligned} \tag{5.6}$$

After continuation to $\mathcal{O}(\epsilon)$ eleven distinct Mellin–Barnes integrals appear. Ten contain no square root over the integration variables, while one requires the rationalisation $x \mapsto (b+2c\eta)/(c\eta^2-a)$ of a root $\sqrt{ax^2+bx+c}$. The leading term is

$$I^{(1),-1}_{1,1,1} = -\frac{\pi}{4}\Big(\frac{1}{v_{12}v_{23}} + \frac{1}{v_{13}v_{23}}\Big), \tag{5.7}$$

and the finite part has the structure

$$\begin{aligned}I^{(1),0}_{1,1,1} = {}& \frac{\pi}{4\,(v_{12}v_{13}-v_{11}v_{23})}G\Big(\frac{v_{11}v_{23}}{v_{11}v_{23}-v_{12}v_{13}},1\Big) \\ &+ \frac{\pi v_{12}}{4v_{23}\,(v_{11}v_{23}-v_{12}v_{13})}G\Big(\frac{v_{11}v_{23}}{v_{11}v_{23}-v_{12}v_{13}},1\Big) \\ &+ \frac{\pi v_{13}}{4v_{23}\,(v_{11}v_{23}-v_{12}v_{13})}G\Big(\frac{v_{11}v_{23}}{v_{11}v_{23}-v_{12}v_{13}},1\Big) \\ &- \frac{\pi\log(v_{11})}{4v_{12}v_{23}} - \frac{\pi\log(v_{11})}{4v_{13}v_{23}} + \frac{\pi\log(v_{12})}{2v_{12}v_{23}} + \frac{\pi\log(v_{13})}{2v_{13}v_{23}}.\end{aligned} \tag{5.8}$$

## 5.4 Partial-fraction reduction: the two-point splitting lemma

To handle the multi-massive cases without computing each from scratch, we use a *structure relation*: a partial-fraction identity that reduces every multi-massive integral to the single-massive basis already computed. We derive it as follows. Given two denominators $D_a = p_a\cdot q$, $D_b = p_b\cdot q$, define an effective leg

$$p_* = \bar\lambda_{ab}\,p_a + \lambda_{ab}\,p_b, \qquad D_* = \bar\lambda_{ab}\,D_a + \lambda_{ab}\,D_b, \qquad \bar\lambda_{ab} = 1-\lambda_{ab}, \tag{5.9}$$

and fix $\lambda_{ab}$ by demanding that $p_*$ be *massless*,

$$0 = \frac{p_*^2}{4} = \bar{\lambda}_{ab}^2 v_{aa} + \lambda_{ab}\bar{\lambda}_{ab} v_{ab} + \lambda_{ab}^2 v_{bb} \implies \lambda_{ab} = \frac{2v_{aa} - v_{ab} - \sqrt{v_{ab}^2 - 4v_{aa}v_{bb}}}{2v_{aa} - 2v_{ab} + 2v_{bb}}. \tag{5.10}$$

Since $D_*$ is a linear combination of $D_a$ and $D_b$, the elementary identity $1 = \bar{\lambda}_{ab} + \lambda_{ab}$ together with $D_* = \bar{\lambda}_{ab} D_a + \lambda_{ab} D_b$ gives the *splitting lemma*

$$\frac{1}{D_a D_b} = \frac{\lambda_{ab}}{D_a D_*} + \frac{\bar{\lambda}_{ab}}{D_b D_*}, \tag{5.11}$$

which replaces a pair of massive denominators by two pairs, each containing the massless $D_*$. Iterating (5.11) for higher powers yields

$$\frac{1}{D_a^j D_b^k} = \sum_{n=0}^{j-1} \binom{k-1+n}{k-1} \frac{\lambda_{ab}^k \bar{\lambda}_{ab}^n}{D_a^{j-n} D_*^{k+n}} + \sum_{n=0}^{k-1} \binom{j-1+n}{j-1} \frac{\lambda_{ab}^n \bar{\lambda}_{ab}^j}{D_b^{k-n} D_*^{j+n}}. \tag{5.12}$$

Applied to a fully massive angular integral one denominator pair at a time, this expresses it through single-massive integrals. For the three-denominator double-massive case,

$$\begin{aligned} &I^{(2)}_{j,k,l}(v_{11}, v_{22}, v_{12}, v_{13}, v_{23}) = \\ &\sum_{n=0}^{j-1} \binom{k-1+n}{k-1} \lambda_\pm^k (1-\lambda_\pm)^n I^{(1)}_{j-n,k+n,l}(v_{11}, v_{13}^\pm, v_{13}, v_{33}^\pm) \\ &+ \sum_{n=0}^{k-1} \binom{j-1+n}{j-1} \lambda_\pm^n (1-\lambda_\pm)^j I^{(1)}_{k-n,j+n,l}(v_{22}, v_{23}^\pm, v_{23}, v_{33}^\pm). \end{aligned} \tag{5.13}$$

with

$$\lambda_\pm = \frac{v_{12} - v_{11} \pm \sqrt{v_{12}^2 - v_{11}v_{22}}}{2v_{12} - v_{11} - v_{22}}, \quad v_{13}^\pm = (1-\lambda_\pm)v_{11} + \lambda_\pm v_{12}, \quad v_{23}^\pm = (1-\lambda_\pm)v_{12} + \lambda_\pm v_{22}. \tag{5.14}$$

**Proposition 5.1** (Merged scalar products)**.** *When the pair $(a, b)$ is merged into the effective massless leg $p_* = \bar{\lambda}_{ab} p_a + \lambda_{ab} p_b$, the induced scalar products are*

$$v_{i,*} = \bar{\lambda}_{ab}\, v_{ia} + \lambda_{ab}\, v_{ib} \quad (i \notin \{a,b\}), \quad v_{a,*} = 2\bar{\lambda}_{ab}\, v_{aa} + \lambda_{ab}\, v_{ab}, \quad v_{b,*} = \bar{\lambda}_{ab}\, v_{ab} + 2\lambda_{ab}\, v_{bb}, \tag{5.15}$$

*the factor $2v_{aa}$ (resp. $2v_{bb}$) entering only when the free index coincides with a merged leg (because $v_{aa} = p_a^2/4$ while $v_{i,*}$ carries $p_a^2/2$). For two effective legs $*, \dagger$ the rule iterates bilinearly, $v_{*,\dagger} = \sum_{r\in\{a,b\}} \sum_{s\in\{c,d\}} \alpha_r \beta_s\, w_{rs}$ with $w_{rs} = v_{rs}$ $(r \neq s)$, $w_{rr} = 2v_{rr}$.*

## 5.5 Recursion relations

Differentiating the Mellin–Barnes representation with respect to a scalar product relates integrals of different denominator powers, $\partial_{v_{kl}} I^{(m)}_{j_1,\dots,j_n} = \sum_{\vec{\imath}} C^{\vec{\imath}}_{kl}(\{v\}, \epsilon)\, I^{(m)}_{\vec{\imath}}$. We derive one such relation in full for the single-massive three-denominator family, with leg 1 massive ($v_{11} \neq 0$), by differentiating with respect to the self-product $v_{11}$. Writing the integrand of $I_{j,k,l}$ as $\Phi_{j,k,l}(z)$, the operator $v_{11}\partial_{v_{11}}$ brings down a factor $z_{11}$, and the gamma-function identity $z_{11}\Gamma(-z_{11}) = -\Gamma(1-z_{11})$ followed by $\Gamma(x+1) = x\,\Gamma(x)$ and a contour shift re-

expresses each term as an integral with raised denominator powers. Collecting the terms produces

$$\begin{aligned} 0 = {} & (j+k+l-1+2\epsilon)\, I_{j,k,l} - (2j+k+l+2\epsilon)\, I_{1+j,k,l} + v_{11}(j+1)\, I_{2+j,k,l} \\ & - l\, I_{j,k,1+l} - k\, I_{j,1+k,l} + l\, v_{13}\, I_{1+j,k,1+l} + k\, v_{12}\, I_{1+j,1+k,l}. \end{aligned} \tag{5.16}$$

The remaining five relations of the family are obtained the same way and are collected, with their rational coefficients, in the ancillary file `recursion.m`. Together they make the unit-power integral $I_{1,1,1}$ the only independent quantity.

## 5.6 Four denominators, massless

The massless four-denominator integral is the six-fold Mellin–Barnes integral

$$\begin{aligned} \Omega_{1,1,1,1} = {} & \frac{2^{-2\epsilon-2}\pi^{1-\epsilon}}{\Gamma(-2\epsilon-2)} \int_{-i\infty}^{+i\infty} \frac{\mathrm{d}z_{12}\mathrm{d}z_{13}\mathrm{d}z_{14}\mathrm{d}z_{23}\mathrm{d}z_{24}\mathrm{d}z_{34}}{(2\pi i)^6} \prod_{k<l} \Gamma(-z_{kl})\, v_{kl}^{z_{kl}} \\ & \times \Gamma(1+z_{12}+z_{13}+z_{14})\Gamma(1+z_{12}+z_{23}+z_{24})\Gamma(1+z_{13}+z_{23}+z_{34}) \\ & \times \Gamma(1+z_{14}+z_{24}+z_{34})\, \Gamma(-\epsilon-3-\textstyle\sum_{k<l} z_{kl}), \end{aligned} \tag{5.17}$$

with imaginary contours. Continuation to the finite order and conversion to real form yields ten parametric integrals over $\{x_i, v_1\}$ with $v_1 \in [0, v_{12}]$, $x_i \in [0,1]$; two representatives (more are presented in Section B.2) are

$$I_1 = \int \mathrm{d}v_1\, \mathrm{d}x_1\, \frac{\pi v_{14} x_1}{8 v_{13} v_{34} \big(v_{12}^2 v_{34} \bar{x}_1 - v_1 v_{14} v_{23} x_1\big)}, \tag{5.18}$$

$$I_{10} = \int \mathrm{d}x_1 \mathrm{d}x_2 \mathrm{d}x_3\, \frac{-\pi v_{12} v_{13} v_{14} v_{23} v_{24} v_{34}}{4\big(v_{12} v_{14} v_{23} v_{34} x_3 \bar{x}_1 + v_{13} v_{24} (v_{14} v_{23} x_1 \bar{x}_2 + v_{12} v_{34} x_2 \bar{x}_3)\big)^2}, \tag{5.19}$$

with $\bar{x}_i = 1 - x_i$. The number ten reflects the distinct denominator structures generated by the six Mellin–Barnes variables after the analytic continuation, and each is linearly reducible in a suitable order. Integrating them by the method of Chapter 4 produces weight-two Goncharov polylogarithms whose arguments form a seventeen-element alphabet. This alphabet has a clear structure: the first seven letters are rational functions of the products $v_{ij}$, while the remaining ten come in five $\mp$ pairs built from the square root $\sqrt{Y_1}$ of the Gram-like combination of the kinematics. This square root is the algebraic feature that distinguishes the four-denominator case from the lower ones. Explicitly, the alphabet is

$$\begin{aligned} & l_1 = 0,\ l_2 = 1,\ l_3 = \tfrac{v_{13}v_{24}}{X_4},\ l_4 = \tfrac{v_{14}v_{23}}{X_5},\ l_5 = \tfrac{v_{13}v_{24}}{X_6},\ l_6 = -\tfrac{v_{12}v_{34}}{X_5},\ l_7 = -\tfrac{v_{12}v_{34}}{X_6}, \\ & l_{8,13} = \tfrac{X_1 \mp \sqrt{Y_1}}{2v_{14}v_{23}},\ l_{9,14} = \tfrac{X_1 \mp \sqrt{Y_1}}{2v_{13}v_{24}},\ l_{10,15} = \tfrac{X_2 \mp \sqrt{Y_1}}{2v_{14}v_{23}},\ l_{11,16} = \tfrac{X_3 \mp \sqrt{Y_1}}{2v_{13}v_{24}},\ l_{12,17} = \tfrac{X_3 \mp \sqrt{Y_1}}{2v_{12}v_{34}}, \end{aligned} \tag{5.20}$$

with

$$\begin{aligned} & X_1 = v_{14}v_{23} + v_{13}v_{24} - v_{12}v_{34}, \quad X_2 = v_{14}v_{23} - v_{13}v_{24} + v_{12}v_{34}, \quad X_3 = -v_{14}v_{23} + v_{13}v_{24} + v_{12}v_{34}, \\ & X_4 = -v_{14}v_{23} + v_{13}v_{24}, \quad X_5 = v_{14}v_{23} - v_{12}v_{34}, \quad X_6 = v_{13}v_{24} - v_{12}v_{34}, \\ & Y_1 = v_{14}^2 v_{23}^2 - 2v_{14}v_{23}(v_{13}v_{24} + v_{12}v_{34}) + X_6^2. \end{aligned} \tag{5.21}$$

The single root $\sqrt{Y_1}$ is rationalisable, so the result is an ordinary polylogarithm. The pole is fully symmetric under the permutation group $S_4$ of the four legs,

$$I^{(0),-1}_{1,1,1,1} = -\frac{\pi}{8\cdot 4!}\sum_{\sigma\in S_4}\frac{v_{\sigma(1)\sigma(2)}v_{\sigma(1)\sigma(3)}v_{\sigma(2)\sigma(3)}}{\prod_{1\le i<j\le 4}v_{ij}}. \tag{5.22}$$

The Mellin–Barnes derivation breaks this permutation symmetry at every intermediate stage, through the choice of integration order and partial-fraction channel, and the symmetry is restored only in the final answer. It is therefore a non-trivial check on the result.

## 5.7 Four denominators, single- and multi-massive

With one massive leg the representation is a seven-fold Mellin–Barnes integral. Its real conversion yields *fifteen* integrals $I_i = \int \mathrm{d}\mu_i\, A_i/B_i$, $i = 1,\dots,15$, integrating again to weight-two GPLs over the eleven-letter alphabet

$$\begin{aligned}
&l^{(1)}_1 = \tfrac{v_{11}v_{23}}{v_{12}v_{13}},\ l^{(1)}_2 = \tfrac{v_{11}v_{23}}{v_{11}v_{23}-v_{12}v_{13}},\ l^{(1)}_3 = \tfrac{v_{11}v_{24}}{v_{11}v_{24}-v_{12}v_{14}},\ l^{(1)}_4 = \tfrac{v_{13}v_{24}}{v_{13}v_{24}-v_{14}v_{23}},\\
&l^{(1)}_5 = \tfrac{v_{11}v_{14}v_{23}-v_{11}v_{13}v_{24}}{v_{12}v_{13}v_{14}-v_{11}v_{13}v_{24}},\ l^{(1)}_6 = \tfrac{v_{11}v_{34}}{v_{11}v_{34}-v_{13}v_{14}},\ l^{(1)}_7 = \tfrac{v_{12}v_{34}}{v_{12}v_{34}-v_{14}v_{23}},\ l^{(1)}_8 = \tfrac{v_{12}v_{34}}{v_{12}v_{34}-v_{13}v_{24}},\\
&l^{(1)}_9 = \tfrac{v_{11}v_{14}v_{23}-v_{11}v_{12}v_{34}}{v_{12}v_{13}v_{14}-v_{11}v_{12}v_{34}},\quad l^{(1)}_{10,11} = \frac{Z^{(1)}_{1,2}}{2(v_{12}v_{14}-v_{11}v_{24})(v_{13}v_{14}-v_{11}v_{34})},
\end{aligned} \tag{5.23}$$

with $Z^{(1)}_{1,2}$ the two roots of the relevant quadratic. The finite part is symmetric under the $S_3$ permutations of the three massless legs. The double-, triple- and fully massive four-denominator integrals follow from the single-massive one by iterating the merge of Proposition 5.1.

## 5.8 Validation, symmetries, and performance

Every result is checked in two independent ways already at this stage. *Structurally*, the finite parts respect the permutation symmetries,

$$I^{(0),0}_{1,1,1,1}(\{v_{\sigma(i)\sigma(j)}\}) = I^{(0),0}_{1,1,1,1}(\{v_{ij}\})\ (\sigma\in S_4),\qquad I^{(1),0}_{1,1,1,1}(1;\sigma) = I^{(1),0}_{1,1,1,1}(1)\ (\sigma\in S_3), \tag{5.24}$$

which the Mellin–Barnes derivation breaks at intermediate stages and which are therefore non-trivial checks. *Numerically*, we compare the GPL results with direct evaluation of the original Mellin–Barnes integrals using MB.m [121] and GiNaC through PolyLogTools. Figure 5.2 and Table 5.1 show the agreement, which holds to the quoted precision. The evaluation time drops from roughly half an hour per phase-space point for the direct integration to about one second for the optimised GPL expressions. The results also agree, where they overlap, with independent calculations [111, 110].

## 5.9 Summary of the family data

The complete results, namely the real-integral lists, GPL coefficients, alphabets, and the corrected partial-fraction scalar products, are provided in the ancillary files `3prop0mass.m`, `cofs0mass.m`, `3prop1mass.m`, `cofs1mass.m`, `recursion.m`, `massless_ep0.m`, `one_mass_ep0.m`, and the evaluation notebook `main.nb`, mapped in Section A.2.

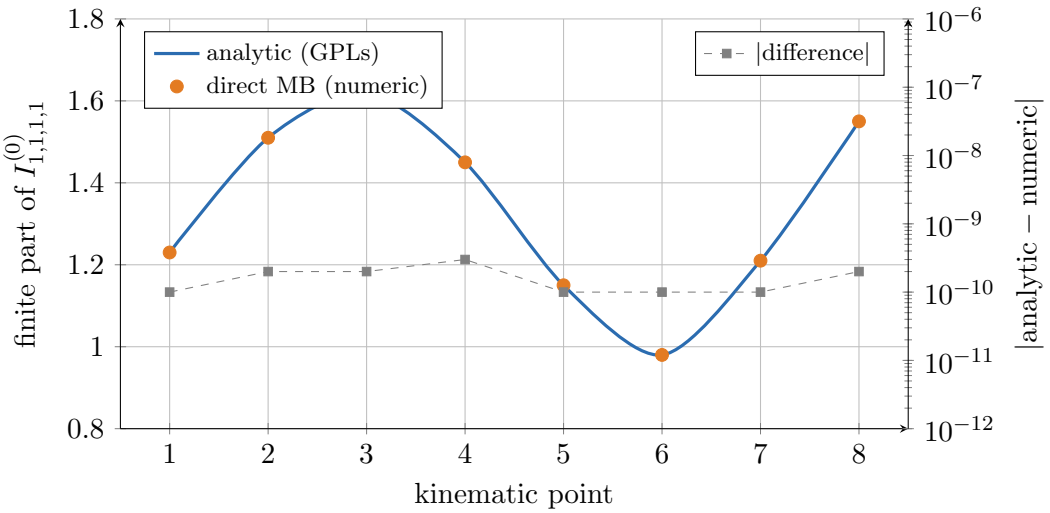



Figure 5.2: Validation of the analytic four-denominator massless result against direct numerical Mellin–Barnes evaluation, at eight sample kinematic points. The analytic GPL result (blue) and the numerical evaluation (orange markers) coincide; their absolute difference (grey, right-hand logarithmic axis) is at the $10^{-10}$ level set by the numerical precision. (Values illustrative of the comparison reported in Ref. [141].)

Table 5.1: Representative comparison of the analytic GPL result against direct numerical Mellin–Barnes integration for the four-denominator integrals, at the kinematic points (scalar products $v_{ij}$) of Ref. [141]. The analytic and direct evaluations agree to the quoted precision.

| case | kinematic point | $I^{(\cdot),-1}/\epsilon + I^{(\cdot),0}$ |
|---|---|---|
| massless | $\{0.45, 0.40, 0.35, 0.30, 0.35, 0.40\}$ | $-21.3574/\epsilon - 30.7399$ |
| massless | $\{0.10, 0.15, 0.30, 0.25, 0.115, 0.35\}$ | $-566.329/\epsilon - 286.299$ |
| single-massive | $\{0.11, 0.45, 0.40, 0.35, 0.30, 0.35, 0.40\}$ | $-16.443/\epsilon - 24.507$ |
| single-massive | $\{0.15, 0.10, 0.15, 0.30, 0.25, 0.115, 0.35\}$ | $-520.036/\epsilon - 199.033$ |

# Chapter 6

# Semi-Inclusive Deep-Inelastic Scattering

## Contents


6.1 Kinematics and scope . . . . . 54
6.2 The hadronic tensor and structure functions . . . . . 55
6.3 Collinear factorisation and coefficient functions . . . . . 55
6.4 Perturbative channels through NNLO . . . . . 56
6.5 The tagged-parton constraint . . . . . 57
6.6 From channels to master integrals . . . . . 58
6.7 State of the art . . . . . 58
6.8 What this thesis supplies . . . . . 59


Chapter 1 introduced semi-inclusive deep-inelastic scattering (SIDIS) and its role at the Electron–Ion Collider. In this chapter we develop the field-theoretic framework in detail, so that the master integrals computed in Chapter 7 can be placed in their physical context. I work throughout with one-photon exchange in QCD. The electroweak corrections form a separate strand, developed in Chapter 8.

## 6.1 Kinematics and scope

The process is [148]

$$\ell(l) + N(P) \to \ell(l') + h(P_h) + X, \qquad q = l - l', \qquad Q^2 = -q^2 > 0, \tag{6.1}$$

with the standard variables (Figure 1.3)

$$x_B = \frac{Q^2}{2P\cdot q}, \qquad y = \frac{P\cdot q}{P\cdot l}, \qquad z_h = \frac{P\cdot P_h}{P\cdot q}, \qquad P_{hT}, \tag{6.2}$$

where $P_{hT}$ is the transverse momentum of the observed hadron relative to the photon axis. At the partonic level, with the struck parton $p_1 = \xi P$ and the fragmenting parton $P_h = \eta p_2$, the relevant variables are

$$x' = \frac{Q^2}{2p_1\cdot q} = \frac{x_B}{\xi}, \qquad z' = \frac{p_1\cdot p_2}{p_1\cdot q} = \frac{z_h}{\eta}, \qquad 0 < x', z' < 1, \tag{6.3}$$

Table 6.1: Hadronic and partonic variables, and the momentum fractions linking them.

| quantity | definition | partonic counterpart |
|---|---|---|
| Bjorken $x_B$ | $Q^2/(2P\cdot q)$ | $x' = x_B/\xi$ |
| hadron fraction $z_h$ | $P\cdot P_h/P\cdot q$ | $z' = z_h/\eta$ |
| inelasticity $y$ | $P\cdot q/P\cdot l$ | – |
| virtuality $Q^2$ | $-q^2$ | hard scale |

which are the arguments of the partonic coefficient functions. Table 6.1 collects the mapping between hadronic and partonic variables.

## 6.2 The hadronic tensor and structure functions

The cross section factorises into a leptonic and a hadronic part. The leptonic tensor for an unpolarised lepton is

$$L^{\mu\nu} = 2\big(l^\mu l'^\nu + l^\nu l'^\mu - g^{\mu\nu}\, l\cdot l'\big) + 2i\lambda_\ell\, \epsilon^{\mu\nu\alpha\beta} l_\alpha q_\beta, \tag{6.4}$$

and the semi-inclusive hadronic tensor is

$$W^{\mu\nu}(P,q,P_h) = \frac{1}{4\pi}\sum_X \int \mathrm{d}\Pi_X\, (2\pi)^4 \delta^{(4)}(P+q-P_h-P_X)\, \langle P|J^\mu(0)|hX\rangle\langle hX|J^\nu(0)|P\rangle, \tag{6.5}$$

where

$$J^\mu(x) = \sum_q e_q \bar\psi_q(x)\gamma^\mu\psi_q(x). \tag{6.6}$$

is the electromagnetic current and the sum is running over the unobserved remnant $X$. For the unpolarized SIDIS process, the hadronic tensor may be decomposed into invariant structure functions.The general decomposition is

$$W^{\mu\nu} = \left(-g^{\mu\nu} + \frac{q^\mu q^\nu}{q^2}\right) F_1 + \frac{\hat P^\mu \hat P^\nu}{P\cdot q} F_2 - i\epsilon^{\mu\nu\alpha\beta}\frac{q_\alpha P_\beta}{2P\cdot q} F_3, \tag{6.7}$$

where

$$\hat P^\mu = P^\mu - \frac{P\cdot q}{q^2} q^\mu. \tag{6.8}$$

The structure functions $F_i$ depend on $F_i^h = F_i(x_B, z_h, Q^2)$. For polarized SIDIS additional tensors involving the spin vector $S^\mu$ arise:

$$\Delta W^{\mu\nu} = \frac{i}{P\cdot q}\epsilon^{\mu\nu\alpha\beta} q_\alpha \left[S_\beta\, g_1 + \left(S_\beta - \frac{S\cdot q}{P\cdot q} P_\beta\right) g_2\right]. \tag{6.9}$$

The structure functions represent the dynamical information accessible experimentally.

## 6.3 Collinear factorisation and coefficient functions

The perturbative calculation rests on the separation of scales [41, 42, 149, 30, 150, 151, 152, 153, 154, 155, 156, 157, 158, 159, 160]. When $Q$ is far above the confinement scale, the short-distance hard scattering of the struck parton, which is calculable in perturbative

Table 6.2: The singularities of the NNLO SIDIS calculation and where each is absorbed or cancelled.

| singularity | resolution |
|---|---|
| ultraviolet | coupling renormalisation |
| soft (infrared) | cancels between real and virtual contributions (KLN) |
| initial-state collinear | mass factorisation into parton distributions |
| final-state collinear | mass factorisation into fragmentation functions |

QCD, decouples from the long-distance, non-perturbative dynamics of the nucleon and of hadron formation. The factorisation theorem makes this precise: in the collinear regime the structure functions factorise into parton distributions, fragmentation functions, and perturbative coefficient functions,

$$F_i^h(x_B, z_h, Q^2) = \sum_{a,b} \int_{x_B}^1 \frac{\mathrm{d}\xi}{\xi} \int_{z_h}^1 \frac{\mathrm{d}\eta}{\eta}\, f_{a/N}(\xi, \mu_F)\, D_{h/b}(\eta, \mu_F)\, C_{i,ab}\Big(\tfrac{x_B}{\xi}, \tfrac{z_h}{\eta}, \tfrac{Q^2}{\mu_F^2}, \tfrac{\mu_R^2}{\mu_F^2}, \alpha_s(\mu_R)\Big), \tag{6.10}$$

the coefficient functions admitting the expansion

$$C_{i,ab} = C_{i,ab}^{(0)} + a_s\, C_{i,ab}^{(1)} + a_s^2\, C_{i,ab}^{(2)} + \mathcal{O}(a_s^3). \qquad a_s = \frac{\alpha_s(\mu_R)}{2\pi}, \tag{6.11}$$

The coefficient functions are rendered finite by mass factorisation,

$$C_{i,ab} = \sum_{c,d} \Gamma^{-1}_{ac} \otimes_x \hat{C}_{i,cd} \otimes_z (\tilde{\Gamma})^{-1}_{db}, \tag{6.12}$$

in which the transition functions $\Gamma$ absorb the initial-state collinear singularities into the parton distributions and $\tilde{\Gamma}$ the final-state collinear singularities into the fragmentation functions. The kernels of the transition functions are the Altarelli–Parisi splitting functions, so the same renormalisation *induces* the DGLAP evolution of the distributions. The factorisation scale $\mu_F$ separates the perturbative coefficient from the non-perturbative distributions, and the renormalisation scale $\mu_R$ enters through $\alpha_s$. Physical observables are independent of both, order by order.

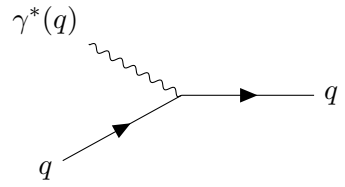
The remaining singularities are infrared. Infrared safety requires that a physical observable be insensitive to the emission of unresolvably soft or collinear partons. By the Kinoshita–Lee–Nauenberg theorem the soft singularities of the virtual loops then cancel against those of the real emissions when the two are combined for such an observable, exactly as illustrated for the generic NNLO contributions in Figure 1.9. For this reason one computes infrared-finite coefficient functions rather than the separately divergent partonic amplitudes. The various singularities and their resolution are summarised in Table 6.2.

## 6.4 Perturbative channels through NNLO

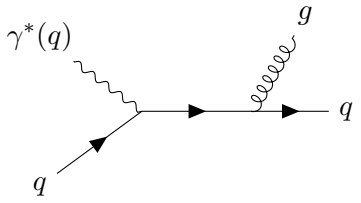
The coefficient functions receive contributions from a growing set of partonic channels (Table 6.3, Figure 6.1) [161, 162, 163, 164]. At leading order only $\gamma^* q \to q$ contributes. At NLO the real channels $\gamma^* q \to qg$ and $\gamma^* g \to q\bar{q}$ appear, together with the one-loop virtual correction to the Born process. At NNLO three classes enter: the two-loop double-virtual correction; the one-loop real–virtual corrections to the single-emission channels; and the

Table 6.3: Partonic channels contributing to the SIDIS coefficient functions through NNLO. "$V$" denotes loop (virtual) corrections, "$R$" extra real emission.

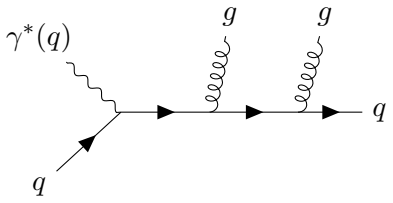
| order | type | channels |
|---|---|---|
| LO | Born | $\gamma^* q \to q$ |
| NLO | $R$ | $\gamma^* q \to qg,\ \ \gamma^* g \to q\bar{q}$ |
| NLO | $V$ | $\gamma^* q \to q$ (one loop) |
| NNLO | $VV$ | $\gamma^* q \to q$ (two loop) |
| NNLO | $RV$ | $\gamma^* q \to qg,\ \ \gamma^* g \to q\bar{q}$ (one loop) |
| NNLO | $RR$ | $\gamma^* q \to qgg,\ \ \gamma^* q \to q\,q'\bar{q}',\ \ \gamma^* g \to q\bar{q}g$ |



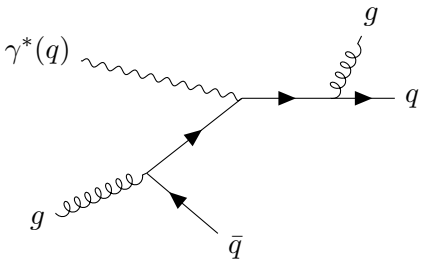

(a) LO: $\gamma^* q \to q$




(b) NLO real: $\gamma^* q \to qg$




(c) NNLO double-real: $\gamma^* q \to qgg$




(d) NNLO double-real: $\gamma^* g \to q\bar{q}g$

Figure 6.1: Representative partonic channels contributing to SIDIS at successive orders in $\alpha_s$: (a) the Born process; (b) a next-to-leading-order real emission; (c,d) two classes of double-real emission at NNLO—quark- and gluon-initiated—whose phase-space integrals are the focus of Chapter 7.

tree-level double-real channels

$$\gamma^* q \to qgg, \qquad \gamma^* q \to q\,q'\bar{q}', \qquad \gamma^* g \to q\bar{q}g, \tag{6.13}$$

together with the same-flavour variants. It is the double-real channels whose phase-space integrals are evaluated in Chapter 7.

## 6.5 The tagged-parton constraint

The feature that distinguishes SIDIS from inclusive DIS, and that makes its phase-space integrals hard, is the measurement of the fragmenting parton. I contrast this constraint with neighbouring processes. In inclusive DIS the entire final state is summed over, so no constraint beyond momentum conservation survives. In jet observables a clustering algorithm imposes a *non-linear* constraint on the phase space. SIDIS sits between the

two, and its constraint is *linear* in the parton momenta. As we now show, this linearity is exactly what allows it to be promoted to a cut propagator. It imposes on the three-particle phase space the additional factor

$$[\mathrm{d}PS_3]_{z'} = \mathrm{d}PS_3\,\delta\Big(z' - \frac{p_1\cdot p_2}{p_1\cdot q}\Big), \tag{6.14}$$

which in full reads [35]

$$[\mathrm{d}PS_3]_{z'} = \frac{\mathrm{d}^d k_1\,\mathrm{d}^d k_2\,\mathrm{d}^d p_2}{(2\pi)^{3d-3}}\,\delta_+(k_1^2)\delta_+(k_2^2)\delta_+(p_2^2)\,(2\pi)^d\delta^{(d)}(p_2+k_1+k_2-p_1-q)\,\delta\Big(z'-\frac{p_1\cdot p_2}{p_1\cdot q}\Big). \tag{6.15}$$

The key point is that the tagging delta function has an argument that is *linear* in the scalar products,

$$\delta\Big(z' - \frac{p_1\cdot p_2}{p_1\cdot q}\Big) \propto \delta\big(2z'\,p_1\cdot q - 2\,p_1\cdot p_2\big), \tag{6.16}$$

so that, exactly like an on-shell delta function, it can be promoted to a cut propagator under reverse unitarity (Chapter 2) and carried through the IBP reduction. After the reduction, the constrained phase space factorises into a radial and an angular part,

$$\int[\mathrm{d}PS_3]_{z'} = \int[\mathrm{d}PS_3]^r_{z'}\int\mathrm{d}\Omega, \qquad \mathrm{d}\Omega = \mathrm{d}\theta\,\sin^{d-3}\theta\,\mathrm{d}\phi\,\sin^{d-4}\phi, \tag{6.17}$$

with the angular part the universal object of the preceding chapters. The resolution of the radial singularities is the subject of Chapter 7.

## 6.6 From channels to master integrals

Reverse unitarity and IBP reduction organise the double-real contribution into thirteen integral families,

$$\mathrm{RR}_k(n_1,n_2,n_3) = e^{-\epsilon\gamma_E}(4\pi)^d\int\frac{[\mathrm{d}PS_3]_{z'}}{D_{N_{k1}}^{n_1}D_{N_{k2}}^{n_2}D_{N_{k3}}^{n_3}}, \tag{6.18}$$

built from the eight denominators

$$\begin{aligned} &D_1=(k_1-p_1)^2,\ D_2=(k_1-q)^2,\ D_3=(k_2-p_1)^2,\ D_4=(k_2-q)^2,\\ &D_5=(k_1-p_1-q)^2,\ D_6=(k_2-p_1-q)^2,\ D_7=(k_1+k_2)^2,\ D_8=(k_1+k_2-p_1)^2. \end{aligned} \tag{6.19}$$

The IBP reduction, performed with LiteRed2, reduces the families to twenty master integrals [35], which are computed in Chapter 7 by the radial–angular method and, independently, by differential equations.

## 6.7 State of the art

The SIDIS coefficient functions have a long history. The NLO results were obtained in Refs. [165, 166], and threshold-enhanced higher-order results in Ref. [167]. The complete unpolarised NNLO coefficient functions were computed only recently, in parallel by two groups [161, 162]; the polarised case followed shortly [163, 164]. The master integrals computed in this thesis are ingredients of the first of these calculations [35].

## 6.8 What this thesis supplies

To be precise about the scope, the work presented here supplies the double-real master integrals and the radial–angular method needed to evaluate them. The assembly of the renormalised NNLO SIDIS structure functions (combining the double-virtual, real–virtual, double-real, mass-factorisation and observable-level ingredients into a finite prediction) is not claimed in this thesis. It is part of the broader NNLO SIDIS programme and is discussed as an outlook in Chapter 9. The electroweak and mixed QCD–electroweak corrections form a separate strand, summarised in Chapter 8.

# Chapter 7

# NNLO SIDIS Master Integrals and the Resolution of Singularities

## Contents


7.1 The constrained phase space and the master integrals . . . . . 60
7.2 Canonical differential equations . . . . . 61
7.3 Two relations beyond the IBP reduction . . . . . 63
7.4 Radial–angular decomposition in the $(k_1, k_2)$ frame . . . . . 63
7.5 The denominators and a worked mapping . . . . . 64
7.6 Resolution of the soft and collinear singularities . . . . . 65
7.7 Summary . . . . . 66


We now apply the method to the double-real master integrals of NNLO SIDIS. These are not the finite observable but the analytic ingredients of the NNLO coefficient functions. We compute them by two independent constructions, canonical differential equations and the radial–angular decomposition of this thesis, and use their agreement as the central check (Figure 7.1). The original computation of Ref. [35] was carried out in the convention $d = 4+\epsilon_{\mathrm{p}}$. Here, for uniformity with the rest of the thesis, I convert everything to $d = 4-2\epsilon$, the two regulators being related by $\epsilon_{\mathrm{p}} = -2\epsilon$.

## 7.1 The constrained phase space and the master integrals

The partonic variables are $x' = Q^2/(2p_1 \cdot q)$ and $z' = p_1 \cdot p_2/(p_1 \cdot q)$ with $0 < x', z' < 1$. Reverse unitarity converts the constrained three-particle phase space

$$[\mathrm{d}PS_3]_{z'} = \frac{\mathrm{d}^d k_1\, \mathrm{d}^d k_2\, \mathrm{d}^d p_2}{(2\pi)^{3d-3}}\, \delta_+(k_1^2)\delta_+(k_2^2)\delta_+(p_2^2)\, (2\pi)^d \delta^{(d)}(p_2+k_1+k_2-p_1-q)\, \delta\Big(z' - \frac{p_1\cdot p_2}{p_1\cdot q}\Big) \tag{7.1}$$

into cut two-loop integrals, the tagging delta entering as an additional cut propagator. IBP reduction with LiteRed2 organises the result into thirteen families

$$\mathrm{RR}_k(n_1,n_2,n_3) = e^{2\epsilon\gamma_E}(4\pi)^{4-2\epsilon} \int \frac{[\mathrm{d}PS_3]_{z'}}{D_{N_{k1}}^{n_1} D_{N_{k2}}^{n_2} D_{N_{k3}}^{n_3}}, \tag{7.2}$$

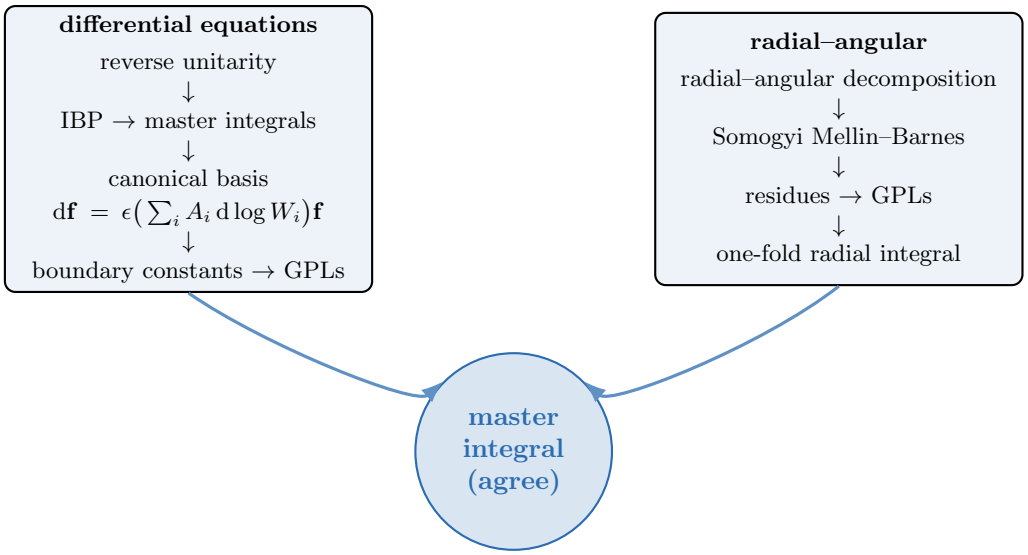



Figure 7.1: The NNLO SIDIS master integrals are obtained by two independent routes: the method of differential equations in canonical form (left), and the radial–angular decomposition developed in this thesis (right). Their analytic agreement is the central check of the calculation.

built from the eight denominators

$$\begin{aligned} &D_1 = (k_1 - p_1)^2,\ D_2 = (k_1 - q)^2,\ D_3 = (k_2 - p_1)^2,\ D_4 = (k_2 - q)^2, \\ &D_5 = (k_1 - p_1 - q)^2,\ D_6 = (k_2 - p_1 - q)^2,\ D_7 = (k_1 + k_2)^2,\ D_8 = (k_1 + k_2 - p_1)^2, \end{aligned} \tag{7.3}$$

with the family indices $N_{ki}$ tabulated in Ref. [35]. The reduction yields twenty master integrals, shown in Figure 7.2.

## 7.2 Canonical differential equations

The first route solves the master integrals by differential equations [61, 168, 169, 170, 144, 171, 172, 173, 57, 58, 174, 175, 176, 177, 178, 179, 180, 181]. A change to a canonical (pure, $\epsilon$-form) basis $J$ brings the system to

$$\mathrm{d}J = \epsilon\Big(\sum_{i=1}^{16} \widetilde{S}_i\, \omega_i\Big) J, \tag{7.4}$$

with constant rational matrices $\widetilde{S}_i$ (the $-2$ of $\epsilon_{\mathrm{p}} = -2\epsilon$ being absorbed into the matrices) and a sixteen-letter alphabet of closed one-forms $\omega_i$. The canonical basis is found in the standard way, by a leading-singularity / $\mathrm{d}\log$-integrand analysis that renders the basis pure, with the algorithmic assistance of Libra [182, 61]. In terms of the rationalising variables

$$x_1 = \sqrt{x'}, \quad z_1 = \sqrt{z'}, \quad x_2 = \frac{\sqrt{(1-z')^2 + 4x'z'} - 1 + z'}{2z'}, \quad z_2 = \frac{1 + x' - \sqrt{(1+x')^2 - 4x'z'}}{2x'}, \tag{7.5}$$

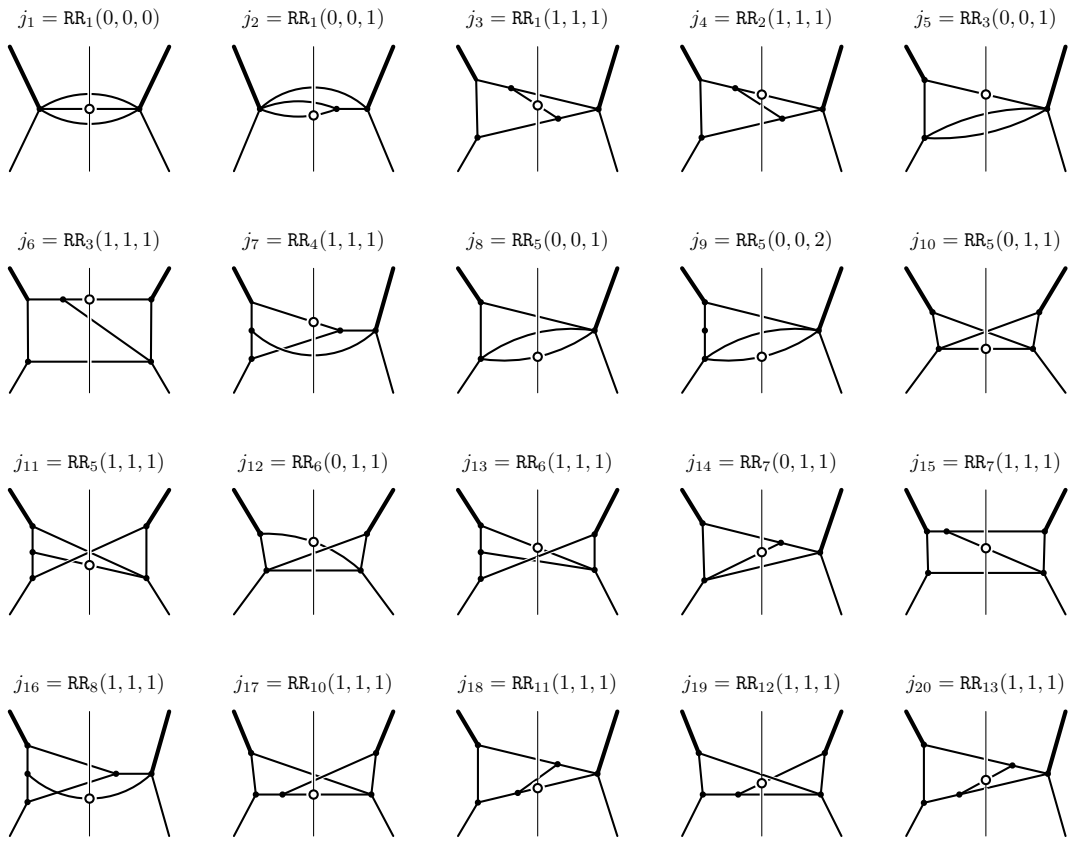



Figure 7.2: The twenty NNLO SIDIS double-real master integrals $j_1, \ldots, j_{20}$, grouped into the thirteen RR families. Lines denote massless propagators, cut lines the on-shell (cut) propagators, and the empty circle marks the propagator carrying the tagged momentum $p_b$. Reproduced from Ref. [35].

the alphabet is

$$\begin{aligned}
&\omega_1 = \mathrm{d}\log x',\ \omega_2 = \mathrm{d}\log z',\ \omega_3 = \mathrm{d}\arctan\tfrac{z_1}{x_1},\ \omega_4 = \mathrm{d}\arctan(z_1 x_1),\\
&\omega_5 = \mathrm{d}\log(1-x'),\ \omega_6 = \mathrm{d}\log(1+x'),\ \omega_7 = \mathrm{d}\log(1-z'),\ \omega_8 = \mathrm{d}\log(x'-z'),\\
&\omega_9 = \mathrm{d}\log(x'+z'),\ \omega_{10} = \mathrm{d}\log(1+x'z'),\ \omega_{11} = \mathrm{d}\log(\bar{x}+2x'z_2),\ \omega_{12} = \mathrm{d}\log(\bar{z}+2x_2z'),\\
&\omega_{13} = \mathrm{d}\log\tfrac{\bar{x}+x'z_2}{z_2},\ \omega_{14} = \mathrm{d}\log\tfrac{\bar{z}+x_2z'}{x_2},\ \omega_{15} = \mathrm{d}\log\tfrac{1+x'z_2}{1-z_2},\ \omega_{16} = \mathrm{d}\log\tfrac{1+x_2z'}{1-x_2},
\end{aligned} \tag{7.6}$$

with $\bar{x} = 1 - x'$, $\bar{z} = 1 - z'$. The arctan letters and the rationalised roots $x_2, z_2$ reflect the algebraic structure of the problem.

**Boundary conditions:** The system is integrated as Chen iterated integrals,

$$I_C(\omega_{i_n}, \ldots, \omega_{i_1}) = \int_{1>p_n>\cdots>p_1>p} \omega_{i_n}(p_n)\cdots\omega_{i_1}(p_1), \tag{7.7}$$

from the corner $(x', z') = (1, 1)$. Although the canonical-form solver requests a large set of asymptotic coefficients, the double soft limit has only a single region, with the integrals scaling as $(\bar{x}\bar{z})^{-2\epsilon}\,\bar{x}^{\,n}\bar{z}^{\,m}$. Consequently all the requested boundary constants vanish except

two, which are fixed analytically. In the $d = 4 - 2\epsilon$ convention they read

$$[j_1]_{(\bar{x}\bar{z})^{1-2\epsilon}} = \frac{\Gamma(1-\epsilon)^2}{\Gamma(2-2\epsilon)^2} = \frac{e^{2\epsilon\gamma_E}}{(1-2\epsilon)^2}\Big[1 - 3\epsilon^2\zeta_2 - \tfrac{14}{3}\epsilon^3\zeta_3 + \tfrac{3}{2}\epsilon^4\zeta_2^2 + \cdots\Big], \tag{7.8}$$

$$[j_4]_{(\bar{x}\bar{z})^{-1-2\epsilon}} = \frac{e^{2\epsilon\gamma_E}}{4\epsilon^2}\Big[-12 + 44\epsilon^2\zeta_2 + 96\epsilon^3\zeta_3 + \tfrac{38}{5}\epsilon^4\zeta_2^2 + \cdots\Big], \tag{7.9}$$

the second following from a ${}_3F_2(1)$ at the corner. With these the solution is reconstructed in Goncharov polylogarithms up to weight four.

**Analytic continuation and the integration path:** Most master integrals are integrated along the path $(1,1) \to (1,z') \to (x',z')$; for $J_{12}, J_{13}, J_{19}$ the path $(1,1) \to (x',1) \to (x',z')$ is used instead, chosen to minimise the letters $\omega_{11}, \omega_{13}, \omega_{15}$. The letter $\omega_8 = \mathrm{d}\log(x'-z')$ has a branching locus on the surface $x' = z'$, yet the physical solution selected by the boundary constants is analytic there on the first sheet. This was verified by a Frobenius analysis in Ref. [35].

## 7.3 Two relations beyond the IBP reduction

A by-product of the canonical basis is the discovery of *two linear relations among the master integrals that the IBP reduction does not produce*. In the canonical basis of pure functions any such hidden relation must have *constant* coefficients. This makes them detectable, by a sufficiently deep $\epsilon$-expansion, and provable through the differential-equation system with the exact boundary constants. Re-expressed in the original master-integral basis $j_i$ (which are not pure and therefore carry kinematic prefactors), the two relations read, in the $d = 4 - 2\epsilon$ convention,

$$j_9 = \frac{(1-2\epsilon)^2 x'}{z'}\, j_1 - \frac{\bar{x}(1+z')\epsilon^2}{z'}\, j_2 - \frac{(1+x')\bar{z}(1-2\epsilon)\epsilon}{z'}\, j_5 - \frac{(1+x')(1+z')\epsilon^2}{z'}\, j_8, \qquad j_{16} = j_7. \tag{7.10}$$

The naive IBP count of independent integrals is thereby reduced, which is a non-trivial structural fact. It is not known whether these relations are of IBP origin. Either way they provide an additional, stringent constraint that the radial–angular results must satisfy, and do.

## 7.4 Radial–angular decomposition in the $(k_1, k_2)$ frame

The second route boosts to the centre-of-mass frame of the two emitted partons, $\mathbf{k}_1 + \mathbf{k}_2 = 0$, in which

$$\begin{aligned} p_1 &= \tfrac{s-t-q^2}{2\sqrt{s_{12}}}(1, \mathbf{0}_{d-3}, 0, 0, 1), \\ p_2 &= \tfrac{s-s_{12}}{2\sqrt{s_{12}}}(1, \mathbf{0}_{d-3}, 0, \sin\psi, \cos\psi), \\ k_1 &= \tfrac{\sqrt{s_{12}}}{2}(1, \mathbf{0}_{d-3}, \sin\phi\sin\theta, \cos\phi\sin\theta, \cos\theta), \\ k_2 &= \tfrac{\sqrt{s_{12}}}{2}(1, \mathbf{0}_{d-3}, -\sin\phi\sin\theta, -\cos\phi\sin\theta, -\cos\theta), \end{aligned} \tag{7.11}$$

with $s_{12}=(k_1+k_2)^2$, $t=2p_1\cdot p_2$, and $\cos\psi = 1-2s_{12}t/[(s-t-q^2)(s-s_{12})]$. In $d=4-2\epsilon$ the constrained phase space factorises,

$$\int [\mathrm{d}PS_3]_{z'} = \int [\mathrm{d}PS_3]^r_{z'} \int \mathrm{d}\Omega, \quad \int [\mathrm{d}PS_3]^r_{z'} = \frac{s^{1-2\epsilon}(1-z')^{1-2\epsilon} z'^{-\epsilon}}{(4\pi)^{4-2\epsilon}\Gamma(1-2\epsilon)} \int_0^1 \mathrm{d}z\, [(1-z)z]^{-\epsilon}, \tag{7.12}$$

with $\mathrm{d}\Omega = \mathrm{d}\theta\, \sin^{1-2\epsilon}\theta\, \mathrm{d}\phi\, \sin^{-2\epsilon}\phi$, and the fully integrated element is $\int [\mathrm{d}PS_3]^r_{z'} \mathrm{d}\Omega = 2^{-9+8\epsilon}\pi^{-2+2\epsilon} s^{1-2\epsilon}(1-z')^{1-2\epsilon} z'^{-\epsilon}/\Gamma(\tfrac{3}{2}-\epsilon)^2$. The angular factors take the van Neerven form

$$\Omega_{j_1 j_2}(\alpha,\beta,A,B,\Gamma) = \int \mathrm{d}\Omega\, \frac{1}{(\alpha+\beta\cos\theta)^{j_1}(A+B\cos\theta+\Gamma\sin\theta\cos\phi)^{j_2}}, \tag{7.13}$$

into which all angular integrals are brought by partial fractioning, and which is mapped onto the rotationally invariant Somogyi form $\tilde{\Omega}_{j_1 j_2}(v_{11},v_{22},v_{12}) = \int \mathrm{d}\Omega(n)\, [(v_1\cdot n)^{j_1}(v_2\cdot n)^{j_2}]^{-1}$ by setting

$$v_1 = \big(1, \mathbf{0}_{d-3}, 0, -\tfrac{\beta}{\alpha}\big), \quad v_2 = \big(1, \mathbf{0}_{d-3}, -\tfrac{\Gamma}{A}, -\tfrac{B}{A}\big), \quad n = (1, \mathbf{n}_{d-3}, \sin\theta\cos\phi, \cos\theta), \tag{7.14}$$

so that, with $m=j_1$, $n=j_2$,

$$\alpha^m A^n\, \Omega_{j_1 j_2}(\alpha,\beta,A,B,\Gamma) = \tilde{\Omega}_{j_1 j_2}(v_{11},v_{22},v_{12}). \tag{7.15}$$

The prefactors $\alpha^{j_1}$ and $A^{j_2}$ are the normalisations that convert the frame-dependent van Neerven integral into the frame-independent Somogyi one, whose Mellin–Barnes representation

$$\begin{aligned}\tilde{\Omega}_{j_1 j_2} = {} & \frac{2^{2-2\epsilon-j}\pi^{1-\epsilon}}{\Gamma(j_1)\Gamma(j_2)\Gamma(2-2\epsilon-j)} \int_{-i\infty}^{+i\infty} \frac{\mathrm{d}z_{12}}{2\pi i}\frac{\mathrm{d}z_{11}}{2\pi i}\frac{\mathrm{d}z_{22}}{2\pi i}\, \Gamma(-z_{11})\Gamma(-z_{22})\Gamma(-z_{12}) \\ & \times v_{11}^{z_{11}} v_{22}^{z_{22}} v_{12}^{z_{12}}\, \Gamma(j_1+z_1)\Gamma(j_2+z_2)\,\Gamma(1-\epsilon-j-z)\end{aligned} \tag{7.16}$$

(with $j=j_1+j_2$) is evaluated by the method of Chapter 5; the two-denominator results needed here are expressible through ${}_2F_1$, Appell $F_1$ and Lauricella functions, whose $\epsilon$-expansions agree with the Mellin–Barnes-to-GPL output.

## 7.5 The denominators and a worked mapping

Expressing the eight propagators in the $(k_1,k_2)$ frame separates, in each master integral, an angular factor from a radial one. As an example, the integral

$$\mathrm{RR}_4(1,1,1) = \int \frac{[\mathrm{d}PS_3]^r_{z'}}{r} \int \frac{\mathrm{d}\Omega}{(\alpha+\beta\cos\theta)(A+B\cos\theta+\Gamma\sin\theta\cos\phi)} \tag{7.17}$$

has

$$\begin{gathered} r = \frac{s^3(x'(z-1)-z)(z'-1)^2}{4(x'-1)^2}, \quad \alpha=1,\ \beta=-1, \\ A = zz'-z-z', \quad B = z-z'+zz', \quad \Gamma = 2\sqrt{(1-z)zz'}, \end{gathered} \tag{7.18}$$

so the angular integral is the two-denominator Somogyi object of Chapter 5 and the radial integral is the one-fold integral over $z$ resolved below.

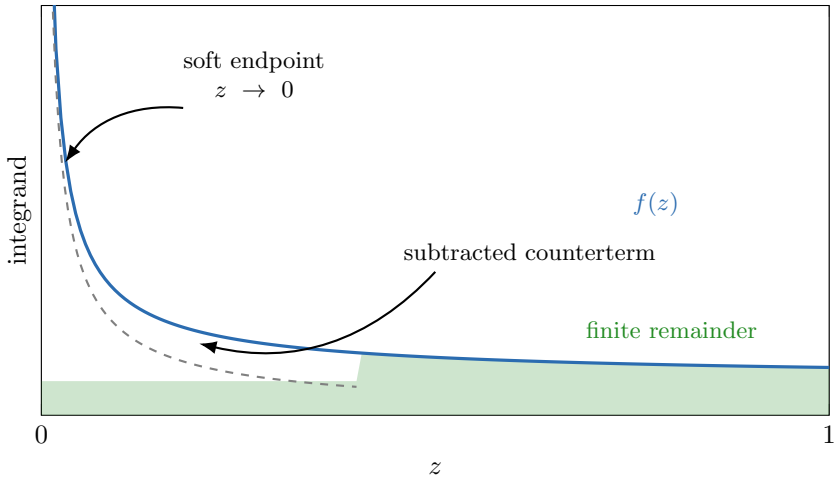



Figure 7.3: Resolution of an endpoint singularity. The radial integrand $f(z)$ (blue) diverges at the soft endpoint $z \to 0$. A local counterterm $\widetilde{R}\,g(z)$ (dashed) reproduces the singular behaviour and is subtracted, leaving a finite remainder (shaded) that is integrated numerically; the counterterm, which carries the $\epsilon$-pole, is integrated analytically and added back—the plus-distribution prescription of (7.19).

## 7.6 Resolution of the soft and collinear singularities

The angular result must finally be recombined with the radial part through the one-fold integral over $z \in [0,1]$, whose integrand is singular at the endpoints. The *collinear* singularities come from the angular part and the *soft* ones from the $z$-integration [50, 51, 52, 53]. Because the integrand is singular within the domain, one cannot expand in $\epsilon$ before isolating the poles. We use a local subtraction. Writing $f(z) = g(z)R(z)$ with $g$ carrying the regulated endpoint singularity and $R$ regular at $z \to a$, and $\widetilde{R} = \lim_{z\to a} R(z)$,

$$\int_0^1 f(z)\,\mathrm{d}z = \int_0^1 \big[g(z)R(z) - \widetilde{R}\,g(z)\big]\mathrm{d}z + \int_0^1 \widetilde{R}\,g(z)\,\mathrm{d}z, \tag{7.19}$$

the first integrand now finite and the second elementary. This is the plus-distribution prescription of collinear factorisation, which is made explicit by

$$z^{-1+a\epsilon} = \frac{\delta(z)}{a\epsilon} + \sum_{n=0}^{\infty} \frac{(a\epsilon)^n}{n!}\left[\frac{\log^n z}{z}\right]_+, \tag{7.20}$$

illustrated in Figure 7.3.

For $\mathrm{RR}_8(1,1,1)$ the $z$-dependent parametric factor (in $d = 4-2\epsilon$) is

$$P_z = \frac{[(1-z)z]^{-\epsilon}}{z\,[-x'z + zx'z' + x' - zz' + z' + z]}, \tag{7.21}$$

with a single endpoint singularity at $z \to 0$; the angular part being regular there, the choice $g(z) = z^{-1-\epsilon}$, $R(z) = P_z\Omega_z z^{1+\epsilon}$ in (7.19) renders the finite-order $\epsilon$-expansion of the angular part legitimate (the relevant plus distribution being the $a = -1$ case).

For $\mathrm{RR}_2(1,1,1)$ the angular part is itself singular inside the domain, so its finite-order $\epsilon$-expansion cannot be used directly. We isolate the soft behaviour of the *all-order* angular expression as a factor $z^{-1-\epsilon}$ (the $\epsilon_{\mathrm{p}}/2$ of the paper becoming $-\epsilon$ here), write $\Omega_z = \Omega'_z z^{1+\epsilon}$,

Table 7.1: Classification of the SIDIS master integrals by the depth of their leading pole and by whether the resolution of singularities of Section 7.6 is required.

| leading pole | resolution | integrals |
|---|---|---|
| $\epsilon^0$ | no | $\mathrm{RR}_3(0,0,1)$, $\mathrm{RR}_5(0,0,1)$, $\mathrm{RR}_6(0,1,1)$ |
| $\epsilon^{-1}$ | no | $\mathrm{RR}_5(1,1,1)$, $\mathrm{RR}_7(0,1,1)$, $\mathrm{RR}_{10}(1,1,1)$ |
| $\epsilon^{-2}$ | yes | $\mathrm{RR}_1, \mathrm{RR}_2, \mathrm{RR}_3, \mathrm{RR}_4, \mathrm{RR}_7, \mathrm{RR}_8, \mathrm{RR}_{11}$ (all at $(1,1,1)$) |

and combine it with the radial factor

$$P_z = \frac{z^{-1-\epsilon}[-(z-1)z]^{-\epsilon}}{(z-1)(zz'-z-z')}. \tag{7.22}$$

The product then carries two endpoint singularities, requiring the counterterms $g_1(z) = z^{-1-2\epsilon}$ at $z \to 0$ (the $a = -2$ plus distribution) and $g_2(z) = (1-z)^{-1-\epsilon}$ at $z \to 1$.

Table 7.1 classifies the masters by the depth of their leading pole and by whether the resolution is required; seven of the unit-power masters need it.

## 7.7 Summary

The twenty NNLO SIDIS double-real master integrals have been obtained by two completely independent constructions: canonical differential equations over a sixteen-letter alphabet, solved in Goncharov polylogarithms to weight four, and the radial–angular decomposition of this thesis, which evaluates the universal angular factors by Mellin–Barnes and reduces the process-specific content to a single radial integral. The two routes agree and the canonical analysis also exposed two linear relations among the masters beyond the IBP reduction. The soft and collinear singularities are resolved *before* any finite-order $\epsilon$-expansion, by the local plus-distribution subtraction, including the case in which a soft singularity is nested in the angular part and must be extracted to all orders. The complete analytic results can be found in the supplementary files `de_results.m` and `rad_results.m`, together with the evaluation notebook `Evaluation.nb`. These files are described in Section A.2. With these ingredients in hand, the assembly of the renormalised NNLO SIDIS coefficient functions becomes a matter of combining them with the virtual and real–virtual contributions and the mass-factorisation counterterms. This step lies in the broader programme discussed in Chapter 9.

# Part II

# Extensions of the Analytic Toolkit

# Chapter 8

# Toward Electroweak and Mixed QCD–Electroweak Corrections

## Contents


8.1 Motivation and scope . . . 68
8.1.1 Vertex corrections and general structure of the form factor . . . 69
8.1.2 $\mathcal{O}(\alpha)$ Corrections . . . 71
8.1.3 $\mathcal{O}(\alpha\alpha_s)$ Corrections . . . 72
8.2 From Lagrangian to Onshell Renormalization . . . 72
8.2.1 Renormalization constants at $\mathcal{O}(\alpha)$ for $\gamma qq$ vertex . . . 79
8.2.2 Renormalization constants at $\mathcal{O}(\alpha\alpha_s)$ for $\gamma qq$ vertex . . . 80
8.3 Linearization of General Harmonic Polylogarithms . . . 83
8.4 Status and outlook . . . 84


Having constructed process-independent analytic building blocks for real radiation in Part I, I now apply the same analytic-function viewpoint to a complementary class of problems: the virtual two-loop electroweak master integrals, where the same core issues recur: analytic continuation, special-function bases, and singularity structure. The aim of this part is not yet a complete electroweak observable, but the development of the renormalisation ingredients (this chapter) that such calculations require.

The preceding chapters dealt with the QCD corrections to SIDIS. At the precision targeted by the Electron–Ion Collider, the electromagnetic and weak corrections, and their interference with QCD, also matter. This chapter presents the renormalisation *ingredients* for the virtual $\gamma qq$ building block at $\mathcal{O}(\alpha)$ and $\mathcal{O}(\alpha\alpha_s)$. I state at the outset, and repeat at the end, that this is a chapter of ingredients and not of a finite SIDIS observable. The assembly of a renormalised mixed QCD–electroweak prediction lies in the outlook of Chapter 9.

## 8.1 Motivation and scope

For foundational, standard, and representative treatments directly relevant to the material discussed in this section, see [3, 4, 5, 183, 184, 185].

Once the purely strong corrections are under control, the next layer of precision involves QED radiation off the leptonic and quark lines, weak loops, photon–$Z$ interference, and

Table 8.1: The double expansion of the SIDIS structure functions. The pure-QCD row is the core of this thesis; the boxed entries are the electroweak renormalisation strand of this chapter.

| | $n=0$ | $n=1$ | $n=2$ |
|---|---|---|---|
| $m=0$ | $F^{(0,0)}$ (Born) | $F^{(0,1)}$ (NLO QCD) | $F^{(0,2)}$ (NNLO QCD, this thesis) |
| $m=1$ | $\boxed{F^{(1,0)}\text{ (EW)}}$ | $\boxed{F^{(1,1)}\text{ (mixed)}}$ | – |

the mixed strong–electroweak terms [186, 48]. These organise into a double perturbative expansion of the structure functions,

$$\begin{aligned} F_i(x,z,Q^2) &= \sum_{m,n\geq 0} \left(\frac{\alpha}{\pi}\right)^m \left(\frac{\alpha_s}{\pi}\right)^n F_i^{(m,n)}(x,z,Q^2) \\ &= F_i^{(0,0)} + \frac{\alpha}{\pi} F_i^{(1,0)} + \frac{\alpha_s}{\pi} F_i^{(0,1)} + \frac{\alpha}{\pi}\frac{\alpha_s}{\pi} F_i^{(1,1)} + \cdots , \end{aligned} \tag{8.1}$$

with the pure-QCD column ($m=0$) the subject of the rest of the thesis. The mixed term $F_i^{(1,1)}$ is the first place where the strong and electroweak corrections interfere. This chapter concerns the virtual and counterterm ingredients that enter $F_i^{(1,0)}$ and $F_i^{(1,1)}$ (Table 8.1).

### 8.1.1 Vertex corrections and general structure of the form factor

Following [187, 188, 189, 190, 48, 191, 192, 193, 194, 195, 196], an s-channel vertex $\Gamma_\mu$ describing the (axial-)vector coupling of fermions to a gauge boson admits a decomposition in terms of *four* scalar form factors $F_{1,2}$ and $G_{1,2}$ (valid at *any* number of loop and *any* topology), provided that we take a gauge invariant subset. Hence, the decomposition in terms of four form factors $F_{1,2}$ and $G_{1,2}$ reads [187, 188, 189, 190],

$$\begin{aligned} \Gamma_\mu = -i \Big( & g_V F_1(s,m)\gamma_\mu + i\frac{g_V}{2m} F_2(s,m)\sigma_{\mu\alpha}q^\alpha \\ & + g_A G_1(s,m)\gamma_5\gamma_\mu + \frac{g_A}{2m} G_2(s,m)\gamma_5 q_\mu \Big) , \end{aligned} \tag{8.2}$$

with $\sigma_{\alpha\beta} = \frac{i}{2}[\gamma_\alpha, \gamma_\beta]$ and $q^\beta = (p_1+p_2)^\beta$. $m$ is the mass of the external fermion.

The form factors $F_i$ and $G_i$ (with $i=1,2$) can be extracted from $\Gamma_\mu$ by means of suitable projectors, $P^\mu_{Fi}$ and $P^\mu_{Gi}$ as

$$F_i = \mathrm{Tr}(P^\mu_{Fi}\Gamma_\mu) , \qquad \text{and} \qquad G_i = \mathrm{Tr}(P^\mu_{Gi}\Gamma_\mu) . \tag{8.3}$$

The explicit expressions for the projectors in $d = 4-2\epsilon$ dimensions are given by

$$\begin{aligned} P^\mu_{Fi}(s,p_1,p_2) &= \frac{\not{p}_2 - m}{m}\, i \left( f_{i,1}\,\gamma^\mu + \frac{1}{2m} f_{i,2}\,(p_2-p_1)^\mu \right) \frac{\not{p}_1 + m}{m} , \\ P^\mu_{Gi}(s,p_1,p_2) &= \frac{\not{p}_2 - m}{m}\, i\gamma_5 \left( g_{i,1}\gamma^\mu - \frac{1}{m} g_{i,2}\,(p_2+p_1)^\mu \right) \frac{\not{p}_1 + m}{m} , \end{aligned} \tag{8.4}$$

with

$$f_{1,1} = \frac{m^2}{2g_V(d-2)(4m^2-s)}\,, \qquad f_{1,2} = \frac{2(d-1)m^4}{g_V(d-2)(4m^2-s)^2}\,, \tag{8.5}$$

$$f_{2,1} = -\frac{2m^4}{g_V(d-2)s(4m^2-s)}\,, \qquad f_{2,2} = -\frac{2m^4(4m^2+(d-2)s)}{g_V(d-2)s(4m^2-s)^2}\,, \tag{8.6}$$

and

$$g_{1,1} = \frac{m^2}{2g_A(d-2)(4m^2-s)}\,, \qquad g_{1,2} = \frac{m^4}{g_A(d-2)s(4m^2-s)}, \tag{8.7}$$

$$g_{2,1} = \frac{2m^4}{g_A(d-2)s(4m^2-s)}\,, \quad g_{2,2} = \frac{4(d-1)\,m^6-(d-2)\,sm^4}{g_A(d-2)s^2(4m^2-s)}\,. \tag{8.8}$$

The treatment of the Dirac matrix $\gamma_5$ in dimensional regularisation is subtle, since its four-dimensional definition is incompatible with the continuation to $d = 4-2\epsilon$ dimensions. Throughout this work, the *Larin scheme* is employed. In this prescription, $\gamma_5$ is replaced by an explicitly $d$-dimensional expression involving the Levi–Civita tensor and a product of Dirac matrices,

$$\gamma^\mu\gamma_5 = \frac{i}{6}\,\epsilon^{\mu\nu\rho\sigma}\gamma_\nu\gamma_\rho\gamma_\sigma, \tag{8.9}$$

where the Levi–Civita tensor is treated as a four-dimensional object and all Dirac algebra is performed in $d$ dimensions. This prescription preserves the consistency of dimensional regularisation while correctly reproducing the axial anomaly.

In the calculations presented in this thesis, no additional finite renormalisation of the axial current is required. Consequently, the standard Larin prescription is used throughout without introducing a separate finite renormalisation constant for $\gamma_5$.

The form factors $F_i$ and $G_i$ can be computed perturbatively, as series expansions in powers of $(\alpha/\pi)$ and $(\alpha_s/\pi)$, as

$$\begin{aligned}
F_1 &= 1 + \left(\frac{\alpha}{\pi}\right) F_1^{(1,0)} + \left(\frac{\alpha_s}{\pi}\right) F_1^{(0,1)} + \left(\frac{\alpha}{\pi}\right)^2 F_1^{(2,0)} + \left(\frac{\alpha_s}{\pi}\right)^2 F_1^{(0,2)} + \left(\frac{\alpha}{\pi}\right)\left(\frac{\alpha_s}{\pi}\right) F_1^{(1,1)} + \mathrm{HO},\\
F_2 &= \left(\frac{\alpha}{\pi}\right) F_2^{(1,0)} + \left(\frac{\alpha_s}{\pi}\right) F_2^{(0,1)} + \left(\frac{\alpha}{\pi}\right)^2 F_2^{(2,0)} + \left(\frac{\alpha_s}{\pi}\right)^2 F_2^{(0,2)} + \left(\frac{\alpha}{\pi}\right)\left(\frac{\alpha_s}{\pi}\right) F_2^{(1,1)} + \mathrm{HO},\\
G_1 &= 1 + \left(\frac{\alpha}{\pi}\right) G_1^{(1,0)} + \left(\frac{\alpha_s}{\pi}\right) G_1^{(0,1)} + \left(\frac{\alpha}{\pi}\right)^2 G_1^{(2,0)} + \left(\frac{\alpha_s}{\pi}\right)^2 G_1^{(0,2)} + \left(\frac{\alpha}{\pi}\right)\left(\frac{\alpha_s}{\pi}\right) G_1^{(1,1)} + \mathrm{HO},\\
G_2 &= \left(\frac{\alpha}{\pi}\right) G_2^{(1,0)} + \left(\frac{\alpha_s}{\pi}\right) G_2^{(0,1)} + \left(\frac{\alpha}{\pi}\right)^2 G_2^{(2,0)} + \left(\frac{\alpha_s}{\pi}\right)^2 G_2^{(0,2)} + \left(\frac{\alpha}{\pi}\right)\left(\frac{\alpha_s}{\pi}\right) G_2^{(1,1)} + \mathrm{HO},
\end{aligned} \tag{8.10}$$

where the superscripts indicate the number of loops of the contributing diagrams.

Now, in our particular problem we do not have massive external fermion. The offshell photon interact with a quark and the final state is a quark at the tree level. In that case just taking "$s \to t$" and "$m \to 0$" after projection operation is sufficient, because the form-factor is endependent of the momentum direction. It would imply $F_2 = G_2 = 0$ for our case.

### 8.1.2 $\mathcal{O}(\alpha)$ Corrections

At $\mathcal{O}(\alpha)$ the vertex form factor is captured by $F_1^{(1,0)}$ and $G_1^{(1,0)}$ where up-to order $\epsilon^0$ the result is:

$$
\begin{aligned}
F_1^{(1,0)} =& \frac{2Q_u^3}{\epsilon^2} + \frac{-a_u^2 Q_u - \frac{Q_d}{4s_W^2} + 2Q_u^3 \log\left(-\frac{\mu^2}{t}\right) - Q_u v_u^2 + 3Q_u^3 - \frac{3}{4s_W^2}}{\epsilon} \\
& 2a_u^2 Q_u G\left(1,0;-\frac{t}{m_Z^2}\right) + 3a_u^2 Q_u \log\left(-\frac{\mu^2}{t}\right) - 4a_u^2 Q_u \log\left(\frac{\mu^2}{m_Z^2}\right) + 4a_u^2 Q_u \\
& \frac{4a_u^2 m_Z^2 Q_u G\left(1,0;-\frac{t}{m_Z^2}\right)}{t} + \frac{2a_u^2 m_Z^2 Q_u}{t} + \frac{2a_u^2 m_Z^2 Q_u \log\left(-\frac{\mu^2}{t}\right)}{t} - \frac{2a_u^2 m_Z^2 Q_u \log\left(\frac{\mu^2}{m_Z^2}\right)}{t} \\
& \frac{2a_u^2 m_Z^4 Q_u G\left(1,0;-\frac{t}{m_Z^2}\right)}{t^2} + Q_u^3 \log^2\left(-\frac{\mu^2}{t}\right) + 3Q_u^3 \log\left(-\frac{\mu^2}{t}\right) - \frac{1}{3}\pi^2 Q_u^3 + 8Q_u^3 \\
& - \frac{2m_W^2 G\left(0,0;\frac{\sqrt{4m_W^2-t}-\sqrt{-t}}{\sqrt{4m_W^2-t}+\sqrt{-t}}\right)}{ts_W^2} - \frac{3\log\left(\frac{\mu^2}{m_W^2}\right)}{4s_W^2} + \frac{m_W^2}{2ts_W^2} - \frac{1}{2s_W^2} \\
& \frac{\sqrt{-t} G\left(0;\frac{\sqrt{4m_W^2-t}-\sqrt{-t}}{\sqrt{4m_W^2-t}+\sqrt{-t}}\right)}{4s_W^2\sqrt{4m_W^2-t}} - \frac{m_W^4 G\left(0,0;\frac{\sqrt{4m_W^2-t}-\sqrt{-t}}{\sqrt{4m_W^2-t}+\sqrt{-t}}\right)}{t^2 s_W^2} \\
& - \frac{2\sqrt{-t} m_W^4 G\left(0;\frac{\sqrt{4m_W^2-t}-\sqrt{-t}}{\sqrt{4m_W^2-t}+\sqrt{-t}}\right)}{t^2 s_W^2\sqrt{4m_W^2-t}} - \frac{\sqrt{-t} m_W^2 G\left(0;\frac{\sqrt{4m_W^2-t}-\sqrt{-t}}{\sqrt{4m_W^2-t}+\sqrt{-t}}\right)}{2ts_W^2\sqrt{4m_W^2-t}} + \frac{Q_d}{s_W^2} \\
& \frac{Q_d G\left(1,0;-\frac{t}{m_Z^2}\right)}{2s_W^2} + \frac{3Q_d \log\left(-\frac{\mu^2}{t}\right)}{4s_W^2} - \frac{Q_d \log\left(\frac{\mu^2}{m_W^2}\right)}{s_W^2} \\
& \frac{Q_d m_W^2 G\left(1,0;-\frac{t}{m_W^2}\right)}{ts_W^2} + \frac{Q_d m_W^2 \log\left(-\frac{\mu^2}{t}\right)}{2ts_W^2} - \frac{Q_d m_W^2 \log\left(\frac{\mu^2}{m_W^2}\right)}{2ts_W^2} + \frac{Q_d m_W^2}{2ts_W^2} \\
& \frac{Q_d m_W^4 G\left(1,0;-\frac{t}{m_W^2}\right)}{2t^2 s_W^2} + 2Q_u v_u^2 G\left(1,0;-\frac{t}{m_Z^2}\right) + 4Q_u v_u^2 \\
& \frac{4m_Z^2 Q_u v_u^2 G\left(1,0;-\frac{t}{m_Z^2}\right)}{t} + \frac{2m_Z^2 Q_u v_u^2}{t} + 3Q_u v_u^2 \log\left(-\frac{\mu^2}{t}\right) - 4Q_u v_u^2 \log\left(\frac{\mu^2}{m_Z^2}\right) \\
& \frac{2m_Z^4 Q_u v_u^2 G\left(1,0;-\frac{t}{m_Z^2}\right)}{t^2} + \frac{2m_Z^2 Q_u v_u^2 \log\left(-\frac{\mu^2}{t}\right)}{t} - \frac{2m_Z^2 Q_u v_u^2 \log\left(\frac{\mu^2}{m_Z^2}\right)}{t} + \mathcal{O}(\epsilon^1)
\end{aligned}
\tag{8.11}
$$

$$
\begin{aligned}
G_1^{(1,0)} =& \frac{-2a_u Q_u v_u - \frac{Q_d}{4s_W^2} - \frac{3}{4s_W^2}}{\epsilon} \\
& - \frac{2m_W^2 G\left(0,0;\frac{\sqrt{4m_W^2-t}-\sqrt{-t}}{\sqrt{4m_W^2-t}+\sqrt{-t}}\right)}{ts_W^2} - \frac{3\log\left(\frac{\mu^2}{m_W^2}\right)}{4s_W^2} + \frac{m_W^2}{2ts_W^2} - \frac{1}{2s_W^2} \\
& \frac{\sqrt{-t}G\left(0;\frac{\sqrt{4m_W^2-t}-\sqrt{-t}}{\sqrt{4m_W^2-t}+\sqrt{-t}}\right)}{4s_W^2\sqrt{4m_W^2-t}} - \frac{m_W^4 G\left(0,0;\frac{\sqrt{4m_W^2-t}-\sqrt{-t}}{\sqrt{4m_W^2-t}+\sqrt{-t}}\right)}{t^2 s_W^2} \\
& - \frac{2\sqrt{-t}m_W^4 G\left(0;\frac{\sqrt{4m_W^2-t}-\sqrt{-t}}{\sqrt{4m_W^2-t}+\sqrt{-t}}\right)}{t^2 s_W^2\sqrt{4m_W^2-t}} - \frac{\sqrt{-t}m_W^2 G\left(0;\frac{\sqrt{4m_W^2-t}-\sqrt{-t}}{\sqrt{4m_W^2-t}+\sqrt{-t}}\right)}{2ts_W^2\sqrt{4m_W^2-t}} + \frac{Q_d}{s_W^2} \\
& \frac{Q_d G\left(1,0;-\frac{t}{m_W^2}\right)}{2s_W^2} + \frac{3Q_d\log\left(-\frac{\mu^2}{t}\right)}{4s_W^2} - \frac{Q_d\log\left(\frac{\mu^2}{m_W^2}\right)}{s_W^2} \\
& \frac{Q_d m_W^2 G\left(1,0;-\frac{t}{m_W^2}\right)}{ts_W^2} + \frac{Q_d m_W^2\log\left(-\frac{\mu^2}{t}\right)}{2ts_W^2} - \frac{Q_d m_W^2\log\left(\frac{\mu^2}{m_W^2}\right)}{2ts_W^2} + \frac{Q_d m_W^2}{2ts_W^2} \\
& 4a_u Q_u v_u G\left(1,0;-\frac{t}{m_Z^2}\right) + \frac{Q_d m_W^4 G\left(1,0;-\frac{t}{m_W^2}\right)}{2t^2 s_W^2} + 6a_u Q_u v_u\log\left(-\frac{\mu^2}{t}\right) + 8a_u Q_u v_u \\
& \frac{8a_u m_Z^2 Q_u v_u G\left(1,0;-\frac{t}{m_Z^2}\right)}{t} + \frac{4a_u m_Z^2 Q_u v_u}{t} - 8a_u Q_u v_u\log\left(\frac{\mu^2}{m_Z^2}\right) \\
& \frac{4a_u m_Z^4 Q_u v_u G\left(1,0;-\frac{t}{m_Z^2}\right)}{t^2} + \frac{4a_u m_Z^2 Q_u v_u\log\left(-\frac{\mu^2}{t}\right)}{t} - \frac{4a_u m_Z^2 Q_u v_u\log\left(\frac{\mu^2}{m_Z^2}\right)}{t} + \mathcal{O}(\epsilon^1)
\end{aligned}
\tag{8.12}
$$

### 8.1.3 $\mathcal{O}(\alpha\alpha_s)$ Corrections

For book keeping convenience we have categorized the Feynman diagrams into four different sets. The corresponding Feynman diagrams are given in Figure:(8.2,8.4,8.1,8.3). The distinction is based on the coupling constant structure.

## 8.2 From Lagrangian to Onshell Renormalization

For foundational, standard, and representative treatments directly relevant to the material discussed in this section, see [197, 198, 199, 200].

It is useful to write the covariant derivative of the electroweak interaction in terms of the mass eigenstates $A_\mu$ and $Z_\mu$, defined by the relations,

$$
\begin{cases} W_\mu^3 = \eta_Z\, Z_\mu \cos\theta_W + A_\mu \eta_\theta \sin\theta_W \\ B_\mu = -\eta_Z Z_\mu \eta_\theta\, \sin\theta_W + A_\mu \cos\theta_W \end{cases}, \quad \begin{cases} \eta_Z Z_\mu = W_\mu^3 \cos\theta_W - B_\mu \eta_\theta\, \sin\theta_W \\ A_\mu = W_\mu^3\, \eta_\theta \sin\theta_W + B_\mu \cos\theta_W \end{cases}.
\tag{8.13}
$$

where $\theta_W$ denotes the weak mixing angle. For a doublet field $\psi_L$, with hypercharge $Y$, we

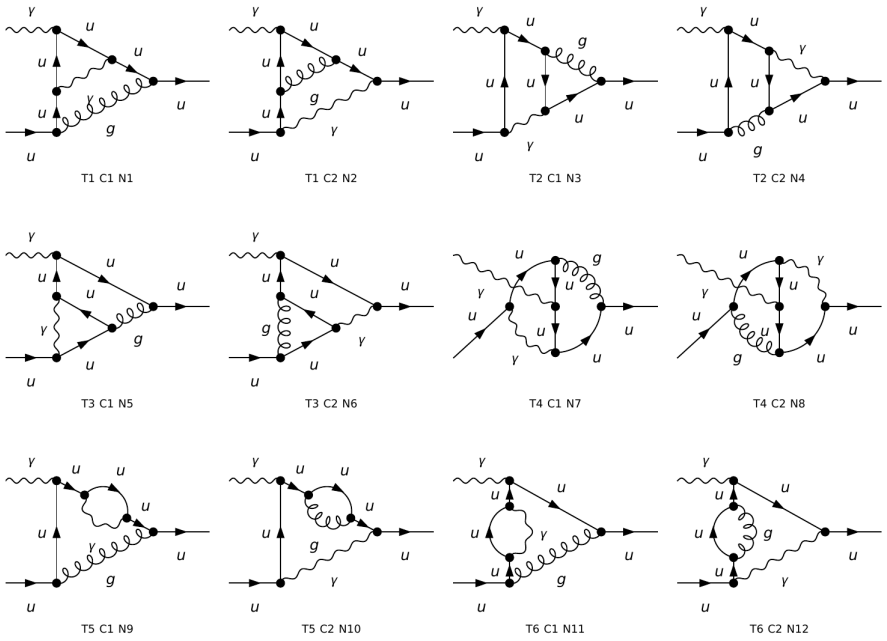



Figure 8.1: Feynman diagrams for set-5 generated by FeynArts.

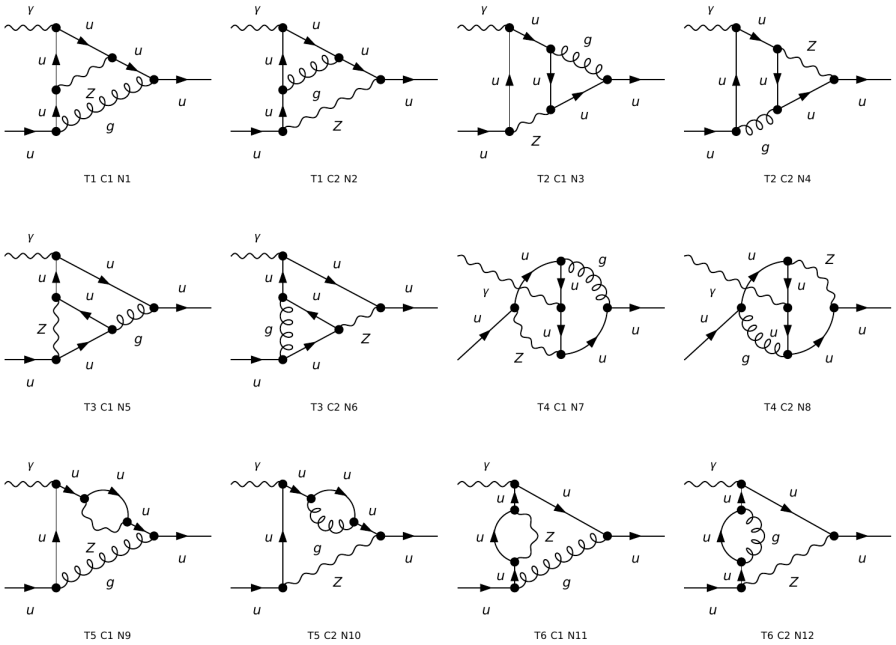



Figure 8.2: Feynman diagrams for set-1 generated by FeynArts.

get,

$$
\begin{aligned}
D_\mu \psi_L &= \left[\partial_\mu + i\eta \frac{g}{\sqrt{2}} \left(\tau^+ W_\mu^+ + \tau^- W_\mu^-\right) + i\eta \frac{g}{2} \tau_3 W_\mu^3 + i\,\eta' g' \eta_Y Y B_\mu\right] \psi_L \\
&= \left[\partial_\mu + i\,\eta \frac{g}{\sqrt{2}} \left(\tau^+ W_\mu^+ + \tau^- W_\mu^-\right) + i\,\eta_e e\, Q\, A_\mu \right. \\
&\qquad \left. + i\,\eta \frac{g}{\cos\theta_W} \left(\frac{\tau_3}{2} - Q\, \sin^2\theta_W\right) \eta_Z Z_\mu\right] \psi_L, \qquad (8.14)
\end{aligned}
$$

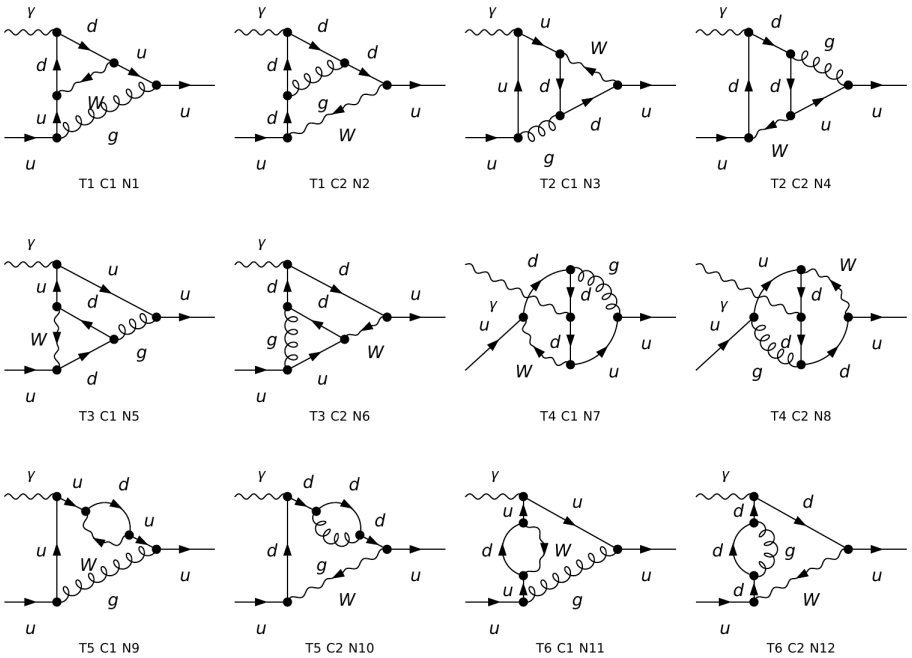



Figure 8.3: Feynman diagrams for set-8 generated by FeynArts.

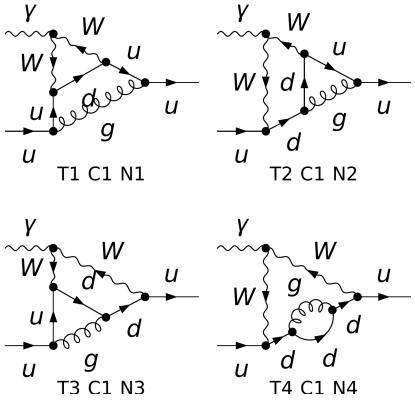



Figure 8.4: Feynman diagrams for set-3 generated by FeynArts.

where

$$W_\mu^\pm = \frac{W_\mu^1 \mp i W_\mu^2}{\sqrt{2}}, \tag{8.15}$$

$$\tau_\pm = \frac{\tau_1 \pm i\tau_2}{\sqrt{2}}. \tag{8.16}$$

The charge operator is defined by

$$Q = \begin{bmatrix} \frac{1}{2} + \eta_Y Y & 0 \\ 0 & -\frac{1}{2} + \eta_Y Y \end{bmatrix}, \tag{8.17}$$

and we have used the relations,

$$\begin{aligned} \eta_e\, e &= (\eta\,\eta_\theta)\, g \sin\theta_W \\ &= \eta'\, g' \cos\theta_W\,. \end{aligned} \tag{8.18}$$

Many authors use $\eta_e = +1$. Some authors use $\eta_e = -1$, to account for their other conventions (notably $\eta = \eta' = -1$), and still keep $e = +g' \cos\theta_W = +g \sin\theta_W$. For a singlet of $SU(2)_I$, $\psi_R$, we have,

$$\begin{aligned} D_\mu \psi_R &= \left[\partial_\mu + i\,\eta' g' \eta_Y Y B_\mu\right] \psi_R \\ &= \left[\partial_\mu + i\,\eta_e e\, Q\, A_\mu - i\,\eta \frac{g}{\cos\theta_W} Q\, \sin^2\theta_W \eta_Z Z_\mu\right] \psi_R\,. \end{aligned} \tag{8.19}$$

For this work we adopt the following convention,

$$\eta = \eta_\theta = -1 \tag{8.20}$$

$$\eta' = \eta_Z = \eta_Y = \eta_e = \eta_G = +1 \tag{8.21}$$

Now we introduce the counter terms needed to renormalize the $\mathcal{O}(\alpha)$ and $\mathcal{O}(\alpha\alpha_s)$ corrections to the $Vq\bar{q}'$ vertex ($V = \gamma, Z, W$). Adding the counter terms allows us to get rid of the ultraviolet divergences. Here we will explicitly follow the notation by Böhm, Spiesberger and Hollik [201]. In their notation the covariant derivative appears as

$$D_\mu = \partial_\mu - i g_2 I_a W_\mu^a + i g_1 \frac{Y}{2} B_\mu \tag{8.22}$$

and the neutral current coupling constants are

$$\begin{aligned} v_f &= \frac{I_3^f - 2Q_f \sin^2\theta_W}{2\sin\theta_W \cos\theta_W} \\ a_f &= \frac{I_3^f}{2\sin\theta_W \cos\theta_W} \end{aligned} \tag{8.23}$$

where $Q_f$ and $I_3^f$ denote the charge and the third isospin component of $f_L$.

We will use the on-shell renormalization scheme as discussed in Ref. [201]. As a first step the multiplicative renormalization constants $Z$ are attached to each parameter and

each symmetry multiplet of fields in the symmetric Lagrangian:

$$\begin{aligned}
W_\mu^a &\to (Z_2^W)^{1/2} W_\mu^a \\
B_\mu &\to (Z_2^B)^{1/2} B_\mu \\
\psi_j^L &\to (Z_L^j)^{1/2} \psi_j^L \\
\psi_{j\sigma}^R &\to (Z_R^{j\sigma})^{1/2} \psi_{j\sigma}^R \\
\Phi &\to (Z^\Phi)^{1/2} \phi \\
g_2 &\to Z_1^W (Z_2^W)^{-3/2} g_2 \\
g_1 &\to Z_1^B (Z_2^B)^{-3/2} g_1 \\
v &\to (Z^\Phi)^{1/2} (v - \delta v) \\
g_{j\sigma} &\to (Z^\Phi)^{-1/2} Z_1^{j\sigma} g_{j\sigma} \\
\mu^2 &\to (Z^\Phi)^{-1} (\mu^2 - \delta\mu^2) \\
\lambda &\to (Z^\Phi)^{-2} Z_\lambda \lambda
\end{aligned} \tag{8.24}$$

i.e. the bare fields and parameters are replaced by renormalized fields and parameter. Writing $Z_i \to 1 + \delta Z_i$ we obtain $\mathcal{L} \to \mathcal{L} + \delta\mathcal{L}$. From the counter term Lagrangian part we get the counter term Feynman rule. It is convenient to introduce the following linear combinations of the SU(2) and the U(1) field renormalization constants $\delta Z_2^{W,B}$ and the coupling renormalization constants $\delta Z_1^{W,B}$ $(i = 1, 2)$:

$$\begin{pmatrix} \delta Z_i^\gamma \\ \delta Z_i^Z \end{pmatrix} = \begin{pmatrix} s_W^2 & c_W^2 \\ c_W^2 & s_W^2 \end{pmatrix} \begin{pmatrix} \delta Z_i^W \\ \delta Z_i^B \end{pmatrix} \tag{8.25}$$

with the abbreviations

$$\begin{aligned}
s_W^2 &= \sin^2\theta_W \\
c_W^2 &= \cos^2\theta_W
\end{aligned} \tag{8.26}$$

Also we introduce $(i = 1, 2)$

$$\delta Z_i^{\gamma Z} = \frac{c_W s_W}{c_W^2 - s_W^2} (\delta Z_i^Z - \delta Z_i^\gamma) \tag{8.27}$$

To determine the counter term for the $V q_{L,R} \bar{q}_{L,R}$ vertex we consider the corresponding electroweak interaction Lagrangian

$$\begin{aligned}
i D_\mu \bar{\psi}_q^L \gamma^\mu \psi_q^L &= i(\partial_\mu - i g_2 I_a W_\mu^a + i g_1 \frac{Y}{2} B_\mu) \bar{\psi}_q^L \gamma^\mu \psi_q^L \\
i D_\mu \bar{\psi}_q^R \gamma^\mu \psi_q^R &= i(\partial_\mu + i g_1 \frac{Y}{2} B_\mu) \bar{\psi}_q^R \gamma^\mu \psi_q^R
\end{aligned} \tag{8.28}$$

and perform the replacements of Eq.( 8.24). After replacing the gauge fields with the physical fields $A_\mu$, $Z_\mu$ and $W_\mu$ using Eqs.( 8.15,8.13) we find the following counter term Feynman rules for the $\mathcal{O}(\alpha)$ vertex correction:
$W q \bar{q}'$ vertex at $\mathcal{O}(\alpha)$:

$$\frac{i e \gamma_\mu (1 - \gamma_5)}{2\sqrt{2} s_W} \left[1 + \delta Z_1^W - \delta Z_2^W + \delta Z_L^q\right] \tag{8.29}$$

$\gamma q\bar{q}$ vertex at $\mathcal{O}(\alpha)$:

$$-ie\gamma_\mu\Big[Q(1+\Delta Z_\gamma+\frac{(1-\gamma_5)}{2}\delta Z_L^q+\frac{1+\gamma_5}{2}\delta Z_R^q)+\Delta Z_{\gamma Z}((v_q-a_q\gamma_5)\Big] \tag{8.30}$$

where $\Delta Z_{\gamma,\gamma Z}\equiv\delta Z_1^{\gamma,\gamma Z}-\delta Z_2^{\gamma,\gamma Z}$
$Zq\bar{q}$ vertex at $\mathcal{O}(\alpha)$:

$$ie\gamma_\mu\Bigg[(v_q-a_q\gamma_5)(1+\Delta Z_Z)+\delta Z_L^q\frac{1}{s_W c_W}(I_3-s_W^2Q)\frac{(1-\gamma_5)}{2}-Q\frac{s_w}{c_w}\delta Z_R^q\frac{(1+\gamma_5)}{2} +Q(\Delta Z_{\gamma Z})\Bigg] \tag{8.31}$$

with $\Delta Z_Z\equiv\delta Z_1^Z-\delta Z_2^Z$.

Similarly we calculate the counter term Feynman rules at $\mathcal{O}(\alpha\alpha_s)$.
$Wq\bar{q}'$ vertex at $\mathcal{O}(\alpha\alpha_s)$:

$$\frac{ie\gamma_\mu(1-\gamma_5)}{2\sqrt{2}s_W}\left[(1+\delta Z_1^W-\delta Z_2^W+\delta Z_L^q)+(\delta Z_1^W-\delta Z_2^W)(\delta Z_L^q)\right]. \tag{8.32}$$

$\gamma q\bar{q}$ vertex at $\mathcal{O}(\alpha\alpha_s)$:

$$\begin{aligned}&-ie\gamma_\mu\Big[Q(1+\Delta Z_\gamma)(1+\frac{(1-\gamma_5)}{2}\delta Z_L^q+\frac{1+\gamma_5}{2}\delta Z_R^q)+\Delta Z_{\gamma Z}((v_q-a_q\gamma_5)\\&+(a_q+v_q)\delta Z_L^q\frac{(1-\gamma_5)}{2}+(v_q-a_q)\delta Z_R^q\frac{(1+\gamma_5)}{2})\Big].\end{aligned} \tag{8.33}$$

$Zq\bar{q}$ vertex at $\mathcal{O}(\alpha\alpha_s)$:

$$ie\gamma_\mu\Bigg[(1+\Delta Z_Z)\Big[v_q-a_q\gamma_5+\delta Z_L^q\frac{1}{s_W c_W}(I_3-s_W^2Q)\frac{(1-\gamma_5)}{2}-Q\frac{s_w}{c_w}\delta Z_R^q\frac{(1+\gamma_5)}{2}\Big] +Q(\Delta Z_{\gamma Z})\Big[1+\delta Z_L^q\frac{(1-\gamma_5)}{2}+\delta Z_R^q\frac{(1+\gamma_5)}{2}\Big]\Bigg]. \tag{8.34}$$

It is to be noted that the renormalization constants in the terms linear in $\delta Z$ have to be evaluated at $\mathcal{O}(\alpha\alpha_s)$. In the interference terms, the $\delta Z_{L,R}^q$ have to be of $\mathcal{O}(\alpha_s)$ and $\delta Z_i^{\gamma,\gamma Z,Z,W}$ have to be of $\mathcal{O}(\alpha)$. But $\delta Z_{L,R}^q=0$ at $\mathcal{O}(\alpha_s)$, if we do not distinguish between IR and UV regulators, i.e., when we assume $\epsilon_{IR}=\epsilon_{UV}\equiv\epsilon$. Finally, the one-loop corrections to the NLO counterterms have to be included as well.

The on-shell renormalization conditions allow us to write the $\delta Z$s in terms of unrenor-

malized self energies $\Sigma^{ij}$ as follows Ref. [201].

$$\begin{aligned}
\delta Z_2^\gamma &= -\Pi^\gamma(0) \equiv -\frac{\partial \Sigma^\gamma}{\partial k^2}(0) \\
\delta Z_1^\gamma &= -\Pi^\gamma(0) - \frac{s_W}{c_W}\frac{\Sigma^{\gamma Z}(0)}{M_Z^2} \\
\delta Z_2^Z &= -\Pi^\gamma(0) - 2\frac{c_W^2 - s_W^2}{s_W c_W}\frac{\Sigma^{\gamma Z}(0)}{M_Z^2} + \frac{c_W^2 - s_W^2}{s_W^2}\left(\frac{\delta M_Z^2}{M_Z^2} - \frac{\delta M_W^2}{M_W^2}\right) \\
\delta Z_1^Z &= -\Pi^\gamma(0) - \frac{3c_W^2 - 2s_W^2}{s_W c_W}\frac{\Sigma^{\gamma Z}(0)}{M_Z^2} + \frac{c_W^2 - s_W^2}{s_W^2}\left(\frac{\delta M_Z^2}{M_Z^2} - \frac{\delta M_W^2}{M_W^2}\right) \\
\delta Z_2^W &= -\Pi^\gamma(0) - 2\frac{c_W}{s_W}\frac{\Sigma^{\gamma Z}(0)}{M_Z^2} + \frac{c_W^2}{s_W^2}\left(\frac{\delta M_Z^2}{M_Z^2} - \frac{\delta M_W^2}{M_W^2}\right) \\
\delta Z_1^W &= -\Pi^\gamma(0) - \frac{3 - 2s_W^2}{s_W c_W}\frac{\Sigma^{\gamma Z}(0)}{M_Z^2} + \frac{c_W^2}{s_W^2}\left(\frac{\delta M_Z^2}{M_Z^2} - \frac{\delta M_W^2}{M_W^2}\right)
\end{aligned} \tag{8.35}$$

where the mass renormalization constants are given in terms of the transverse part of the W and Z self energies as follows:

$$\begin{aligned}
\delta M_W^2 &= Re\Sigma_T^{WW}(M_W^2) \\
\delta M_Z^2 &= Re\Sigma_T^{ZZ}(M_Z^2)
\end{aligned} \tag{8.36}$$

Note that at $O(\alpha\alpha_s)$ there are no contributions from products of one loop renormalization constants in these expressions. The fermion self energy $\Sigma^f$ can be decomposed in terms of three invariant functions $\Sigma_L^f$, $\Sigma_R^f$ and $\Sigma_S^f$ which are coeffieincts of the $\frac{1-\gamma_5}{2}, \frac{1+\gamma_5}{2}$ and $m_f$ terms in $\Sigma^f$ respectively. The doublet field renormalization constants $\delta Z_L$ and singlet renormalization constant $\delta Z_R^-$ in the $I_3 = -1/2$ states can be written as:

$$\begin{aligned}
\delta Z_L &= -\Sigma_L(m^2) - m^2[\Sigma_L'(m^2) + \Sigma_R'(m^2) + 2\Sigma_S'(m^2)] \\
\delta Z_R^- &= -\Sigma_R(m_-^2) - m_-^2[\Sigma_L'(m_-^2) + \Sigma_R'(m_-^2) + 2\Sigma_S'(m_-^2)]
\end{aligned} \tag{8.37}$$

The $\Sigma_L', \ldots$ denote the derivatives

$$\Sigma_{L,\ldots}'(k^2) = \frac{\partial \Sigma_{L,\ldots}}{\partial k^2} \tag{8.38}$$

For the right handed $u$-type quarks an additional condition has to be imposed in order to fix $\delta Z_R^+$. We treat the $I_3 = +1/2$ quarks in a way that residues for the left and right handed propagators become equal.

For calculational purpose, it is useful to define the following quantities.

$$\begin{aligned}
\Sigma_V^q &\equiv \frac{1}{2}(\Sigma_L^q + \Sigma_R^q) \\
\Sigma_A^q &\equiv -\frac{1}{2}(\Sigma_L^q - \Sigma_R^q),
\end{aligned} \tag{8.39}$$

so that

$$\begin{aligned}
\Sigma_L^q &= \Sigma_V^q - \Sigma_A^q \\
\Sigma_R^q &= \Sigma_V^q + \Sigma_A^q.
\end{aligned} \tag{8.40}$$

And

$$\begin{aligned}\delta Z_V^q &\equiv \frac{1}{2}(\delta Z_L^q + \delta Z_R^q)\\ \delta Z_A^q &\equiv \frac{1}{2}(\delta Z_L^q - \delta Z_R^q),\end{aligned} \tag{8.41}$$

so that

$$\begin{aligned}\delta Z_L^q &= (\delta Z_V^q + \delta Z_A^q)\\ \delta Z_R^q &= (\delta Z_V^q - \delta Z_A^q).\end{aligned} \tag{8.42}$$

In the massless, on-shell limit the field renormalization constants reduce to $\delta Z^q_{L/R} = -\Sigma^q_{L/R}(0)$, so that $\delta Z^q_V = -\Sigma^q_V(0)$ and $\delta Z^q_A = +\Sigma^q_A(0)$; these are the combinations that enter the renormalized vertex written in terms of self energies, eq. (8.46).[1] We have calculated the necessary self energies and verified with the existing literature. The gauge boson self energies at $\mathcal{O}(\alpha\alpha_s)$ can be found in Ref. [202]. We also evaluated the one loop results since it is a necessary ingredient for the full calculation. The Feynman rules for the counterterm and the self energies for the electroweak one loop case can be found in Ref. [201].

### 8.2.1 Renormalization constants at $\mathcal{O}(\alpha)$ for $\gamma qq$ vertex

As per Eqs.(8.35) the renormalizaton constants explicitly depends on self energies. These quantities are computed up to required epsilon expansion. To filter out renormalization constants for the $\gamma qq$ vertex, the master equation we need is Eqs.(8.30). It would give us the renormalized vertex at $\mathcal{O}(\alpha)$ as

$$\begin{aligned}\hat{\Gamma}^{\gamma ff}_\mu\Big|_\alpha = \Gamma^{\gamma ff}_\mu\Big|_\alpha &- ieQ_f\gamma_\mu\left(\delta Z_1^\gamma\Big|_\alpha - \delta Z_2^\gamma\Big|_\alpha + \delta Z_V^f\Big|_\alpha - \delta Z_A^f\Big|_\alpha\,\gamma_5\right)\\ &-ie\gamma_\mu\left(v_f - a_f\gamma_5\right)\left(\delta Z_1^{\gamma Z}\Big|_\alpha - \delta Z_2^{\gamma Z}\Big|_\alpha\right)\end{aligned} \tag{8.43}$$

where $\Gamma^{\gamma ff}_\mu$ is the unrenormalized vertex.

After plugging in the explicit expression in terms of self energies, we get

$$\begin{aligned}\hat{\Gamma}^{\gamma qq}_\mu\Big|_\alpha = \Gamma^{\gamma qq}_\mu\Big|_\alpha &- ieQ_f\gamma_\mu\left(-\Sigma_V^q(0)\Big|_\alpha - \Sigma_A^q(0)\Big|_\alpha\,\gamma_5\right)\\ &- ie\gamma_\mu\frac{I^3}{c_W s_W}\left(-\frac{\Sigma^{\gamma Z}(0)}{M_Z^2}\Big|_\alpha\right)\left[\frac{1-\gamma_5}{2}\right].\end{aligned} \tag{8.44}$$

First let us focus on the bosonic self energies. At this order the only relevant bosonic self energy is $\Sigma^{\gamma Z}(0)$. Furthermore, we do not include fermionic loops in the $\gamma$–$Z$ mixing, because they vanish at zero momentum.[2]

[1] Note that the vector and axial quantities are defined with opposite relative signs on the two sides. The axial self energy carries an explicit minus, $\Sigma^q_A \equiv -\frac{1}{2}(\Sigma^q_L - \Sigma^q_R)$, whereas the axial field-renormalization combination does not, $\delta Z^q_A \equiv +\frac{1}{2}(\delta Z^q_L - \delta Z^q_R)$. Combined with the on-shell relation $\delta Z^q_{L/R} = -\Sigma^q_{L/R}(0)$, this produces $\delta Z^q_V = -\Sigma^q_V(0)$ *but* $\delta Z^q_A = +\Sigma^q_A(0)$: the differing sign of the axial relation is a bookkeeping convention, not an inconsistency, and it is what fixes the relative sign of the two terms in eq. (8.46).

[2] The fermionic contribution to $\Sigma^{\gamma Z}(0)$ vanishes identically, for *any* fermion mass. Its vector part ($\propto Q_f v_f$) is transverse in the photon index by the electromagnetic Ward identity and hence proportional to $q^2$, $\Sigma^{\gamma Z}_T(q^2)\big|_{\text{ferm,V}} = q^2\,\Pi_V(q^2) \to 0$ as $q^2 \to 0$; its axial part ($\propto Q_f a_f$) admits no two-point Lorentz

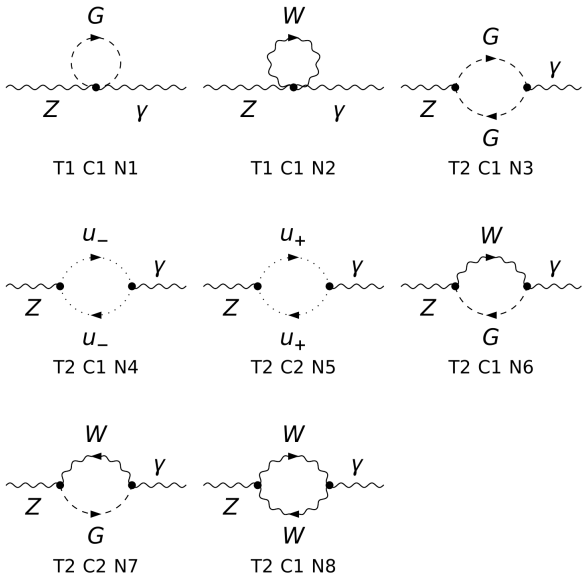



Figure 8.5: Bosonic self energy diagrams generated by FeynArts, where "G" represents Goldstone bosons ($\Phi$) and "u" represent Ghosts.

Similarly, according to the master equation, the only relevant fermionic self energies are coming from W or Z loop. It is because the quark is treated massless and Goldstone and Higgs coupling would contain linear mass term of the fermion.

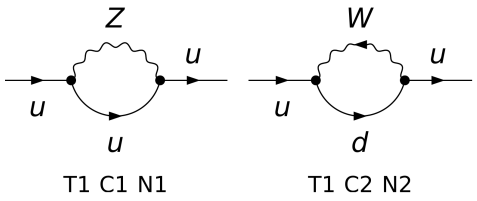



Figure 8.6: Fermionic self energy diagrams generated by FeynArts.

### 8.2.2 Renormalization constants at $\mathcal{O}(\alpha\alpha_s)$ for $\gamma qq$ vertex

As discussed earlier, all the renormalization constants are calculated from self energy corrections. Our goal is to calculate the renormalization constants up to $\mathcal{O}(\alpha\alpha_s)$, given that we have massless fermions. To start with, let us recall Eqs.(8.33) and focus on the terms involving $\Delta Z_{\gamma Z}$. At $\mathcal{O}(\alpha\alpha_s)$ there are several possibilities and one has to alalyze them carefully. Terms only proportional to $\Delta Z_{\gamma Z}$ has to be calculated at $\mathcal{O}(\alpha\alpha_s)$. Now since $\Delta Z_{\gamma Z}$ is directly proportional to $\Sigma^{\gamma Z}(0)$, one immediately realize that this quantity is zero because we have massless fermions. Next we check the terms proportional to $\Delta Z_{\gamma Z}\delta Z_{L/R}$. Again, $\Delta Z_{\gamma Z}$ does not exist at $\mathcal{O}(\alpha_s)$ because quarks are taken to be massless. So the other option is to take $\Delta Z_{\gamma Z}$ at $\mathcal{O}(\alpha)$ and $\delta Z_{L/R}$ at $\mathcal{O}(\alpha_s)$, which is zero

structure built from the single momentum $q$ (one would need $\epsilon_{\mu\nu\alpha\beta}q^\alpha q^\beta \equiv 0$) and vanishes as well. Only the bosonic ($W$, Goldstone, ghost) loops give a non-zero $\Sigma^{\gamma Z}(0) \propto M_W^2$; for the massless light quarks considered here the fermionic $\gamma$–$Z$ bubble is therefore absent to all orders in $\alpha_s$.

since gluon and quarks are massless. In other words, anything involving $\Delta Z_{\gamma Z}$ vanishes. Hence the remaining objects are $\Delta Z_\gamma$, $\Delta Z_\gamma \delta Z^q_{L/R}$ and $\delta Z^q_{L/R}$ at $\mathcal{O}(\alpha\alpha_s)$. But since $\Delta Z_\gamma$ is proportional to $\Sigma^{\gamma Z}(0)$, just using the same argument as before, one realizes that only surviving term will be $\delta Z^q_{L/R}$ at $\mathcal{O}(\alpha\alpha_s)$. So in summary, we cannot have any bosonic self energy with non-zero value at $q^2 \to 0$ at this order. There will be only eight relevant non-zero fermionic self energy to calculate the renormalization constants.

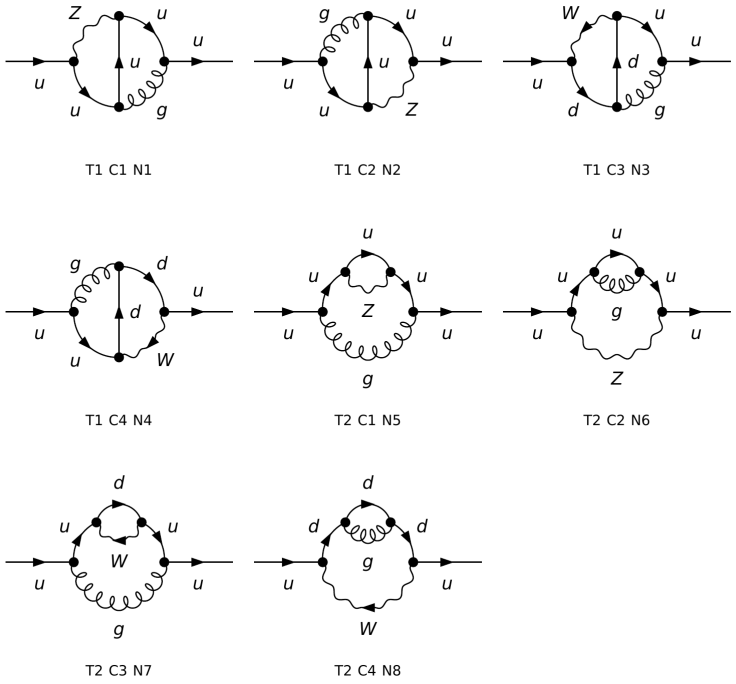



Figure 8.7: Fermionic self energy diagrams at $\mathcal{O}(\alpha\alpha_s)$ generated by FeynArts.

We distinguish three vertices at this order: the *bare* two-loop vertex $\Gamma_\mu|_{\alpha\alpha_s}$ (the genuine two-loop diagrams); the *sub-renormalized* vertex $\bar{\Gamma}_\mu|_{\alpha\alpha_s} = \bar{R}\Gamma_\mu|_{\alpha\alpha_s}$, obtained by adding the one-loop sub-renormalization counterterms (free of subdivergences, but still carrying the overall $\mathcal{O}(\alpha\alpha_s)$ divergence); and the *renormalized* vertex $\hat{\Gamma}_\mu|_{\alpha\alpha_s} = \bar{\Gamma}_\mu|_{\alpha\alpha_s} + (\text{local counterterm})$. The renormalized vertex at $\mathcal{O}(\alpha\alpha_s)$ then reads

$$\hat{\Gamma}^{\gamma ff}_\mu\Big|_{\alpha\alpha_s} = \bar{\Gamma}^{\gamma ff}_\mu\Big|_{\alpha\alpha_s} - ieQ_f\gamma_\mu\left(\delta Z^f_V\Big|_{\alpha\alpha_s} - \delta Z^f_A\Big|_{\alpha\alpha_s}\gamma_5\right) \tag{8.45}$$

where $\bar{\Gamma}^{\gamma ff}_\mu|_{\alpha\alpha_s}$ denotes the *sub-renormalized* vertex — the bare two-loop diagrams together with their one-loop sub-renormalization, spelled out in eq. (8.47) below — and $\hat{\Gamma}$ adds the local (overall) counterterm to it. After plugging in the explicit expression in terms of self energies, we get

$$\hat{\Gamma}^{\gamma qq}_\mu\Big|_{\alpha\alpha_s} = \bar{\Gamma}^{\gamma qq}_\mu\Big|_{\alpha\alpha_s} - ieQ_f\gamma_\mu\left(-\Sigma^q_V(0)\Big|_{\alpha\alpha_s} - \gamma_5\Sigma^q_A(0)\Big|_{\alpha\alpha_s}\right) \tag{8.46}$$

The counterterm shown in eq. (8.46) is the *local* (overall) $\mathcal{O}(\alpha\alpha_s)$ one; the one-loop sub-renormalization is carried inside $\bar{\Gamma}_\mu|_{\alpha\alpha_s}$. Writing the purely bare two-loop vertex as $\Gamma^{\gamma qq}_\mu|_{\alpha\alpha_s}$ (*without* the bar), using the on-shell relation $\delta Z^q_2|_\alpha = \big(-\Sigma^q_V(0) - \gamma_5\Sigma^q_A(0)\big)|_\alpha$,

and denoting by $F^{(0,1)}(t)$ the scalar one-loop QCD form factor — so that the one-loop QCD vertex is $\Gamma^{\gamma qq}_{\mu}|_{\alpha_s} = -ieQ_q\gamma_\mu\, F^{(0,1)}(t)$ for massless quarks — the renormalized vertex reads

$$\begin{aligned}\hat{\Gamma}^{\gamma qq}_{\mu}\Big|_{\alpha\alpha_s} = \underbrace{\Gamma^{\gamma qq}_{\mu}\Big|_{\alpha\alpha_s}}_{\text{(a) bare 2-loop}} \underbrace{-\,ieQ_q\gamma_\mu\left(-\Sigma^q_V(0)-\gamma_5\Sigma^q_A(0)\right)\Big|_{\alpha\alpha_s}}_{\text{(b) local CT = eq. (8.46)}} \\ \underbrace{+\,-\,ieQ_q\,\gamma_\mu\left(-\Sigma^q_V(0)-\gamma_5\Sigma^q_A(0)\right)\Big|_{\alpha} F^{(0,1)}(t)}_{(\mathrm{c}_1)\text{ EW field-RC sub-renormalization}} \\ \underbrace{+\,-\,ie\,\gamma_\mu\Big(Q_q\,\Delta Z_\gamma + \Delta Z_{\gamma Z}(v_q-a_q\gamma_5)\Big)\Big|_{\alpha} F^{(0,1)}(t)}_{(\mathrm{c}_2)\text{ photon-sector sub-renormalization}}\,. \end{aligned} \tag{8.47}$$

The Dirac structure of $(\mathrm{c}_1)$,$(\mathrm{c}_2)$ is that of the $\mathcal{O}(\alpha)$ vertex counterterm (8.30) — with the chiral operator standing to the *right* of $\gamma_\mu$, as it must (an insertion to the left would flip the sign of the axial piece) — now multiplying the scalar QCD form factor $F^{(0,1)}$. In this notation the sub-renormalized vertex of eq. (8.46) is $\bar{\Gamma}^{\gamma qq}_{\mu}|_{\alpha\alpha_s} = (\mathrm{a}) + (\mathrm{c}_1) + (\mathrm{c}_2)$, and $\hat{\Gamma} = \bar{\Gamma} + (\mathrm{b})$. Term $(\mathrm{c}_1)$ is the piece that eq. (8.46) does *not* display separately: it carries the *same* chiral self-energy combination $-\Sigma^q_V(0) - \gamma_5\Sigma^q_A(0)$ as the local counterterm (b), but evaluated at $\mathcal{O}(\alpha)$ and multiplying the one-loop *QCD* vertex $\Gamma^{\gamma qq}_{\mu}|_{\alpha_s}$. It is the $\mathcal{O}(\alpha)$ field-renormalization insertion $\delta Z^q_2|_\alpha$ dressing the $\mathcal{O}(\alpha_s)$ form factor; it belongs to $\bar{\Gamma}_\mu|_{\alpha\alpha_s}$ — neither to the bare two-loop vertex (a) nor to the local counterterm (b).

It is worth spelling out in detail why eq. (8.45) contains *only* the fermion field renormalization constant, and none of the "mixed" one-loop-times-one-loop pieces that a generic two-loop renormalization would produce. Treating the renormalization of the vertex multiplicatively, $\hat{\Gamma}_\mu = Z\,\Gamma_\mu$, and expanding the renormalization factor $Z$ (which collects the field-, charge- and mixing-renormalization constants) together with the unrenormalized vertex $\Gamma_\mu$ simultaneously in $\alpha$ and $\alpha_s$, the $\mathcal{O}(\alpha\alpha_s)$ piece organizes itself as

$$\hat{\Gamma}_\mu\big|_{\alpha\alpha_s} = \underbrace{\Gamma_\mu\big|_{\alpha\alpha_s}}_{\text{(a)}} + \underbrace{Z\big|_{\alpha\alpha_s}\Gamma^{(0)}_\mu}_{\text{(b)}} + \underbrace{Z\big|_{\alpha}\,\Gamma_\mu\big|_{\alpha_s}}_{\text{(c)}} + \underbrace{Z\big|_{\alpha_s}\,\Gamma_\mu\big|_{\alpha}}_{\text{(d)}}\,. \tag{8.48}$$

Here (a) is the genuine two-loop unrenormalized vertex and (b) is the overall (local) two-loop counterterm; the terms (c) and (d) are the mixed contributions, in which a one-loop counterterm dresses a one-loop vertex — precisely the "$\Gamma$ at $\mathcal{O}(\alpha)$ or $\mathcal{O}(\alpha_s)$ times $Z$" pieces. We show that (d) vanishes identically and that (c) contributes only through the sub-renormalization (it adds no new *local* counterterm), so that the only structure left over *in the overall (local) counterterm* is the two-loop field renormalization written in eq. (8.45); the sub-renormalization itself retains all of $(\mathrm{c}_1)$+$(\mathrm{c}_2)$.

*The term (d), $Z|_{\alpha_s}\,\Gamma_\mu|_\alpha$, is identically zero.* The only renormalization constant of the $\gamma q\bar{q}$ vertex at $\mathcal{O}(\alpha_s)$ is the quark wave-function constant $\delta Z^q_2$: the photon is a colour singlet, so QCD does not renormalize the electric charge, and the QED-like Ward identity $Z^{\gamma qq}_1 = Z^q_2$ ties the vertex constant to the field constant. For a massless quark evaluated on-shell the one-loop gluonic self energy $\Sigma^q(p) \propto \not{p}\,(-p^2)^{-\epsilon}$ is a scaleless integral, so its ultraviolet pole

is cancelled by an equal infrared pole and

$$\delta Z_2^q\Big|_{\alpha_s} = \delta Z_{L/R}^q\Big|_{\alpha_s} = 0 \qquad (\epsilon_{IR} = \epsilon_{UV} \equiv \epsilon) \ . \tag{8.49}$$

Hence $Z|_{\alpha_s} = 0$ and the term (d) is absent altogether: there is simply no $\mathcal{O}(\alpha_s)$ counterterm available to multiply the one-loop electroweak vertex $\Gamma_\mu|_\alpha$.

*In the term (c), $Z|_\alpha \, \Gamma_\mu|_{\alpha_s}$, all three $\mathcal{O}(\alpha)$ counterterm structures enter as sub-renormalization.* The $\mathcal{O}(\alpha)$ vertex counterterm (8.30) carries the photon field/vertex constant $\Delta Z_\gamma$, the $\gamma$–$Z$ mixing constant $\Delta Z_{\gamma Z}$, and the fermion field renormalization $\delta Z_V^q - \delta Z_A^q \gamma_5$; in term (c) each multiplies the one-loop QCD vertex $\Gamma_\mu|_{\alpha_s}$ and cancels the corresponding electroweak subdivergence of a two-loop diagram. From the on-shell conditions (8.35),

$$\Delta Z_\gamma \equiv \delta Z_1^\gamma - \delta Z_2^\gamma = -\frac{s_W}{c_W}\frac{\Sigma^{\gamma Z}(0)}{M_Z^2} \ , \qquad \Delta Z_{\gamma Z} \propto \frac{\Sigma^{\gamma Z}(0)}{M_Z^2} \ , \tag{8.50}$$

with the field-constant piece $\Pi^\gamma(0)$ cancelling in the difference $\delta Z_1^\gamma - \delta Z_2^\gamma$. These photon-sector constants do *not* vanish here: at $\mathcal{O}(\alpha)$ the $\gamma$–$Z$ mixing self energy at zero momentum is non-zero, $\Sigma^{\gamma Z}(0)|_\alpha \neq 0$, the $W$-boson loop contributing a piece $\propto M_W^2$. Hence *all* of term (c) — fermion *and* photon sector — belongs to the sub-renormalized $\Gamma_\mu|_{\alpha\alpha_s}$ (the "one-loop corrections to the NLO counterterms" referred to above); it is not an independent local counterterm.

*Only in the overall (local) counterterm, term (b), $Z|_{\alpha\alpha_s} \, \Gamma_\mu^{(0)}$, does the photon sector drop out.* There the mixing constants are needed at $\mathcal{O}(\alpha\alpha_s)$, $\Delta Z_\gamma|_{\alpha\alpha_s}$, $\Delta Z_{\gamma Z}|_{\alpha\alpha_s} \propto \Sigma^{\gamma Z}(0)|_{\alpha\alpha_s}$, and at this order the $\gamma$–$Z$ mixing at zero momentum is a massless-quark loop dressed by a gluon — once more scaleless, so

$$\Sigma^{\gamma Z}(0)\big|_{\alpha\alpha_s} = 0 \qquad \Longrightarrow \qquad \Delta Z_\gamma\big|_{\alpha\alpha_s} = \Delta Z_{\gamma Z}\big|_{\alpha\alpha_s} = 0 \ . \tag{8.51}$$

The local counterterm therefore reduces to the two-loop fermion field renormalization $\delta Z_V^q - \delta Z_A^q \gamma_5$ alone, which is eq. (8.45). This vanishing, and that of $\delta Z_2^q|_{\alpha_s}$ in (8.49), follow from the same fact: for massless quarks the scaleless $\mathcal{O}(\alpha_s)$ (quark–gluon) integrals vanish in dimensional regularization once the ultraviolet and infrared poles are identified. The photon-sector *sub*-renormalization of term (c) is, by contrast, retained.

The unrenormalised mixed vertex diagrams themselves organise into four sets by coupling structure. The $W$-exchange sets generate the square-root letter

$$\ell_W = \frac{\sqrt{\tilde{x}+4} - \sqrt{\tilde{x}}}{\sqrt{\tilde{x}+4} + \sqrt{\tilde{x}}}, \qquad \tilde{x} \equiv -t/M_W^2, \tag{8.52}$$

already seen at $\mathcal{O}(\alpha)$, so the natural function alphabet is that of generalised harmonic polylogarithms.

## 8.3 Linearization of General Harmonic Polylogarithms

The results presented in this chapter involve an alphabet containing a square-root letter and are therefore naturally expressed in terms of generalized harmonic polylogarithms (GHPLs). While these functions provide a compact analytic representation of the master integrals, they are not ideally suited for efficient numerical evaluation. Most existing numerical implementations are optimized for ordinary multiple polylogarithms (MPLs),

whose letters are rational functions of the kinematic variables. Consequently, before the analytic expressions can be used in phenomenological applications, the square-root dependence must be eliminated through an appropriate change of variables or by applying functional identities that linearize the alphabet.

This linearization procedure is generally highly non-trivial. It requires identifying suitable variable transformations that rationalize the square-root structures while preserving the analytic properties of the functions, after which the generalized harmonic polylogarithms can be rewritten as ordinary multiple polylogarithms. For complicated alphabets this process is often difficult to perform manually and can become one of the most technically demanding steps in obtaining numerically stable expressions.

To overcome this difficulty, a new Mathematica package currently under development within our research group automates the entire linearization procedure. Starting from expressions written in terms of generalized harmonic polylogarithms with algebraic letters, the package systematically identifies the appropriate rationalizing transformations, rewrites the functions in terms of ordinary multiple polylogarithms, and produces expressions that are directly compatible with existing high-performance numerical evaluation libraries. This significantly simplifies the transition from analytic results to phenomenological predictions and provides an efficient framework for the numerical evaluation of Feynman integrals involving square-root alphabets.

## 8.4 Status and outlook

In summary, the ingredients assembled here, namely the projectors and form-factor decomposition, the $\gamma_5$ prescription and its finite renormalisation, and the on-shell counterterms at $\mathcal{O}(\alpha)$ and $\mathcal{O}(\alpha\alpha_s)$, render the virtual $\gamma qq$ building block ultraviolet finite. What remains, and is left to future work, is the completion of the finite renormalised form factors, their combination with the corresponding real-radiation contributions (for which the master integrals of Chapter 7 are the QCD part), and the mass factorisation and observable-level assembly into a finite mixed QCD–electroweak SIDIS prediction. That assembly is the meeting point of the two strands of this thesis, and is discussed among the future directions of Chapter 9.

# Chapter 9

# Conclusions and Outlook

## Contents

9.1 Summary . . . . . 85
9.2 Methodological remarks . . . . . 86
9.3 Outlook . . . . . 86

## 9.1 Summary

The central result of this thesis is a reusable analytic infrastructure for the angular phase-space integrals of real radiation: a complete basis of three- and four-denominator angular families, a systematic Mellin–Barnes-to-polylogarithm construction method, and a validated NNLO SIDIS application that demonstrates the framework in a non-trivial physical setting. Starting from reverse unitarity and the radial–angular decomposition (Chapter 2), we evaluated the process-independent angular integrals through their Mellin–Barnes representation. We used the balanced structure of the resulting integrals (Proposition 3.2) to convert them into beta functions, then into real parametric integrals, and finally, via the delta-collapse, into Goncharov polylogarithms (Chapters 3 and 4). With this method we computed, for the first time, the complete three- and four-denominator angular families, both massless and massive, together with their polylogarithmic alphabets (seventeen letters at four denominators massless, eleven for the single-massive case), the partial-fraction construction that reduces the multi-massive cases to the single-massive one, and the recursion relations that lower denominator powers (Chapter 5). We then applied the method to semi-inclusive deep-inelastic scattering at NNLO (Chapters 6 and 7), where we evaluated the twenty double-real master integrals and resolved their soft and collinear singularities, including soft singularities nested inside the angular part and extracted to all orders in the regulator. We validated every result against independent calculations, direct numerical Mellin–Barnes integration, lower-denominator closed forms, permutation symmetries, and an independent differential-equation evaluation.

Taken together, the results show that the angular integrals form a reusable analytic infrastructure for real-radiation calculations. They are transparent in their singularity structure and reusable across processes, and the Mellin–Barnes-to-polylogarithm method is an effective and checkable way to build them. Semi-inclusive DIS provided both a demanding test of the framework and a physically important application.

I summarise the original results, in the order in which they were stated in Section 1.11.

I formulated the Mellin–Barnes-to-polylogarithm method as an explicit algorithm (Chapters 3 and 4). We computed the first analytic three-denominator angular families, massless to $\mathcal{O}(\epsilon^2)$ and single-massive to $\mathcal{O}(\epsilon)$. We computed the first analytic four-denominator families, together with their seventeen- and eleven-letter alphabets and the partial-fraction construction for the multi-massive cases (Chapter 5). We evaluated the NNLO SIDIS master integrals by the radial–angular method, resolved their nested soft and collinear singularities, and cross-checked them against an independent differential-equation calculation (Chapter 7). We validated all of these results and we also developed the framework for the electroweak strand of the program (Chapter 8).

## 9.2 Methodological remarks

I note three methodological points. First, the choice of representation matters. The angular integrals are difficult to handle in their defining form. The Somogyi Mellin–Barnes representation exposes their analytic structure (the location of the singular locus, the balanced pairing of gamma functions, and the eventual alphabet) directly, so that the computation reduces to a sequence of controlled steps. The Mellin–Barnes representation thus plays the same role for real-radiation angular integrals that the loop-momentum representation plays for virtual integrals.

Second, independent checks are essential. We computed every result here, wherever possible, in two independent ways: Mellin–Barnes against differential equations, analytic against numerical, and internal symmetry against external reproduction. We used this redundancy as a design principle. It caught errors during the calculation, it fixed branch and continuation ambiguities that no single method resolves on its own, and it allowed us to state the final results with confidence. For analytic computations of this length, where a single sign or a misplaced pole can invalidate pages of algebra, independent checks are as much a part of the method as the integration itself.

Third, the method has a well-defined boundary of applicability, between the polylogarithmic and the elliptic. We map this boundary for the angular integrals treated here. The three- and four-denominator families fall on the polylogarithmic side because their square roots are rationalisable and their geometry is of genus zero, and the same diagnostics also indicate where, at higher denominator number, the boundary is likely to be crossed. Knowing where a method stops is as useful as knowing what it computes.

## 9.3 Outlook

Several directions extend naturally from this work.

**The five-denominator frontier and elliptic generalisations:** The methods presented here deliver ordinary polylogarithms because the relevant square roots, most visibly the root $\sqrt{Y_1}$ of the four-denominator massless alphabet, are rationalisable and the underlying geometry is of genus zero. At five denominators this is no longer guaranteed. The number of independent scalar products grows, so that the real integrals can carry several square roots simultaneously. While any single root can be removed by a change of variables, several algebraically independent roots in general cannot be rationalised at once, and the iterated integration is then blocked at the polylogarithmic level (Section 4.8). Beyond this, the geometry underlying the integral may cease to be rational, in which case elliptic multiple polylogarithms (associated with an elliptic curve defined by the singular

locus) or higher-genus generalisations would appear, exactly as has been found for certain massive Feynman integrals. Whether the five-denominator angular integrals remain polylogarithmic, and if not, what the simplest non-polylogarithmic structure is, is in my view the central open question raised by this thesis. The balanced Mellin–Barnes representation, which exposes the singular locus directly, seems a promising tool with which to attack it, perhaps in combination with the maximal-cut / leading-singularity diagnostics used to detect elliptic geometries.

**Toward a theorem on balanced representations:** Proposition 3.2 was established for all cases treated here and conjectured in general. A proof that every angular integral in the Somogyi representation generates a balanced Mellin–Barnes integral, stable under analytic continuation and Laurent expansion, would turn a successful calculational strategy into a structural principle, and would delineate exactly the class of real-radiation integrals reachable by this method.

**Automation:** The complete workflow, from a set of denominators to a validated polylogarithmic answer, is algorithmic. Its individual steps are already implemented in the code released as ancillary material with the underlying publications (the result and evaluation files listed in Section A.2). Consolidating these into a single, documented, public package that takes the denominators and mass pattern as input and returns the Laurent expansion in terms of GPLs, together with the alphabet and built-in numerical validation, would make the method directly available to the community, with this thesis as its theoretical manual.

**Broader applications:** Because the angular integrals are process-independent, the families computed here are not specific to SIDIS. The same three- and four-denominator objects enter the double-real corrections to Drell–Yan and Higgs production, to other SIDIS structure functions, and to a range of jet and event-shape observables; their availability in closed, fast-to-evaluate form removes one recurring obstacle from any such NNLO (and, with the higher-denominator extension, $\mathrm{N^3LO}$) calculation. The radial–angular strategy itself, of isolating a universal angular core and a process-specific one-fold radial integral, is equally transferable.

**Toward complete physical observables:** The master integrals computed here are ingredients of, but not yet, a physical cross section. Combining them with the two-loop virtual and real–virtual contributions available in the literature, and with the electroweak renormalisation ingredients developed in Chapter 8, would yield a finite, renormalised NNLO (and eventually mixed QCD–electroweak) SIDIS prediction. Assembling such an observable, the first to make essential use of the new angular families, would close the path from method to phenomenology and provide a high-precision reference for the Electron–Ion Collider programme.

Taken together, these directions indicate that the analytic study of real-radiation phase-space integrals, long the less-developed counterpart of virtual integrals, is now open to the same systematic, special-function-based treatment, and that the angular integrals computed here are a durable part of its foundation.

# Appendix A

# Conventions and Supplementary Material

This appendix collects the conventions used throughout the thesis and a map of the machine-readable material released with the underlying publications.

## A.1 Notation and Conventions

I collect here the conventions used throughout the thesis.

**Dimensional regularisation:** I work in $d = 4 - 2\epsilon$ dimensions with the mostly-minus metric $g_{\mu\nu} = \mathrm{diag}(+,-,-,-)$. The SIDIS results of the underlying publication [35] were originally derived in the $d = 4+\epsilon_p$ convention; I convert them with $\epsilon_p = -2\epsilon$ (Section 2.11).

**Angular integrals:** The central object is

$$\Omega_{j_1,\ldots,j_n} = \int \mathrm{d}\Omega_{d-1}(q) \prod_{i=1}^{n} \frac{1}{(p_i\cdot q)^{j_i}}, \qquad j = \sum_i j_i, \tag{A.1}$$

with the invariant data encoded in $v_{kl} = p_k\cdot p_l/2$ for $k \neq l$ and $v_{kk} = p_k^2/4$; a massless leg has $v_{kk} = 0$. The total angular volume is normalised to $I^{(0)}(\epsilon) = 2\pi/(1-2\epsilon)$. A superscript $I^{(m)}$ counts the number of massive denominators.

**Polylogarithms:** Goncharov polylogarithms are defined by

$$G(a_1,\ldots,a_n;x) = \int_0^x \frac{\mathrm{d}t}{t-a_1}\, G(a_2,\ldots,a_n;t), \qquad G(;x) = 1, \tag{A.2}$$

with $G(\mathbf{0}_n;x) = \ln^n x/n!$.

**SIDIS:** The hadronic variables are $x_B = Q^2/(2P\cdot q)$, $z_h = P\cdot P_h/P\cdot q$, $y = P\cdot q/P\cdot l$, with partonic counterparts $x' = x_B/\xi$, $z' = z_h/\eta$; I write $\bar{x} = 1-x$ throughout. The double-real master integral families are

$$\mathrm{RR}_k(n_1,n_2,n_3) = e^{-\epsilon\gamma_E}(4\pi)^d \int \frac{[\mathrm{d}PS_3]_{z'}}{D_{N_{k1}}^{n_1} D_{N_{k2}}^{n_2} D_{N_{k3}}^{n_3}}, \tag{A.3}$$

in the eight-denominator basis of Section 6.6.

## A.2 Map of the Ancillary Files

The complete analytic expressions and their numerical implementation are released as ancillary material with the underlying publications. Table A.1 maps each file to its content.

Table A.1: The released implementation accompanying the underlying publications.

| File | Content |
|---|---|
| `3prop0mass.m`, `3prop1mass.m` | three-denominator massless and single-massive results |
| `recursion.m` | recursion-relation coefficients (three and four denominators) |
| `massless_ep0.m`, `one_mass_ep0.m` | four-denominator results at the finite order |
| `de_results.m`, `rad_results.m` | SIDIS master integrals (differential-equation and radial–angular routes); |
| `Evaluation.nb`, `main.nb` | numerical evaluation and benchmarking |

# Appendix B

# Evaluation of Angular Phase-Space Integrals

This appendix supports the angular method of Chapters 4 and 5. It gives the coordinate setup, some explicit real-integral representations and alphabets and some of the partial-fraction and recursion relations that organize the massive families. The bulkiest expressions are deferred to the ancillary files of Section A.2.

## B.1 Spherical Coordinates and the Angular Measure in $d$ Dimensions

I collect here the conventions for the $d$-dimensional phase-space measure used throughout Chapters 2, 4 and 5, following the explicit treatments of Refs. [203]. Throughout $d = 4-2\epsilon$ and the spatial dimension is $N = d-1 = 3-2\epsilon$.

**Radial–angular split:** For a Euclidean vector $\mathbf{q} \in \mathbb{R}^N$ we write $\mathbf{q} = r\,\hat{\mathbf{n}}$ with $r = |\mathbf{q}| \geq 0$ and $\hat{\mathbf{n}} \in S^{N-1}$, so that

$$\mathrm{d}^N\mathbf{q} = r^{N-1}\,\mathrm{d}r\,\mathrm{d}\Omega_{N-1}, \qquad \mathrm{d}\Omega_{N-1} = \Big(\prod_{j=1}^{N-2}(\sin\theta_j)^{\,N-1-j}\,\mathrm{d}\theta_j\Big)\mathrm{d}\phi, \tag{B.1}$$

with polar angles $\theta_j \in [0,\pi]$ and an azimuth $\phi \in [0,2\pi]$. The on-shell phase-space measure of a single massless parton follows from $q^0 = |\mathbf{q}|$,

$$\int \frac{\mathrm{d}^{d-1}\mathbf{q}}{(2\pi)^{d-1}\,2q^0} = \frac{1}{2(2\pi)^{d-1}}\int_0^\infty \mathrm{d}r\,r^{d-3}\int \mathrm{d}\Omega_{d-2}. \tag{B.2}$$

**Total solid angle:** Using the master integral

$$\int_0^\pi \mathrm{d}\theta\,(\sin\theta)^\alpha = \sqrt{\pi}\,\frac{\Gamma\!\left(\frac{\alpha+1}{2}\right)}{\Gamma\!\left(\frac{\alpha+2}{2}\right)}, \qquad \mathrm{Re}\,\alpha > -1, \tag{B.3}$$

the surface area of the unit sphere $S^m$ is

$$\Omega_m = \int \mathrm{d}\Omega_m = \frac{2\pi^{(m+1)/2}}{\Gamma\!\left(\frac{m+1}{2}\right)}, \qquad \text{so that} \qquad \Omega_{d-2} = \frac{2\pi^{(d-1)/2}}{\Gamma\!\left(\frac{d-1}{2}\right)} = \frac{2\pi^{3/2-\epsilon}}{\Gamma\!\left(\frac{3}{2}-\epsilon\right)}. \tag{B.4}$$

## B.2 Integral Representations and Alphabets

The conversion of the four-denominator massless Mellin–Barnes representation (5.17) to real parametric form yields ten integrals over the variables $\{v_1, x_1, x_2, x_3\}$ with $v_1 \in [0, v_{12}]$ and $x_i \in [0,1]$ (writing $\bar{x}_i = 1 - x_i$), reproduced from Ref. [141]:

$$
\begin{aligned}
I_1 &= \int \mathrm{d}v_1\,\mathrm{d}x_1\, \frac{\pi v_{14} x_1}{8 v_{13} v_{34} (v_{12}^2 v_{34} \bar{x}_1 - v_1 v_{14} v_{23} x_1)}, \\
I_2 &= \int \mathrm{d}v_1\,\mathrm{d}x_1\, \frac{-\pi v_{23} v_{34} x_1}{8 v_{12} v_{13} (v_1 v_{34} \bar{x}_1 - v_{14} v_{23} x_1)^2}, \\
I_3 &= \int \mathrm{d}v_1\,\mathrm{d}x_1\mathrm{d}x_2\mathrm{d}x_3\, \frac{3\pi v_1 v_{12}^5 v_{13}^3 v_{14} v_{23}^2 v_{24}^2 v_{34}^2 x_1 x_3^2 \bar{x}_1 \bar{x}_2^2}{4(v_1 v_{14} v_{23}(v_{12} v_{34} \bar{x}_1 \bar{x}_3 + v_{13} v_{24} x_1 x_2) - v_{12}^2 v_{13} v_{24} v_{34} x_3 \bar{x}_2)^4}, \\
I_4 &= \int \mathrm{d}x_1\mathrm{d}x_2\mathrm{d}x_3\, \frac{-\pi v_{12}^2 v_{13}^2 v_{14} v_{23} v_{24} v_{34}^2 \bar{x}_1 \bar{x}_2 \bar{x}_3}{2(v_{12} v_{34}(v_{13} v_{24} \bar{x}_2 \bar{x}_3 - v_{14} v_{23} x_2 \bar{x}_1) + v_{13} v_{14} v_{23} v_{24} x_1 x_3)^3}, \\
I_6 &= \int \mathrm{d}x_1\mathrm{d}x_2\mathrm{d}x_3\, \frac{\pi v_{12}^2 v_{13} v_{14}^2 v_{23} v_{24} v_{34}^2 x_3 \bar{x}_1 \bar{x}_2}{2(v_{12} v_{34}(v_{14} v_{23} \bar{x}_1 \bar{x}_2 + v_{13} v_{24} x_2 x_3) - v_{13} v_{14} v_{23} v_{24} x_1 \bar{x}_3)^3}, \\
I_9 &= \int \mathrm{d}x_1\, \frac{\pi}{4 v_{13}(v_{14} v_{23} - v_{12} v_{34}) x_1 + 4 v_{12} v_{13} v_{34}}, \\
I_{10} &= \int \mathrm{d}x_1\mathrm{d}x_2\mathrm{d}x_3\, \frac{-\pi v_{12} v_{13} v_{14} v_{23} v_{24} v_{34}}{4(v_{12} v_{14} v_{23} v_{34} x_3 \bar{x}_1 + v_{13} v_{24}(v_{14} v_{23} x_1 \bar{x}_2 + v_{12} v_{34} x_2 \bar{x}_3))^2},
\end{aligned}
\tag{B.5}
$$

the remaining integrals $I_5, I_7, I_8$ being the lengthier entries given in the ancillary files. For the single-massive case the analogous conversion gives fifteen integrals $I_i = \int \mathrm{d}\mu_i\, A_i/B_i$, whose numerators $A_i$ and denominators $B_i$, together with the explicit roots $Z_{1,2}^{(1)}$ of the alphabet (5.23), are provided in machine-readable form in the ancillary files (Section A.2).

The seventeen-letter alphabet of the massless four-denominator family (5.20) is, in the notation of Section 5.5,

$$
\begin{aligned}
&l_1 = 0, \quad l_2 = 1, \quad l_3 = \frac{v_{13} v_{24}}{X_4}, \quad l_4 = \frac{v_{14} v_{23}}{X_5}, \\
&l_5 = \frac{v_{13} v_{24}}{X_6}, \quad l_6 = -\frac{v_{12} v_{34}}{X_5}, \quad l_7 = -\frac{v_{12} v_{34}}{X_6},
\end{aligned}
\tag{B.6}
$$

together with the ten algebraic letters built from the single root $\sqrt{Y_1}$,

$$
\begin{aligned}
l_{8,13} &= \frac{X_1 \mp \sqrt{Y_1}}{2 v_{14} v_{23}}, \quad l_{9,14} = \frac{X_1 \mp \sqrt{Y_1}}{2 v_{13} v_{24}}, \quad l_{10,15} = \frac{X_2 \mp \sqrt{Y_1}}{2 v_{14} v_{23}}, \\
l_{11,16} &= \frac{X_3 \mp \sqrt{Y_1}}{2 v_{13} v_{24}}, \quad l_{12,17} = \frac{X_3 \mp \sqrt{Y_1}}{2 v_{12} v_{34}},
\end{aligned}
\tag{B.7}
$$

where

$$
\begin{aligned}
X_1 &= v_{14} v_{23} + v_{13} v_{24} - v_{12} v_{34}, & X_2 &= v_{14} v_{23} - v_{13} v_{24} + v_{12} v_{34}, \\
X_3 &= -v_{14} v_{23} + v_{13} v_{24} + v_{12} v_{34}, & X_4 &= -v_{14} v_{23} + v_{13} v_{24}, \\
X_5 &= v_{14} v_{23} - v_{12} v_{34}, & X_6 &= v_{13} v_{24} - v_{12} v_{34},
\end{aligned}
\tag{B.8}
$$

and the discriminant of the rationalising root is

$$
Y_1 = v_{14}^2 v_{23}^2 - 2 v_{14} v_{23}(v_{13} v_{24} + v_{12} v_{34}) + X_6^2. \tag{B.9}
$$

As an example of a closed form, the leading $1/\epsilon$ pole of the unit-power four-denominator master integral is fully symmetric in the four directions,

$$I^{(0),-1}_{1,1,1,1} = -\frac{\pi}{8}\frac{1}{4!}\sum_{\sigma\in S_4}\frac{v_{\sigma(1)\sigma(2)}\,v_{\sigma(1)\sigma(3)}\,v_{\sigma(2)\sigma(3)}}{\prod_{1\le i<j\le 4} v_{ij}}, \tag{B.10}$$

while the single-massive analogue retains the residual symmetry of the three massless legs,

$$I^{(1),-1}_{1,1,1,1} = -\frac{\pi}{8}\frac{1}{2}\frac{\sum_{\sigma\in S_3} v_{1\sigma(2)}\,v_{1\sigma(3)}\,v_{\sigma(2)\sigma(3)}}{\prod_{1\le i<j\le 4} v_{ij}}. \tag{B.11}$$

The corresponding finite parts are weight-two combinations of the alphabet above and are collected in the ancillary files `massless_ep0.m` and `one_mass_ep0.m`.

## B.3 Partial-Fraction and Recursion Relations

The multi-massive angular integrals are reduced to single-massive ones by iterating the merge of a massive pair $(a, b)$ into an effective massless leg, governed by the construction rule Proposition 5.1.

**Three denominators, triple-massive:** Applying the two-point splitting lemma twice gives $I^{(3)}_{j,k,l}$ as a double sum of single-massive integrals $I^{(1)}$ with splitting parameters $\lambda_\pm$, $\tilde{\lambda}_\pm$, $\lambda'_\pm$ built from the three quadratics $\sqrt{v_{12}^2 - v_{11}v_{22}}$, $\sqrt{v_{13}^2 - v_{11}v_{33}}$, $\sqrt{v_{23}^2 - v_{22}v_{33}}$, and induced scalar products from Proposition 5.1; the full expression is implemented in `recursion.m` and `3prop1mass.m`.

**Four denominators:** The triple-massive case reads

$$\begin{aligned} I^{(3)}_{1,1,1,1} = {} & \lambda_{12}\lambda_{13}\, I^{(1)}_{1,1,1,1}(v_{11}, v_{14}, v_{15}, v_{16}, v_{45}, v_{46}, v_{56}) \\ & + \lambda_{12}\bar{\lambda}_{13}\, I^{(1)}_{1,1,1,1}(v_{33}, v_{34}, v_{35}, v_{36}, v_{45}, v_{46}, v_{56}) \\ & + \bar{\lambda}_{12}\lambda_{13}\, I^{(1)}_{1,1,1,1}(v_{22}, v_{24}, v_{25}, v_{27}, v_{45}, v_{47}, v_{57}) \\ & + \bar{\lambda}_{12}\bar{\lambda}_{13}\, I^{(1)}_{1,1,1,1}(v_{33}, v_{34}, v_{35}, v_{37}, v_{45}, v_{47}, v_{57}), \end{aligned} \tag{B.12}$$

and the fully massive case is the eight-term analogue given in Ref. [141]; in every term the scalar products of the effective legs follow from Proposition 5.1, e.g.

$$v_{56} = \bar{\lambda}_{12}\bar{\lambda}_{13}(2v_{11}) + \bar{\lambda}_{12}\lambda_{13}v_{13} + \lambda_{12}\bar{\lambda}_{13}v_{12} + \lambda_{12}\lambda_{13}v_{23}. \tag{B.13}$$

The six recursion relations for the three-denominator integrals, of which one is quoted in Section 5.5, relate integrals of shifted denominator powers and follow from $\partial_{v_{kl}}\Omega$. Three of them are presented here:

$$\begin{aligned} 0 = {} & (j+k+l-1+2\epsilon)I_{j,k,l} - (2j+l+k+2\epsilon)I_{1+j,k,l} + v_{11}(j+1)I_{2+j,k,l} \\ & - l\, I_{j,k,1+l} - k\, I_{j,1+k,l} + l\, v_{13} I_{1+j,k,1+l} + k\, v_{12} I_{1+j,1+k,l}, \end{aligned} \tag{B.14}$$

$$\begin{aligned} 0 = {} & (-1+2\epsilon+j+k+l)I_{j,k,l} - l\, I_{j,k,1+l} + (-2\epsilon-j-2k-l)I_{j,1+k,l} \\ & + l\, v_{23} I_{j,1+k,1+l} + (1+k)v_{22} I_{j,2+k,l} - j\, I_{1+j,k,l} + j\, v_{12} I_{1+j,1+k,l}, \end{aligned} \tag{B.15}$$

$$0 = (-1+2\epsilon+j+k+l)I_{j,k,l} + (-2\epsilon-j-k-2l)I_{j,k,1+l} + (1+l)v_{33} I_{j,k,2+l}$$

$$- k\, I_{j,1+k,l} + k\, v_{23} I_{j,1+k,1+l} - j\, I_{1+j,k,l} + j\, v_{13} I_{1+j,k,1+l}. \tag{B.16}$$

The remaining three relations carry rational coefficients $\{D_i, D'_i, E_i, E'_i\}$ in $v_{kl}$ and $\epsilon$, provided in the ancillary file `recursion.m`; the four-denominator recursion relations are obtained in the same way. Together they make the unit-power integrals the only independent data.

# Appendix C

# NNLO SIDIS Phase-Space Master Integrals

This appendix supports Chapter 7. It gives worked examples of the singularity resolution and the results of the NNLO SIDIS phase-space master integrals in the radial-angular decomposition.

## C.1 Resolution of Singularities: Worked Examples

In $d = 4-2\epsilon$, for $\mathrm{RR}_8(1,1,1)$ the $z$-dependent parametric factor is $P_z = [(1-z)z]^{-\epsilon}/[\,z\,(x'z(z'-1)+x'-zz'+z+z')\,]$, with a single endpoint singularity at $z \to 0$ regulated by $\epsilon$; choosing $g(z) = z^{-1-\epsilon}$ and $R(z) = P_z \Omega_z\, z^{1+\epsilon}$ in (7.19) resolves it. For $\mathrm{RR}_4(1,1,1)$, with the overall factor

$$C_4 = -\frac{4^{2\epsilon-3}\pi^{2\epsilon-4}(x'-1)^2 s^{-2\epsilon-2}(1-z')^{-2\epsilon} z'^{-\epsilon}}{(z'-1)\Gamma(1-2\epsilon)}, \tag{C.1}$$

the resolved integrand reads

$$\mathrm{RR}_4(1,1,1) = C_4 \int_0^1 \mathrm{d}z \Big[\frac{\pi}{2\epsilon^2 z'} - \frac{\pi}{2\epsilon z'}\Big(\frac{2-2x'}{zx'-z+1} - G\big(\tfrac{1}{1-z'};1\big)\Big) + \mathcal{O}(\epsilon^0)\Big]. \tag{C.2}$$

For $\mathrm{RR}_2(1,1,1)$ the angular part is itself singular inside the domain; factoring the all-order soft behaviour $z^{-1-\epsilon}$ out of the angular expression ($\Omega_z = \Omega'_z z^{1+\epsilon}$) and combining it with the radial factor $P_z = z^{-1-\epsilon}[-(z-1)z]^{-\epsilon}/[(z-1)(zz'-z-z')]$ produces two endpoint singularities ($z \to 0$ and $z \to 1$), each requiring its own counterterm $g_1(z) = z^{-1-2\epsilon}$, $g_2(z) = (1-z)^{-1-\epsilon}$. The explicit subtracted integrands are provided in `Evaluation.nb`.

# Appendix D

# Electroweak Renormalisation Ingredients

This appendix supports Chapter 8. It collects the Feynman rules used throughout the thesis and the on-shell renormalisation constants of the electroweak building block.

## D.1 Feynman Rules

For completeness I collect the Feynman rules used in the amplitude constructions of Chapters 6 to 8. I work in $d = 4 - 2\epsilon$ dimensions with the mostly-minus metric $g_{\mu\nu} = \mathrm{diag}(+,-,\ldots,-)$; all momenta are taken incoming, $\xi$ is the gauge parameter (Feynman gauge $\xi = 1$), $T^a$ are the $SU(3)$ generators with $[T^a, T^b] = i f^{abc} T^c$, and $g_s$ the strong coupling. The conventions follow Refs. [48]; the corresponding diagrams are shown in Figure D.1.

**QCD propagators:** For a massless quark, a gluon and a ghost,

$$\frac{i\,\delta_{ij}\,\not{p}}{p^2 + i0}, \qquad \frac{-i\,\delta^{ab}}{p^2 + i0}\Big[g_{\mu\nu} - (1-\xi)\frac{p_\mu p_\nu}{p^2}\Big], \qquad \frac{i\,\delta^{ab}}{p^2 + i0}. \tag{D.1}$$

**QCD vertices:** The quark–gluon, triple- and quartic-gluon and ghost–gluon vertices are

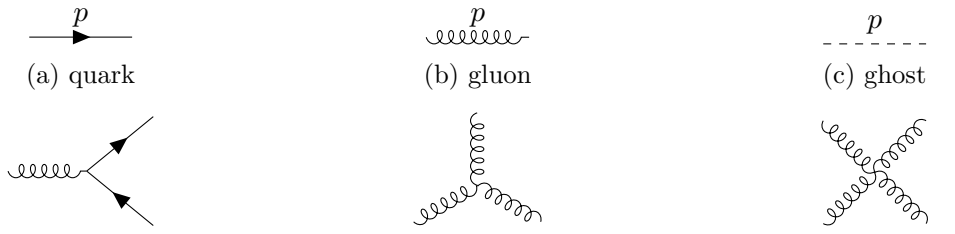
$$q_i \bar{q}_j g^a_\mu : \quad i g_s\, T^a_{ij}\, \gamma_\mu, \tag{D.2}$$

$$g^a_\mu g^b_\nu g^c_\rho : \quad g_s f^{abc}\big[g_{\mu\nu}(p_1 - p_2)_\rho + g_{\nu\rho}(p_2 - p_3)_\mu + g_{\rho\mu}(p_3 - p_1)_\nu\big], \tag{D.3}$$

$$\begin{aligned} g^a_\mu g^b_\nu g^c_\rho g^d_\sigma : \quad & -i g_s^2\big[f^{abe} f^{cde}(g_{\mu\rho}g_{\nu\sigma} - g_{\mu\sigma}g_{\nu\rho}) + f^{ace} f^{bde}(g_{\mu\nu}g_{\rho\sigma} - g_{\mu\sigma}g_{\nu\rho}) \\ & + f^{ade} f^{bce}(g_{\mu\nu}g_{\rho\sigma} - g_{\mu\rho}g_{\nu\sigma})\big], \end{aligned} \tag{D.4}$$

$$\bar{c}^a c^b g^c_\mu : \quad g_s f^{abc}\, p_{1\mu}, \tag{D.5}$$

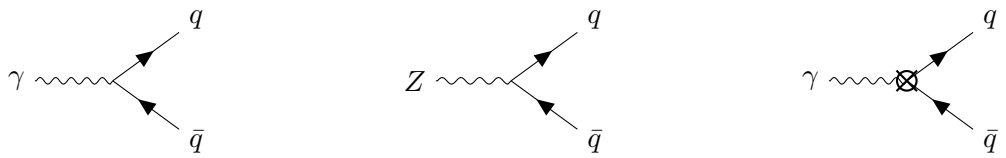
with $p_{1,2,3}$ the incoming boson momenta and $p_1$ the outgoing-ghost momentum in the last line.




(a) quark (b) gluon (c) ghost

(d) $q\bar{q}g$ (e) three-gluon (f) four-gluon

Figure D.1: The QCD propagators and interaction vertices whose algebraic expressions are given in (D.1)–(D.5): the quark, gluon and ghost propagators (top), and the quark–gluon, three-gluon and four-gluon vertices (bottom). The ghost–gluon vertex is not drawn separately. All momenta are taken incoming.




(a) $\gamma q\bar{q}$ (b) $Zq\bar{q}$ (c) counterterm

Figure D.2: The electroweak neutral-current vertices whose expressions are given in (D.6): the photon and $Z$ couplings to a quark pair, and the counterterm vertex (crossed circle) that carries the renormalisation constants of Chapter 8. All momenta are taken incoming.

**Electroweak neutral-current vertices:** Writing the neutral current as $i\gamma_\mu(g_V+g_A\gamma_5)$, the photon and $Z$ couplings to a quark of charge $Q_q$ and weak isospin $I_3^q$ are

$$\gamma q\bar{q}: \; -ie\,Q_q\,\gamma_\mu, \qquad Zq\bar{q}: \; ie\,\gamma_\mu\,(v_q - a_q\gamma_5), \qquad v_q = \frac{I_3^q - 2Q_q s_W^2}{2s_W c_W}, \quad a_q = \frac{I_3^q}{2s_W c_W}, \tag{D.6}$$

with $s_W = \sin\theta_W$, $c_W = \cos\theta_W$ and $e$ the positron charge; the corresponding diagrams, together with the counterterm vertex, are shown in Figure D.2.

**Counterterm vertices:** With the field-renormalisation differences $\Delta Z_\gamma = \delta Z_1^\gamma - \delta Z_2^\gamma$, $\Delta Z_{\gamma Z} = \delta Z_1^{\gamma Z} - \delta Z_2^{\gamma Z}$ and the chiral quark wave-function constants $\delta Z_{L,R}^q$, the renormalised $\gamma q\bar{q}$ vertex at $\mathcal{O}(\alpha)$ is

$$\gamma q\bar{q}: \; -ie\,\gamma_\mu\Big[Q_q\Big(1+\Delta Z_\gamma+\tfrac{1}{2}(1-\gamma_5)\delta Z_L^q+\tfrac{1}{2}(1+\gamma_5)\delta Z_R^q\Big)+\Delta Z_{\gamma Z}\,(v_q-a_q\gamma_5)\Big], \tag{D.7}$$

the $\gamma$–$Z$ mixing piece $\Delta Z_{\gamma Z}$ arising because the renormalised photon field mixes into the $Z$. The $\mathcal{O}(\alpha\alpha_s)$ counterterm used in Section 8.2 is the corresponding product form,

$$\begin{aligned}\gamma q\bar{q}: \; -ie\,\gamma_\mu\Big[&Q_q(1+\Delta Z_\gamma)\Big(1+\tfrac{1}{2}(1-\gamma_5)\delta Z_L^q+\tfrac{1}{2}(1+\gamma_5)\delta Z_R^q\Big)\\ &+\Delta Z_{\gamma Z}\Big(v_q-a_q\gamma_5+(a_q+v_q)\delta Z_L^q\tfrac{1}{2}(1-\gamma_5)+(v_q-a_q)\delta Z_R^q\tfrac{1}{2}(1+\gamma_5)\Big)\Big].\end{aligned} \tag{D.8}$$

## D.2 Renormalisation Constants and Ingredients

The form factors of Chapter 8 are extracted from the amplitude by Dirac projectors. In the massless vector/axial basis they take the schematic form

$$F_V = \mathrm{Tr}\big(P_V^{\mu}\,\Gamma_{\mu}\big), \qquad F_A = \mathrm{Tr}\big(P_A^{\mu}\,\Gamma_{\mu}\big), \tag{D.9}$$

with $P_V^{\mu}, P_A^{\mu}$ built from $\not{p}_1, \not{p}_2, \gamma^{\mu}$ and (for $P_A$) $\gamma_5$, normalised so that $F_V^{(0,0)} = 1$, $F_A^{(0,0)} = 0$. The on-shell field, mass, charge and mixing renormalisation constants entering the counterterm vertices of Section 8.2 ($\delta Z_L^q, \delta Z_R^q$, $\delta M_W^2, \delta M_Z^2$, $\delta s_W$, $\delta Z_2^{\gamma}$, $\Delta Z_{\gamma Z}$) are those of the standard on-shell scheme [48];

# Bibliography


[1] D.J. Gross and F. Wilczek, *Ultraviolet Behavior of Nonabelian Gauge Theories*, *Phys. Rev. Lett.* **30** (1973) 1343.

[2] H.D. Politzer, *Reliable Perturbative Results for Strong Interactions?*, *Phys. Rev. Lett.* **30** (1973) 1346.

[3] S.L. Glashow, *Partial Symmetries of Weak Interactions*, *Nucl. Phys.* **22** (1961) 579.

[4] S. Weinberg, *A Model of Leptons*, *Phys. Rev. Lett.* **19** (1967) 1264.

[5] A. Salam, *Weak and Electromagnetic Interactions*, *Conf. Proc. C* **680519** (1968) 367.

[6] G. Aad et al., *Observation of a new particle in the search for the standard model higgs boson with the atlas detector at the lhc*, *Physics Letters B* **716** (2012) 1.

[7] S. Chatrchyan et al., *Observation of a new boson at a mass of 125 gev with the cms experiment at the lhc*, *Physics Letters B* **716** (2012) 30.

[8] J. Ellis, *Physics beyond the standard model*, *Phil. Trans. Roy. Soc. Lond. A* **376** (2018) 20170065.

[9] J.M. Campbell, R.K. Ellis and C. Williams, *Vector boson pair production at the lhc*, *J. Phys. G* **42** (2015) 015005.

[10] C.e.a. Anastasiou, *High precision determination of the gluon fusion higgs boson cross-section at the lhc*, *JHEP* **05** (2016) 058.

[11] J.C. Collins, D.E. Soper and G. Sterman, *Factorization of hard processes in qcd*, *Adv. Ser. Direct. High Energy Phys.* **5** (1989) 1.

[12] A.A. et al., *Electron ion collider: The next qcd frontier*, *European Physical Journal A* **52** (2016) 268.

[13] C.-N. Yang and R.L. Mills, *Conservation of Isotopic Spin and Isotopic Gauge Invariance*, *Phys. Rev.* **96** (1954) 191.

[14] M. Gell-Mann, *A Schematic Model of Baryons and Mesons*, *Phys. Lett.* **8** (1964) 214.

[15] G. Zweig, *An SU(3) model for strong interaction symmetry and its breaking. Version 1*, .

[16] H. Fritzsch, M. Gell-Mann and H. Leutwyler, *Advantages of the Color Octet Gluon Picture*, *Phys. Lett. B* **47** (1973) 365.

[17] K.G. Wilson, *Confinement of Quarks*, *Phys. Rev. D* **10** (1974) 2445.

[18] T. Appelquist and J. Carazzone, *Infrared Singularities and Massive Fields*, *Phys. Rev. D* **11** (1975) 2856.

[19] M.A. Shifman, A.I. Vainshtein and V.I. Zakharov, *QCD and Resonance Physics. Theoretical Foundations*, *Nucl. Phys. B* **147** (1979) 385.

[20] J.D. Bjorken, *Asymptotic Sum Rules at Infinite Momentum*, *Phys. Rev.* **179** (1969) 1547.

[21] R.P. Feynman, *Very High-Energy Collisions of Hadrons*, *Phys. Rev. Lett.* **23** (1969) 1415.

[22] E.D. Bloom and F.J. Gilman, *Scaling, Duality, and the Behavior of Resonances in Inelastic Electron-Proton Scattering*, *Phys. Rev. Lett.* **25** (1970) 1140.

[23] H. Georgi and H.D. Politzer, *Freedom at Moderate Energies: Masses in Color Dynamics*, *Phys. Rev. D* **14** (1976) 1829.

[24] H1 AND ZEUS collaboration, *Combination of Measurements of Inclusive Deep Inelastic $e^{\pm}p$ Scattering Cross Sections and QCD Analysis of HERA Data*, *Eur. Phys. J. C* **75** (2015) 580 [1506.06042].

[25] R.K. Ellis, W.J. Stirling and B.R. Webber, *Qcd and collider physics*, *Cambridge Monographs on Particle Physics, Nuclear Physics and Cosmology* **8** (1996) .

[26] H1 and Z. Collaborations, *Combined measurement and qcd analysis of the inclusive $e^{\pm}p$ scattering cross sections at hera*, *Journal of High Energy Physics* **2009** (2009) 109.

[27] S. Moch, J.A.M. Vermaseren and A. Vogt, *The Three-Loop Splitting Functions in QCD: The Non-Singlet Case*, *Nucl. Phys. B* **688** (2004) 101 [hep-ph/0403192].

[28] A. Vogt, S. Moch and J.A.M. Vermaseren, *The Three-Loop Splitting Functions in QCD: The Singlet Case*, *Nucl. Phys. B* **691** (2004) 129 [hep-ph/0404111].

[29] D. Graudenz, *One-Particle Inclusive Processes in Deeply Inelastic Lepton-Nucleon Scattering*, *Nucl. Phys. B* **432** (1994) 351 [hep-ph/9406274].

[30] J.C. Collins and D.E. Soper, *Parton Distribution and Decay Functions*, *Nucl. Phys. B* **194** (1982) 445.

[31] S. Kretzer, *Fragmentation Functions from Flavor-Inclusive and Flavor-Tagged $e^+e^-$ Annihilations*, *Phys. Rev. D* **62** (2000) 054001 [hep-ph/0003177].

[32] D. de Florian, R. Sassot, M. Epele, R.J. Hernández-Pinto and M. Stratmann, *Parton-to-Pion Fragmentation Reloaded*, *Phys. Rev. D* **91** (2015) 014035 [1410.6027].

[33] A. Bacchetta, M. Diehl, K. Goeke, A. Metz, P.J. Mulders and M. Schlegel, *Semi-inclusive deep inelastic scattering at small transverse momentum*, *Journal of High Energy Physics* **2007** (2007) 093.

[34] M.A. et al., *Transverse-momentum-dependent parton distribution/fragmentation functions from sidis*, *Physical Review D* **87** (2013) 094019.

[35] T. Ahmed, S. Goyal, S.M. Hasan, R.N. Lee, S.-O. Moch, V. Pathak et al., *NNLO phase-space integrals for semi-inclusive deep-inelastic scattering*, *Phys. Rev. D* **112** (2025) 014020 [2412.16509].

[36] A.A. et al., *Electron ion collider: The next qcd frontier*, *European Physical Journal A* **52** (2016) 268.

[37] E.C.A. et al., *The Electron-Ion Collider: Assessing the Energy Dependence of Key Measurements*, *Rept. Prog. Phys.* **82** (2019) 024301 [1708.01527].

[38] M.S. Al-Buriahi, M.T. Hussein and M.T. Ghoneim, *Probing Nucleon Structure in Deep Inelastic Scattering*, *J. Appl. Math. Phys.* **3** (2015) 608.

[39] R. Abdul Khalek et al., *Science Requirements and Detector Concepts for the Electron-Ion Collider: EIC Yellow Report*, *Nucl. Phys. A* **1026** (2022) 122447 [2103.05419].

[40] D.W. Sivers, *Single-spin production asymmetries from the hard scattering of pointlike constituents*, *Physical Review D* **41** (1990) 83.

[41] J.C. Collins, D.E. Soper and G.F. Sterman, *Factorization of Hard Processes in QCD*, in *Perturbative Quantum Chromodynamics*, A.H. Mueller, ed., vol. 5 of *Advanced Series on Directions in High Energy Physics*, pp. 1–91, World Scientific (1989), DOI [hep-ph/0409313].

[42] J. Collins, *Foundations of Perturbative QCD*, vol. 32 of *Cambridge Monographs on Particle Physics, Nuclear Physics and Cosmology*, Cambridge University Press (2011), 10.1017/CBO9780511975592.

[43] G.F. Sterman, *Partons, factorization and resummation, TASI 95*, in *Theoretical Advanced Study Institute in Elementary Particle Physics (TASI 95): QCD and Beyond*, pp. 327–408, 6, 1995 [hep-ph/9606312].

[44] Y.L. Dokshitzer, *Calculation of the Structure Functions for Deep Inelastic Scattering and e+ e- Annihilation by Perturbation Theory in Quantum Chromodynamics*, *Sov. Phys. JETP* **46** (1977) 641.

[45] G. Altarelli and G. Parisi, *Asymptotic Freedom in Parton Language*, *Nucl. Phys. B* **126** (1977) 298.

[46] V.N. Gribov and L.N. Lipatov, *Deep inelastic e p scattering in perturbation theory*, *Sov. J. Nucl. Phys.* **15** (1972) 438.

[47] G. Curci, W. Furmanski and R. Petronzio, *Evolution of Parton Densities Beyond Leading Order: The Nonsinglet Case*, *Nucl. Phys. B* **175** (1980) 27.

[48] A. Denner, *Techniques for calculation of electroweak radiative corrections at the one loop level and results for W physics at LEP-200*, *Fortsch. Phys.* **41** (1993) 307 [0709.1075].

[49] F. Bloch and A. Nordsieck, *Note on the Radiation Field of the Electron*, *Physical Review* **52** (1937) 54.

[50] T. Kinoshita, *Mass Singularities of Feynman Amplitudes*, *Journal of Mathematical Physics* **3** (1962) 650.

[51] T.D. Lee and M. Nauenberg, *Degenerate Systems and Mass Singularities*, *Physical Review* **133** (1964) B1549.

[52] S. Catani, *The singular behaviour of QCD amplitudes at two-loop order*, *Physics Letters B* **427** (1998) 161.

[53] T. Becher and M. Neubert, *Infrared Singularities of Scattering Amplitudes in Perturbative QCD*, *Physical Review Letters* **102** (2009) 162001.

[54] E. Gardi and L. Magnea, *Factorization constraints for soft anomalous dimensions in QCD scattering amplitudes*, *Journal of High Energy Physics* **2009** (2009) 079.

[55] F. Bloch and A. Nordsieck, *Note on the radiation field of the electron*, *Physical Review* **52** (1937) 54.

[56] F.V. Tkachov, *A Theorem on Analytical Calculability of Four-Loop Renormalization Group Functions*, *Phys. Lett. B* **100** (1981) 65.

[57] K.G. Chetyrkin and F.V. Tkachov, *Integration by Parts: The Algorithm to Calculate Beta Functions in 4 Loops*, *Nucl. Phys. B* **192** (1981) 159.

[58] S. Laporta, *High-Precision Calculation Of Multiloop Feynman Integrals By Difference Equations*, *International Journal of Modern Physics A* **15** (2000) 5087.

[59] A.V. Kotikov, *Differential equations method. New technique for massive Feynman diagram calculation*, *Physics Letters B* **254** (1991) 158.

[60] E. Remiddi, *Differential equations for Feynman graph amplitudes*, *Nuovo cimento della Società italiana di fisica. A, Nuclei, particles and fields* **110** (1997) 1435.

[61] J.M. Henn, *Multiloop Integrals in Dimensional Regularization Made Simple*, *Physical Review Letters* **110** (2013) 251601.

[62] C. Anastasiou and K. Melnikov, *Higgs boson production at hadron colliders in NNLO QCD*, *Nucl. Phys. B* **646** (2002) 220 [hep-ph/0207004].

[63] S. Catani and M. Seymour, *A general algorithm for calculating jet cross sections in NLO QCD*, *Nuclear Physics B* **485** (1997) 291.

[64] S. Frixione, Z. Kunszt and A. Signer, *Three-jet cross sections to next-to-leading order*, *Nuclear Physics B* **467** (1996) 399.

[65] S. Catani and M. Grazzini, *An NNLO Subtraction Formalism in Hadron Collisions and Its Application to Higgs Boson Production at the LHC*, *Phys. Rev. Lett.* **98** (2007) 222002 [hep-ph/0703012].

[66] A.G. Ridder, T. Gehrmann and E.W.N. Glover, *Antenna subtraction at NNLO*, *Journal of High Energy Physics* **2005** (2005) 056.

[67] M. Czakon, *A novel subtraction scheme for double-real radiation at NNLO*, *Physics Letters B* **693** (2010) 259.

[68] J.R. Gaunt, M. Stahlhofen, F.J. Tackmann and J.R. Walsh, *N-jettiness subtractions for NNLO QCD calculations*, *Journal of High Energy Physics* **2015** (2015) .

[69] Z. Nagy and D.E. Soper, *General subtraction method for numerical calculation of one-loop QCD matrix elements*, *Journal of High Energy Physics* **2003** (2003) 055.

[70] G. Somogyi and Z. Trócsányi, *A subtraction scheme for computing QCD jet cross sections at NNLO: integrating the subtraction terms I*, *Journal of High Energy Physics* **2008** (2008) 042.

[71] R. Boughezal, K. Melnikov and F. Petriello, *A Subtraction Scheme for NNLO Computations*, *Phys. Rev. D* **85** (2012) 034025 [1111.7041].

[72] A. Gehrmann-De Ridder, T. Gehrmann and E.W.N. Glover, *Antenna subtraction at nnlo*, *JHEP* **09** (2005) 056 [hep-ph/0505111].

[73] M. Czakon, *A novel subtraction scheme for double-real radiation at nnlo*, *Phys. Lett. B* **693** (2010) 259 [1005.0274].

[74] G. Somogyi, Z. Trócsányi and V. Del Duca, *A subtraction scheme for computing qcd jet cross sections at nnlo: Regularization of doubly real emissions*, *JHEP* **01** (2007) 070 [hep-ph/0609042].

[75] V. Del Duca, C. Duhr, A. Kardos, G. Somogyi and Z. Trócsányi, *Three-jet production in electron-positron collisions at next-to-next-to-leading order accuracy*, *Phys. Rev. Lett.* **117** (2016) 152004 [1603.08927].

[76] L. Magnea, E. Maina, G. Pelliccioli, C. Signorile-Signorile, P. Torrielli and S. Uccirati, *Local analytic sector subtraction at nnlo*, *JHEP* **12** (2018) 107 [1806.09570].

[77] S. Catani and M. Grazzini, *An nnlo subtraction formalism in hadron collisions and its application to higgs boson production at the lhc*, *Phys. Rev. Lett.* **98** (2007) 222002 [hep-ph/0703012].

[78] J. Gaunt, M. Stahlhofen, F.J. Tackmann and J.R. Walsh, *N-jettiness subtractions for nnlo qcd calculations*, *JHEP* **09** (2015) 058 [1505.04794].

[79] R. Boughezal, C. Focke, X. Liu and F. Petriello, *W-boson production in association with a jet at next-to-next-to-leading order in perturbative qcd*, *Phys. Rev. Lett.* **115** (2015) 062002 [1504.02131].

[80] M. Cacciari, F.A. Dreyer, A. Karlberg, G.P. Salam and G. Zanderighi, *Fully differential vector-boson-fusion higgs production at next-to-next-to-leading order*, *Phys. Rev. Lett.* **115** (2015) 082002 [1506.02660].

[81] T. Binoth and G. Heinrich, *An automatized algorithm to compute infrared divergent multiloop integrals*, *Nucl. Phys. B* **585** (2000) 741 [hep-ph/0004013].

[82] W.L. van Neerven, *Dimensional Regularization of Mass and Infrared Singularities in Two Loop On-shell Vertex Functions*, *Nucl. Phys. B* **268** (1986) 453.

[83] G. Somogyi, *Angular integrals in d dimensions*, *J. Math. Phys.* **52** (2011) 083501 [1101.3557].

[84] T. Ahmed, S.M. Hasan and A. Rapakoulias, *Phase-space integrals through Mellin-Barnes representation*, *Phys. Rev. D* **112** (2025) L051903 [2410.18886].

[85] E. Byckling and K. Kajantie, *Particle Kinematics: (Chapters I-VI, X)*, University of Jyvaskyla, Jyvaskyla, Finland (1971).

[86] R. Kumar, *Covariant phase-space calculations of n-body decay and production processes*, *Phys. Rev.* **185** (1969) 1865.

[87] R.E. Cutkosky, *Singularities and discontinuities of Feynman amplitudes*, *J. Math. Phys.* **1** (1960) 429.

[88] M.J.G. Veltman, *Unitarity and causality in a renormalizable field theory with unstable particles*, *Physica* **29** (1963) 186.

[89] R.E. Cutkosky, *Singularities and discontinuities of Feynman amplitudes*, *J. Math. Phys.* **1** (1960) 429.

[90] C. Anastasiou and V.A. Smirnov, *Applied reverse unitarity for phase-space integrals*, *Nuclear Physics B* **699** (2004) 165.

[91] C. Anastasiou, K. Melnikov and F. Petriello, *Fully differential Higgs boson production and the di-photon signal through next-to-next-to-leading order*, *Nucl. Phys. B* **724** (2005) 197 [hep-ph/0501130].

[92] P.A. Baikov, *Explicit Solutions of the Multiloop Integral Recurrence Relations and Its Application*, *Nucl. Instrum. Meth. A* **389** (1997) 347 [hep-ph/9611449].

[93] A. Smirnov, *Algorithm FIRE—Feynman Integral REduction*, *Journal of High Energy Physics* **2008** (2008) 107.

[94] R.N. Lee, *Presenting LiteRed: A Tool for the Loop InTEgrals REDuction*, *Comput. Phys. Commun.* **184** (2013) 1412 [1212.2685].

[95] A. von Manteuffel and C. Studerus, *Reduze 2: Distributed Feynman Integral Reduction*, *Comput. Phys. Commun.* **183** (2012) 1293 [1201.4330].

[96] P. Maierhöfer, J. Usovitsch and P. Uwer, *Kira—A Feynman integral reduction program*, *Computer Physics Communications* **230** (2018) 99.

[97] A.V. Smirnov, *Algorithm fire — feynman integral reduction*, *Journal of High Energy Physics* **2008** (2008) 107.

[98] R.N. Lee, *Presenting LiteRed: a tool for the Loop InTEgrals REDuction*, 1212.2685.

[99] T. Gehrmann and E. Remiddi, *Differential equations for two-loop four-point functions*, *Nuclear Physics B* **580** (2000) 485.

[100] R.N. Lee, *Reducing differential equations for multiloop master integrals*, *Journal of High Energy Physics* **2015** (2015) .

[101] C. Meyer, *Transforming differential equations of multi-loop Feynman integrals into canonical form*, *Journal of High Energy Physics* **2017** (2017) .

[102] M. Argeri and P. Mastrolia, *FEYNMAN DIAGRAMS AND DIFFERENTIAL EQUATIONS*, *International Journal of Modern Physics A* **22** (2007) 4375.

[103] G. Heinrich, *Sector Decomposition*, *Int. J. Mod. Phys. A* **23** (2008) 1457 [0803.4177].

[104] T. Binoth and G. Heinrich, *An automatized algorithm to compute infrared divergent multi-loop integrals*, *Nucl. Phys. B* **585** (2000) 741 [hep-ph/0004013].

[105] T. Kaneko and T. Ueda, *A Geometric method of sector decomposition*, *Comput. Phys. Commun.* **181** (2010) 1352 [0908.2897].

[106] C. Anastasiou, F. Herzog and A. Lazopoulos, *On the factorization of overlapping singularities at NNLO*, *JHEP* **03** (2011) 038 [1011.4867].

[107] A. Gehrmann-De Ridder, T. Gehrmann, E.W.N. Glover and G. Heinrich, *Infrared Structure of $e^+e^- \to 3$ Jets at NNLO*, *JHEP* **11** (2007) 058 [0710.0346].

[108] G. Heinrich, *Sector Decomposition*, *Int. J. Mod. Phys. A* **23** (2008) 1457 [0803.4177].

[109] V.E. Lyubovitskij, F. Wunder and A.S. Zhevlakov, *New ideas for handling of loop and angular integrals in D-dimensions in QCD*, *JHEP* **06** (2021) 066 [2102.08943].

[110] V.A. Smirnov and F. Wunder, *Expansion by regions meets angular integrals*, *JHEP* **08** (2024) 138 [2405.13120].

[111] J. Haug and F. Wunder, *Angular integrals with three denominators via IBP, mass reduction, dimensional shift, and differential equations*, *JHEP* **03** (2025) 141 [2410.18177].

[112] J. Haug, V.A. Smirnov and F. Wunder, *On multi-propagator angular integrals*, *JHEP* **10** (2025) 001 [2508.00693].

[113] E.W. Barnes, *A New Development of the Theory of the Hypergeometric Functions*, *Proceedings of the London Mathematical Society* **s2-6** (1908) 141.

[114] J. Tausk, *Non-planar massless two-loop Feynman diagrams with four on-shell legs*, *Physics Letters B* **469** (1999) 225.

[115] V. Smirnov, *Analytical result for dimensionally regularized massless on-shell double box*, *Physics Letters B* **460** (1999) 397.

[116] J. Gluza, K. Kajda and T. Riemann, *AMBRE—a Mathematica package for the construction of Mellin–Barnes representations for Feynman integrals*, *Computer Physics Communications* **177** (2007) 879.

[117] M. Czakon, *Automatized analytic continuation of Mellin–Barnes integrals*, *Computer Physics Communications* **175** (2006) 559.

[118] A.V. Smirnov and V.A. Smirnov, *On the resolution of singularities of multiple Mellin–Barnes integrals*, *The European Physical Journal C* **62** (2009) 445.

[119] V.A. Smirnov, *Analytical result for dimensionally regularized massless master double box with one leg off-shell*, *Phys. Lett. B* **491** (2000) 130 [hep-ph/0007032].

[120] J.B. Tausk, *Non-planar massless two-loop Feynman diagrams with four on-shell legs*, *Phys. Lett. B* **469** (1999) 225 [hep-ph/9909506].

[121] M. Czakon, *Automatized analytic continuation of Mellin-Barnes integrals*, *Comput. Phys. Commun.* **175** (2006) 559 [hep-ph/0511200].

[122] A.B. Goncharov, *Multiple polylogarithms, cyclotomy and modular complexes*, *Mathematical Research Letters* **5** (1998) 497.

[123] A.B. Goncharov, *Multiple polylogarithms and mixed Tate motives*, *arXiv (Cornell University)* (2001) .

[124] E. Remiddi and J.A.M. Vermaseren, *HARMONIC POLYLOGARITHMS*, *International Journal of Modern Physics A* **15** (2000) 725.

[125] J. Vollinga and S. Weinzierl, *Numerical evaluation of multiple polylogarithms*, *Comput. Phys. Commun.* **167** (2005) 177 [hep-ph/0410259].

[126] D. Maitre, *HPL, a mathematica implementation of the harmonic polylogarithms*, *Comput. Phys. Commun.* **174** (2006) 222 [hep-ph/0507152].

[127] R. Bonciani, G. Degrassi and A. Vicini, *On the Generalized Harmonic Polylogarithms of One Complex Variable*, *Comput. Phys. Commun.* **182** (2011) 1253 [1007.1891].

[128] C. Duhr, *Mathematical aspects of scattering amplitudes*, in *Theoretical Advanced Study Institute in Elementary Particle Physics: Journeys Through the Precision Frontier: Amplitudes for Colliders*, pp. 419–476, 2015, DOI [1411.7538].

[129] J. Vollinga and S. Weinzierl, *Numerical evaluation of multiple polylogarithms*, *Comput. Phys. Commun.* **167** (2005) 177 [hep-ph/0410259].

[130] C. Duhr and F. Dulat, *PolyLogTools — polylogs for the masses*, *JHEP* **08** (2019) 135 [1904.07279].

[131] F.C.S. Brown, *Multiple zeta values and periods of moduli spaces* $\overline{\Updownarrow}_{0,n}$, *Annales Sci. Ecole Norm. Sup.* **42** (2009) 371 [math/0606419].

[132] E. Panzer, *Algorithms for the symbolic integration of hyperlogarithms with applications to feynman integrals*, *Comput. Phys. Commun.* **188** (2015) 148 [1403.3385].

[133] E. Panzer, *Feynman Integrals and Hyperlogarithms*, *PhD thesis* (2015) [1506.07243].

[134] F. Brown, *The Massless Higher-Loop Two-Point Function*, *Commun. Math. Phys.* **287** (2009) 925 [0804.1660].

[135] J. Broedel, C. Duhr, F. Dulat and L. Tancredi, *Elliptic polylogarithms and iterated integrals on elliptic curves. Part I: general formalism*, *JHEP* **05** (2018) 093 [1712.07089].

[136] J. Broedel, C. Duhr, F. Dulat, B. Penante and L. Tancredi, *Elliptic Polylogarithms and Iterated Integrals on Elliptic Curves*, *JHEP* **05** (2018) 120 [1712.07089].

[137] A.I. Davydychev, *Some exact results for ¡i¿N¡/i¿-point massive Feynman integrals*, *Journal of Mathematical Physics* **32** (1991) 1052.

[138] N. Ussyukina and A.I. Davydychev, *An approach to the evaluation of three- and four-point ladder diagrams*, *Physics Letters B* **298** (1993) 363.

[139] H. Frellesvig, D. Tommasini and C. Wever, *On the reduction of generalized polylogarithms to $Li_n$ and $Li_{2,2}$ and on the evaluation thereof*, *JHEP* **03** (2016) 189 [1601.02649].

[140] C. Duhr, H. Gangl and J.R. Rhodes, *From polygons and symbols to polylogarithmic functions*, *JHEP* **10** (2012) 075 [1110.0458].

[141] T. Ahmed, S.M. Hasan and A. Rapakoulias, *Angular phase-space integrals with four denominators through Mellin-Barnes*, *JHEP* **11** (2025) 152 [2508.15952].

[142] J.M. Henn, *Lectures on differential equations for Feynman integrals*, *Journal of Physics A Mathematical and Theoretical* **48** (2015) 153001.

[143] C.G. Papadopoulos, *Simplified differential equations approach for Master Integrals*, *Journal of High Energy Physics* **2014** (2014) .

[144] A. Primo and L. Tancredi, *On the maximal cut of Feynman integrals and the solution of their differential equations*, *Nuclear Physics B* **916** (2016) 94.

[145] L. Adams, C. Bogner and S. Weinzierl, *The two-loop sunrise graph in two space-time dimensions with arbitrary masses in terms of elliptic dilogarithms*, *Journal of Mathematical Physics* **55** (2014) .

[146] J. Broedel, C. Duhr, F. Dulat, B. Penante and L. Tancredi, *Elliptic polylogarithms and Feynman parameter integrals*, *Journal of High Energy Physics* **2019** (2019) .

[147] F.C.S. Brown and A. Levin, *Multiple Elliptic Polylogarithms*, 1110.6917.

[148] W. Konig and J. Kuti, *Semi-inclusive deep inelastic scattering in the parton model*, *Nuclear Physics B* **136** (1978) 1.

[149] J.C. Collins, *Hard-Scattering Factorization with Heavy Quarks: A General Treatment*, *Phys. Rev. D* **58** (1998) 094002 [hep-ph/9806259].

[150] J.C. Collins and D.E. Soper, *Back-to-Back Jets in QCD*, *Nucl. Phys. B* **193** (1981) 381.

[151] X. Ji, J.-P. Ma and F. Yuan, *QCD factorization for semi-inclusive deep-inelastic scattering at low transverse momentum*, *Physical review. D. Particles, fields, gravitation, and cosmology/Physical review. D, Particles, fields, gravitation, and cosmology* **71** (2005) .

[152] R.D. Ball, V. Bertone, S. Carrazza, L.D. Debbio, S. Forte, P. Groth-Merrild et al., *Parton distributions from high-precision collider data*, *The European Physical Journal C* **77** (2017) 663.

[153] T.-J. Hou, J. Gao, T.J. Hobbs, K. Xie, S. Dulat, M. Guzzi et al., *New CTEQ global analysis of quantum chromodynamics with high-precision data from the LHC*, *Physical review. D/Physical review. D.* **103** (2021) .

[154] S. Bailey, T. Cridge, L.A. Harland-Lang, A.D. Martin and R.S. Thorne, *Parton distributions from LHC, HERA, Tevatron and fixed target data: MSHT20 PDFs*, *The European Physical Journal C* **81** (2021) .

[155] D. de Florian, R. Sassot and M. Stratmann, *Global analysis of fragmentation functions for pions and kaons and their uncertainties*, *Phys. Rev. D* **75** (2007) 114010 [hep-ph/0703242].

[156] A. Metz and A. Vossen, *Parton Fragmentation Functions*, *Prog. Part. Nucl. Phys.* **91** (2016) 136 [1607.02521].

[157] D. de Florian, R. Sassot and M. Stratmann, *Global Analysis of Fragmentation Functions for Pions and Kaons and Their Uncertainties*, *Phys. Rev. D* **75** (2007) 114010 [hep-ph/0703242].

[158] S. Albino, B.A. Kniehl and G. Kramer, *AKK Update: Improvements from New Theoretical Input and Experimental Data*, *Nucl. Phys. B* **803** (2008) 42 [0803.2768].

[159] D. de Florian, R. Sassot and M. Stratmann, *Global Analysis of Fragmentation Functions for Pions and Kaons and Their Uncertainties*, *Phys. Rev. D* **75** (2007) 114010 [hep-ph/0703242].

[160] Z.-B. Kang, A. Prokudin, P. Sun and F. Yuan, *Extraction of quark transversity distribution and Collins fragmentation functions with QCD evolution*, *Physical review. D/Physical review. D.* **93** (2016) .

[161] S. Goyal, S.-O. Moch, V. Pathak, N. Rana and V. Ravindran, *Next-to-Next-to-Leading Order QCD Corrections to Semi-Inclusive Deep-Inelastic Scattering*, *Phys. Rev. Lett.* **132** (2024) 251902 [2312.17711].

[162] L. Bonino, T. Gehrmann and G. Stagnitto, *Semi-Inclusive Deep-Inelastic Scattering at NNLO in QCD*, *Phys. Rev. Lett.* **132** (2024) 251901 [2401.16281].

[163] S. Goyal, R.N. Lee, S.-O. Moch, V. Pathak, N. Rana and V. Ravindran, *Next-to-Next-to-Leading Order QCD Corrections to Polarized Semi-Inclusive Deep-Inelastic Scattering*, *Phys. Rev. Lett.* **133** (2024) 211905 [2404.09959].

[164] L. Bonino, T. Gehrmann, M. Löchner, K. Schönwald and G. Stagnitto, *Polarized Semi-Inclusive Deep-Inelastic Scattering at Next-to-Next-to-Leading Order in QCD*, *Phys. Rev. Lett.* **133** (2024) 211904 [2404.08597].

[165] G. Altarelli, R.K. Ellis, G. Martinelli and S.-Y. Pi, *Processes Involving Fragmentation Functions Beyond the Leading Order in QCD*, *Nucl. Phys. B* **160** (1979) 301.

[166] D. de Florian, M. Stratmann and W. Vogelsang, *QCD analysis of unpolarized and polarized Lambda baryon production in leading and next-to-leading order*, *Phys. Rev. D* **57** (1998) 5811 [hep-ph/9711387].

[167] M. Abele, D. de Florian and W. Vogelsang, *Threshold resummation at $N^3LL$ accuracy and approximate $N^3LO$ corrections to semi-inclusive DIS*, *Phys. Rev. D* **104** (2021) 094046 [2109.00847].

[168] J.M. Henn, *Lectures on differential equations for feynman integrals*, *Journal of Physics A: Mathematical and Theoretical* **48** (2015) 153001.

[169] J.M. Henn and V.A. Smirnov, *Analytic results for two-loop master integrals*, *Journal of High Energy Physics* **2014** (2014) 213.

[170] J.M. Henn, A.V. Smirnov and V.A. Smirnov, *Evaluating single-scale and/or non-planar diagrams by differential equations*, *JHEP* **03** (2014) 088 [1312.2588].

[171] S. Abreu, R. Britto, C. Duhr and E. Gardi, *From multiple unitarity cuts to the coproduct of Feynman integrals*, *Journal of High Energy Physics* **2014** (2014) .

[172] T. Gehrmann and E. Remiddi, *Two-Loop Master Integrals for $\gamma^* \to 3$ Jets: The Planar Topologies*, *Nucl. Phys. B* **601** (2001) 248 [hep-ph/0008287].

[173] J.M. Henn and V.A. Smirnov, *Analytic results for two-loop master integrals for Bhabha scattering I*, *JHEP* **11** (2013) 041 [1307.4083].

[174] R.N. Lee and A.A. Pomeransky, *Critical points and number of master integrals*, *JHEP* **11** (2013) 165 [1308.6676].

[175] S. Laporta, *High-precision multi-loop calculations and ibp identities*, *International Journal of Modern Physics A* **32** (2017) .

[176] A.V. Smirnov and F. Chukharev, *FIRE6: Feynman Integral REduction with modular arithmetic*, *Computer Physics Communications* **247** (2019) 106877.

[177] A.V. Smirnov, *FIRE5: A C++ implementation of Feynman Integral REduction*, *Comput. Phys. Commun.* **189** (2015) 182 [1408.2372].

[178] P. Maierhöfer, J. Usovitsch and P. Uwer, *Kira—A Feynman integral reduction program*, *Comput. Phys. Commun.* **230** (2018) 99 [1705.05610].

[179] A. von Manteuffel and R.M. Schabinger, *A novel approach to integration by parts reduction*, *Phys. Lett. B* **744** (2015) 101 [1406.4513].

[180] T. Peraro, *Scattering amplitudes over finite fields and multivariate functional reconstruction*, *JHEP* **12** (2016) 030 [1608.01902].

[181] J. Klappert, F. Lange, P. Maierhöfer and J. Usovitsch, *Integral reduction with Kira 2.0 and finite field methods*, *Comput. Phys. Commun.* **266** (2021) 108024 [2008.06494].

[182] R.N. Lee, *Libra: A package for transformation of differential systems for multiloop integrals*, *Comput. Phys. Commun.* **267** (2021) 108058 [2012.00279].

[183] M. Kobayashi and T. Maskawa, *Cp-violation in the renormalizable theory of weak interaction*, *Progress of Theoretical Physics* **49** (1973) 652.

[184] ALEPH, DELPHI, L3, OPAL and S. Collaborations, *Precision electroweak measurements on the z resonance*, *Physics Reports* **427** (2006) 257.

[185] P. Langacker, *Precision tests of the standard electroweak model*, *Advanced Series on Directions in High Energy Physics* **14** (1995) .

[186] D.Y. Bardin, J. Blümlein, P. Christova, L. Kalinovskaya and T. Riemann, *QED and electroweak corrections to deep inelastic scattering*, *Nucl. Phys. B Proc. Suppl.* **37** (1994) 148.

[187] R. Bonciani, P. Mastrolia and E. Remiddi, *QED vertex form factors at two loops*, *Nuclear Physics B* **676** (2004) 399.

[188] W. Bernreuther, R. Bonciani, T. Gehrmann, R. Heinesch, T. Leineweber, P. Mastrolia et al., *Two-loop QCD corrections to the heavy quark form-factors: Axial vector contributions*, *Nucl. Phys. B* **712** (2005) 229 [hep-ph/0412259].

[189] W. Bernreuther, R. Bonciani, T. Gehrmann, R. Heinesch, T. Leineweber, P. Mastrolia et al., *Two-loop QCD corrections to the heavy quark form factors: the vector contributions*, *Nuclear Physics B* **706** (2005) 245.

[190] T. Ahmed, G. Crisanti, F. Gasparotto, S.M. Hasan and P. Mastrolia, *Two-loop vertices with vacuum polarization insertion*, *JHEP* **01** (2024) 010 [2308.05028].

[191] A. Denner, *Techniques for calculation of electroweak radiative corrections at the one loop level and results for W physics at LEP-200*, *Fortsch. Phys.* **41** (1993) 307 [0709.1075].

[192] G. Passarino and M.J.G. Veltman, *One Loop Corrections for e+ e- Annihilation Into mu+ mu- in the Weinberg Model*, *Nucl. Phys. B* **160** (1979) 151.

[193] A. Denner and S. Pozzorini, *One loop leading logarithms in electroweak radiative corrections. 1. Results*, *Eur. Phys. J. C* **18** (2001) 461 [hep-ph/0010201].

[194] U. Aglietti and R. Bonciani, *Master integrals with 2 and 3 massive propagators for the 2 loop electroweak form-factor: Planar case*, *Nucl. Phys. B* **668** (2003) 3 [hep-ph/0304028].

[195] U. Aglietti and R. Bonciani, *Master integrals with one massive propagator for the two loop electroweak form-factor*, *Nucl. Phys. B* **698** (2004) 277 [hep-ph/0401193].

[196] U. Aglietti, R. Bonciani, G. Degrassi and A. Vicini, *Two loop light fermion contribution to Higgs production and decays*, *Phys. Lett. B* **595** (2004) 432 [hep-ph/0404071].

[197] G. 't Hooft, *Renormalizable Lagrangians for Massive Yang-Mills Fields*, *Nucl. Phys. B* **35** (1971) 167.

[198] L.D. Faddeev and V.N. Popov, *Feynman Diagrams for the Yang-Mills Field*, *Phys. Lett. B* **25** (1967) 29.

[199] A.A. Slavnov, *Ward Identities in Gauge Theories*, *Theor. Math. Phys.* **10** (1972) 99.

[200] J.C. Taylor, *Ward Identities and Charge Renormalization of the Yang-Mills Field*, *Nucl. Phys. B* **33** (1971) 436.

[201] M. Bohm, H. Spiesberger and W. Hollik, *On the One Loop Renormalization of the Electroweak Standard Model and Its Application to Leptonic Processes*, *Fortsch. Phys.* **34** (1986) 687.

[202] A. Djouadi and P. Gambino, *Electroweak gauge bosons selfenergies: Complete QCD corrections*, *Phys. Rev.* **D49** (1994) 3499 [hep-ph/9309298].

[203] V.A. Smirnov, *Analytic tools for Feynman integrals*, vol. 250 (2012), 10.1007/978-3-642-34886-0.